



저작자표시-비영리-변경금지 2.0 대한민국

이용자는 아래의 조건을 따르는 경우에 한하여 자유롭게

- 이 저작물을 복제, 배포, 전송, 전시, 공연 및 방송할 수 있습니다.

다음과 같은 조건을 따라야 합니다:



저작자표시. 귀하는 원저작자를 표시하여야 합니다.



비영리. 귀하는 이 저작물을 영리 목적으로 이용할 수 없습니다.



변경금지. 귀하는 이 저작물을 개작, 변형 또는 가공할 수 없습니다.

- 귀하는, 이 저작물의 재이용이나 배포의 경우, 이 저작물에 적용된 이용허락조건을 명확하게 나타내어야 합니다.
- 저작권자로부터 별도의 허가를 받으면 이러한 조건들은 적용되지 않습니다.

저작권법에 따른 이용자의 권리는 위의 내용에 의하여 영향을 받지 않습니다.

이것은 [이용허락규약\(Legal Code\)](#)을 이해하기 쉽게 요약한 것입니다.

[Disclaimer](#)

공학박사 학위논문

**Functionalized and Structurally
Enhanced ECM Scaffolds:
Advancing Regenerative Medicine**

기능화와 구조특성 강화를 통한 세포외 기질 지지체

기반의 재생 치료제 개발

2023년 08월

서울대학교 대학원

공과대학 바이오엔지니어링 협동과정

김범석

Abstract

Functionalized and Structurally Enhanced ECM Scaffolds: Advancing Regenerative Medicine

Beom Seok Kim

Interdisciplinary Program for Bioengineering

The Graduate School of Engineering

Seoul National University

Decellularized ECM (dECM) play a crucial role in the development of advanced biomaterials for regenerative medicine. This thesis presents an in-depth investigation of decellularization techniques, specifically incorporating dECM to regenerative application using additive

engineering skills and more conservative process to fabricate dECM scaffold. The current decellularization methods and dECM applications presented partial loss of extracellular matrix and unstable structural support in tissue environments, that possibly correlated to regeneration ability of dECM *in vivo*. To amend this problem, in the further chapters, the protein loading cryogel fabrication and supercritical fluid-based technology were applied to develop ideal dECM derived biomaterial.

The brain dECM cryogels were fabricated by cross-linking method utilizing heparin sulfate which have negative charge features. This approach aimed to mimic the complex composition of native brain tissues and growth factor loading affinity for support of neural tissue formation. The cryogel sustained their 3D structure in various stress conditions and controlled of growth factor releasing kinetics. The brain dECM cryogels exhibited excellent biocompatibility, allowing cell adhesion, proliferation, and tissue-like growth within the scaffold.

The comparative study of decellularization methods revealed the superiority of the supercritical fluid technique in preserving the native tissue architecture and extracellular matrix (ECM) components. By eliminating cellular components while retaining crucial ECM proteins,

this technique offers a promising approach to create biomimetic scaffolds. Quantitative analysis of tissue protein contents demonstrated the higher preservation of ECM (collagen, GAG), and other key proteins when using the supercritical fluid technique. Moreover, supercritical flow-based decellularization method showed higher neuronal cell differentiation efficiency and formal nerve tissue regeneration also.

Overall, this thesis highlights the potential of cryogels as three-dimensional scaffolds and additive loading of specific growth factor improves regeneration ability of own dECM and shows application versatility in tissue engineering applications. Additionally, the utilization of the supercritical fluid technique for efficient decellularization, preserving the native ECM components, and maintaining the structural integrity of tissues.

These techniques provide a platform for developing advanced biomaterials that closely mimic the native tissue environment, offering potential for regenerative medicine and tissue engineering approaches.

Keyword : Decellularization, Heparin sulfate, Supercritical fluid, Extracellular matrix

Student number : 2018-28861

Table of content

Abstract.....	i
Table of content	v
List of Figures.....	xiv
List of Tables	xvi
CHAPTER ONE: INTRODUCTION	1
1.1 Overview.....	1
1.2 Objective of the thesis.....	2
1.3 Organization of thesis	4
CHAPTER TWO:.....	5
THE SCIENTIFIC BACKGROUND AND RESEARCH PROGRESS	5
2.1 Biomaterials for tissue engineering.....	5
2.1.1 Polymeric material for tissue engineering and their applications	
5	

2.1.2 Decellularized ECM for tissue engineering.....	1 3
2.1.3 Application of decellularization technique to tissue engineering	
1 8	
2.2 Decellularization principle and methods	2 5
2.2.1 Principle of decellularization process and traditional	
decellularization methods	2 5
2.2.2 Supercritical fluid-based decellularization	3 0
CHAPTER THREE:.....	3 8
FABRICATION OF NGF RELEASING CRYOGEL WITH BRAIN	
DECELLULARIZED ECM FOR TBI (TRAUMATIC BRAIN INJURY)	
TREATMENT.....	3 8
3.1 Introduction.....	3 8
3.2 Materials and method.....	4 2
3.2.1 Decellularization of brain tissue.....	4 2
3.2.2 Paraffin sectioning of brain tissues.....	4 3
3.2.2.1 H&E staining of brain tissues.....	4 3

3.2.2.2 Trichrome staining of brain tissues	4 4
3.2.2.3 Safranin-O staining.....	4 5
3.2.2.4 DNA quantification in brain tissues	4 5
3.2.2.5 Hydroxy proline quantification in brain tissues	4 6
3.2.2.6 DMMB assays for quantifications of sGAG	4 7
3.2.3 Characterization of brain dECM and heparin derived cryogels	4 8
3.2.3.1 Preparation of brain dECM and heparin derived cryogel	4 8
3.2.3.2 Reaction efficiency calculation	4 8
3.2.3.3 FTIR analysis of cryogel	4 9
3.2.3.4 Microstructure analysis of cryogel.....	4 9
3.2.3.5 Swelling ratio calculation of cryogel.....	4 9
3.2.4 Mechanical property characterization of cryogel.....	5 0
3.2.4.1 Compressive modulus measurements of cryogels.....	5 0
3.2.4.2 Rheological property characterization of cryogels.....	5 0
3.2.4.3 Cryogel injectability test.....	5 1

3.2.5 Heparin mediated protein sustain release kinetics measurement.....	5	1
3.2.6 PC12 cells culture and differentiation.....	5	1
PC12 differentiation with cryogel encapsulated NGF	5	1
3.2.6.1 PC12 culture on the cryogel.....	5	2
3.2.6.2 β -3tubulin staining of PC12 cells.....	5	2
3.2.7 Regeneration of TBI animal model with cryogel.....	5	3
3.2.7.1 Brain defect model design and cryogel application in vivo ..	5	3
3.2.7.2 Fluorescence staining of brain tissues.....	5	3
3.2.8 Statistics analysis.....	5	4
3.3 Results.....	5	6
3.3.1 Decellularization of the brain tissue and component characterization native tissue and brain dECM.....	5	7
3.3.2 Fabrication and characterization of brain dECM based cryogel.....	6	0
3.3.3 Rheological property characterization of fabricated brain dECM derived cryogel.....	6	3

3.3.4	Characterization of injectability of fabricated cryogels.....	6 4
3.3.5	Heparin dependent protein loading efficiency of cryogels and NGF correlated PC12 cell differentiation ratio characterization....	6 6
3.3.6	PC12 culture and differentiation on the NGF loaded cryogels	7 0
3.3.7	<i>In vivo</i> application of cryogel (De1.0HS0.3) and characterization of vessel formation.....	7 1
3.3.8	<i>In vivo</i> application of cryogel (De1.0HS0.3) and characterization of neuronal cell migration in host tissues	7 5
3.3.9	<i>In vivo</i> application of cryogel (De1.0HS0.3) and characterization of neuronal cell recruitment in to the cryogel network .	7 8
3.4	Discussion	7 9
3.5	Conclusion.....	9 3
3.6	Supplementary figure	9 6
4.1	Introduction.....	1 0 0
4.2	Material & methods	1 0 4
4.2.1	Isolation and decellularization of sciatic nerve tissues	1 0 5
4.2.2	Histological assessment of sciatic nerve tissues.....	1 0 6

4.2.2.1 Paraffin sectioning of nerve tissues	1	0	6
4.2.2.2 H&E staining of nerve tissues	1	0	7
4.2.2.3 Trichrome staining of nerve tissues	1	0	7
4.2.2.4 Safranin-O staining.....	1	0	8
4.2.3 ECM characterization in nerve tissues	1	0	9
4.2.3.1 DMMB assay for quantifications of sGAG.....	1	0	9
4.2.3.2 DNA quantification in nerve tissues	1	0	9
4.2.3.3 Hydroxyproline quantification in nerve tissues	1	1	0
4.2.3.4 Proteomic evaluation of tissue samples	1	1	1
4.2.4 Mechanical property characterization of nerve tissues	1	1	2
4.2.4.1 Extension force test of nerve tissues.....	1	1	2
4.2.4.2 Compression force test	1	1	2
4.2.5 Neuronal cell culture	1	1	2
4.2.5.1 PC12 cell cultures for proliferation and differentiation.	1	1	2
4.2.5.2 PC12 cell differentiation on nerve tissues	1	1	3
4.2.5.3 PC12 cell imaging with confocal microscopy.....	1	1	3

4.2.6 Surface image of decellularized ECM with SEM.....	1	1	4
4.2.7 In vivo experiment and characterization of regeneration of tissues	1	1	4
4.2.7.1 Nerve tissue implants to subcutaneous area for immune reaction characterization.....	1	1	4
4.2.7.2 dECM implantation in sciatic nerve defect model.....	1	1	5
4.2.7.3 Gait analysis of sciatic nerve defect model.....	1	1	5
4.2.7.4 Evaluation of muscular tissue regeneration.....	1	1	6
4.2.7.5 Histological assessment of sciatic nerve tissues.....	1	1	6
4.2.7.6 Luxol fast blue staining of regenerated nerve tissues.....	1	1	7
4.2.8 Statistics analysis.....	1	1	7
4.3 Results.....	1	1	9
4.3.1. Decellularized ECM scaffold fabrication and characterization of ECM.....	1	2	0
4.3.2 Mechanical characterization of decellularized tissue samples	1	2	3
4.3.3 PC12 differentiation on native and decellularized tissue slice samples	1	2	6

4.3.4 Immune cell infiltration of implanted tissue samples.....	1 3 0
4.3.5 Motor function and muscular tissue regeneration after implantation <i>in vivo</i>	1 3 2
4.3.6 Nerve tissue regeneration assessment after tissue implantation <i>in vivo</i>	1 3 5
4.4 Discussion	1 3 7
4.5 Conclusion.....	1 4 7
4.6 Supplementary figure	1 4 9
CHAPTER FIVE: CONCLUDING REMARKS	1 5 4
BIBLIOGRAPHY	1 5 6
국문초록.....	1 5 7

List of Figures

Figure 2.1 Commonly applied synthetic polymers to tissue engineering. Copy right (2009), Royal Society of Chemicals.-----	8
Figure 2.2 Natural derived polymers for tissue engineering and cell responsive abilities. Copy right (2021), springer nature -----	11
Figure 2.3 Scheme of 3D scaffold application to <i>in vivo</i> , cell environments by providing of chemical and physical cues -----	17
Figure 2.4 Description about host immune cell and ECM interaction in tissue environments..-----	17
Figure 2.5 dECM applications in various tissue engineering strategies -----	24
Figure 2.6 Basic information of super critical flow process -----	34
Figure 3. 1 ECM structure analysis and quantification in native and decellularized brain tissues (dECM). -----	56
Figure 3. 2 ECM structure analysis and quantification in native and decellularized brain tissues (dECM).-----	59
Figure 3.3 Rheological characteristics measurements of the cryogels -----	62
Figure 3.4 Injectability characterization of the cryogels-----	65
Figure 3.5 Sustain release profile of the proteins and characterization of neuronal cell differentiation ability followed by releasing of NGF from cryogels -----	67
Figure 3.6 3D culture of PC12 cells on NGF encapsulated cryogels for 21 days. -- -----	70
Figure 3.7 In vivo brain defect model development and assessments of vascularization of brain tissues. -----	72
Figure 3.8 Neuronal tissue regeneration assessment post implantation of cryogels in infarct area of host tissues. -----	74
Figure 3.3 Neuronal tissue regeneration assessment post implantation in implanted crygel. areas:-----	77
Figure S3.1 Zeta potential of heparin sulfate and decellularized brain ECM-----	96
Figure. S3.2 Immune cell population of infarct area after surgery A) Representative	

images of Iba-1 images in infarct area of host tissues -----	97
Figure S3.3 Immune cell population in implanted cryogel area-----	98
Figure 4.1 Composition analysis of native tissue and decellularized tissues processed with different decellularization methods-----	119
Figure 4.2 Mechanical characterization of native and decellularized tissues. (A) Representative image of extension test method of wet tissue-----	123
Figure 4. 3 PC12 cell culture and differentiation on nerve tissue slices. (A-B) Class III β -tubulin and actin staining of PC12 cell cultured on native and decellularized tissues.-----	125
Figure 4.4 PC12 cell culture and differentiation on nerve tissue slices for a long- term period. (A) PC12 cell differentiation on nerve tissues for 21 days-----	128
Figure 4.5 Immune cell infiltration ratio characterization of native tissues and dECM after implantation to skin area-----	129
Figure 4. 6 Muscular regeneration and motor function recovery <i>in vivo</i> . (A) Nerve tissue implantation at nerve gap defects -----	131
Figure 4. 7 Gap-43 and S-100 fluorescence staining of sciatic nerves post- implantation at 4,8 weeks.-----	134
Figure 4. 8 Luxol fast blue staining of cross sectioned regenerated nerves after 8weeks.-----	136
Figure S4. 1 Polymeric composition analysis and contents measurements of decellularized tissues processed with various decellularization methods -----	149
Figure S4. 2 SEM image of native tissues and decellularized tissues -----	150
Figure S4. 3 PC12 differentiation cultured on TCP plates with/without NGF---	151
Figure S4.4 Fluorescence data of PC12 cells cultured for 3,7 days on nerve tissue slcies.-----	152
Figure S4. 5 Quantitative data of native tissues. (A) Gap-43, S-100 staining of native tissues.-----	153

List of Tables

Table 2.1 Description about traditional decellularization methods -----	29
Table 1.2 Supercritical fluid based decellularization with various parameter conditions and tissue sources.-----	37
Table 3.1 Decellularized ECM and heparin sulfate concentrations in each cryogel group.-----	59

CHAPTER ONE:

INTRODUCTION OF THE OVERALL

TOPIC OF THESIS

1.1 Overview

Tissue engineering is one of the clinical investigation methods for treatment of surgical defect and non-homeostasis symptoms of human body. In this subject, biomaterials have been studied to treat volumetric tissue loss and tissue necrosis by supplying tissue compatible 3D structure for tissue remodeling. Many kinds of natural derived polymers like chitosan, hyaluronic acid, purified collagens were used for tissue regeneration which need long term screening and accurate medicinal. Those polymers were applied with further engineering steps, polymer surface modification and loading of cell responsive factors, in it to provide ideal tissue environments. For this reason, the non-programmed regenerative biomaterials, decellularized extracellular matrix (dECM) were incorporated to regeneration strategies due to their native tissue derived regenerative potentials and 3D structural biomimicry. In this thesis, on the base of decellularization concept, tissue regenerative

biomaterial fabrication studies are presented from application of dECM based growth factor releasing cryogel fabrication method to cutting- edge decellularization technology for more conservative dECM extraction.

1.2 Objective of the thesis

The final goal of this thesis is to introduce of new strategies for application of decellularized ECM (dECM) to tissue engineering. In this manuscript, extraction of decellularized extracellular matrix (dECM) and fabrication of dECM scaffolds were performed for treatment of volumetric tissue defects that requiring long term medical intervention.

The potential of regeneration and high composition of cell compatible molecules and complex polymer compositions are unique characteristics of dECM. This macromolecular material has been commonly used as solution or hydrogel forms to be applied in cell and tissue engineering. However, the dECM, that even freshly prepared as described above, still need additive delivery systems and more preservative strategies to maximize their regenerative ability for long term treatment of tissue defect. Due to unstable solution form and weak

mechanical strength of thermally crosslinked dECM hydrogel were easily dissipated in tissue environments, to handle this problem, a 4- (4,6-Dimethoxy-1,3,5-triazin-2-yl)-4-methylmorpholinium chloride (DMTMM) crosslinked cryogel system were studied to form a 3D porous skeletal structures using brain dECM along with heparin sulfate charge materials which can add protein releasing ability to cross-linked cryogel. The cryogel could control growth factor releasing amount and provide stable 3D supportive structure to tissue environments for neural cell recruitments.

The innate regenerative molecules in dECM can be diluted and extracted with consecutive step of solvent changing decellularization process. To maintain stable regenerative potential of dECM, preservation of cell responsive protein and cell binding ECM components in dECM were considered as one of the strategies for fabricating of dECM based scaffold. To fabricate maximally preserved dECM scaffold, super critical fluid-based (carbon dioxide: CO₂) decellularization method, investigated and compared with traditional chemical (sodium dodecyl sulfate: SDS) based one to confirm their superior preservation ability of tissue innate proteins and polymer components after decellularization process

enhancing regeneration in tissues.

1.3 Organization of thesis

This thesis demonstrated about fabrication of dECM based biomaterials and application for tissue engineering and regenerative medicines.

In chapter two, scientific backgrounds of the general biomaterial and dECM applications were presented. Furthermore, the traditional decellularization and supercritical fluid-based methods were addressed.

In chapter three, the brain dECM based NGF releasing cryogel were introduced for neural tissue regeneration in traumatic brain injury (TBI). This subject focus on the delivery of dECM in fully cross-linked form for long-term implant with highly concentrated growth factors.

In Chapter Four, a comparative study of two different decellularization methods, supercritical fluid and traditional SDS-based, was presented for fabricating a nerve implants. The superiority of methods was proven through the quantification of their tissue protein contents, changes in mechanical properties, and cell and tissue reactivities after the process.

CHAPTER TWO:

THE SCIENTIFIC BACKGROUND AND RESEARCH PROGRESS

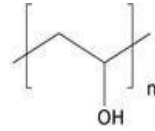
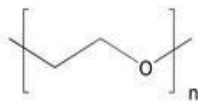
2.1 Biomaterials for tissue engineering

2.1.1 Polymeric material for tissue engineering and their applications

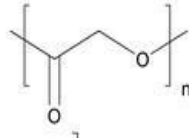
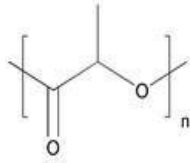
Cases about tissue regeneration have been studied due to their low reproducibility and functional recovery of damaged tissues [1, 2]. When tissue defect and traumatic diseases occurred in normal tissue, it is hard to regenerate and restore same histological homogeneity and structural characteristics of original tissue that existed before tissue loss [2, 3]. Although, the host's inherent regenerative ability forms volumetric 3D structures (new tissues) following the tissue defect after injury. These newly formed tissues often comprise a high proportion of simple connective tissues and fibrosis assets, which cannot fully mimic the functional native tissues [4]. The irregular tissue formation in

defect area disturbs functional tissue infiltration to injured area and harmonization between surrounding normal tissues and new tissues [5]. There were many regenerative strategies that have been studied using stem cells and medicines for formal tissue recovery [2, 6, 7]. The use of living cells or tissue regenerative molecules in tissue regeneration strategies has indeed demonstrated improvements in tissue recovery after defects. However, there are limitations associated with their application, particularly regarding quality control of living cells and insufficient quantity for treating bulk tissue defects [8-10]. The cell delivery and soluble form of medicinal treatment limited to use in tissue defect due to their low targeting efficiency and absence of regulating systems for proper applications without vehicles [11, 12]. Although, cell stemness, were capable of to provoke cellular activity of host tissues. However, it is hard to maintain their regenerative functions and reproducible cell cycles during or before treatment to tissue defects [13]. And even their stemness can be variable with source and lineage, even with the environment that stem cells exposed [14, 15]. For this reason, tissue regeneration strategies need another conceptualization about not only apply regenerative potential materials that activate cells in host tissues-endogenous regeneration but the structural support to volumetric tissue lesion.

Researchers have been exploring the use of 3D polymer scaffolds to promote tissue regeneration, aiming to activate the host cells with structural support [16]. Furthermore, the 3D scaffolds also introduced for providing of cell binding basement as well as delivering of living organisms and proteins in polymer networks rather than injecting solution form or relying on unstable cell therapies with uncertain efficacy and reproducibility [17, 18]. The 3D solid networks that maintain a three-dimensional structure, offer structural stability similar to original tissue and provide temporal encapsulation of various regeneration niche for cell activity inducing comprehensive formal tissue formation.

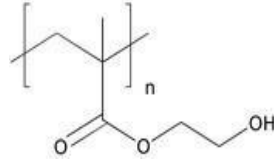
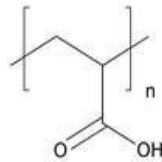


poly(ethylene glycol) (PEG) poly(vinylalcohol) (PVA)



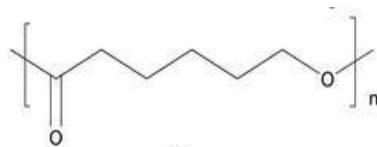
poly(lactic acid) (PLA)

poly(glycolic acid) (PGA)



poly(acrylic acid) (PAA)

poly(2-hydroxyethyl methacrylate) (PHEMA)



poly(caprolactone) (PCL)

Figure 2.1 Commonly applied synthetic polymers to tissue engineering. Copy right (2009), Royal Society of Chemicals

As mentioned earlier, biomaterials with three-dimensional structures have various advantages in the field of tissue engineering. They offer

simple mechanisms while allowing for modification to enable diverse applications. It is important to determine the appropriate materials and crosslinking methods for the intended application, as well as define the potential applications based on the unique characteristics of the chosen materials. Among the kinds of bio-polymers, polyesters are widely utilized in tissue engineering due to their versatile characteristics (Figure 2.1). Polyesters are particularly well-suited for conforming to irregular tissue defects, and the chemical residues of these polymers can be modified to control solubility in water and biodegradability within tissues [19]. Polyesters such as poly ϵ -caprolactone (PCL), polylactic acid (PLA), polyglycolic acid (PGA), and poly lactic-co-glycolic acid (PLGA) copolymer are commonly used in tissue engineering. The PGA is a highly biodegradable polymer with hydrophilic characteristics, making it suitable for cell experiments and animal studies [20]. On the other hand, the PLA has a lower biodegradability compared to PGA due to the presence of methyl groups, which makes it suitable for applications requiring long-term tissue retention [21]. To regulate the degradation rate, the copolymer PLGA was developed, allowing for construction of tissue and mild biodegradation of three-dimensional structures by controlling chemical moieties conjugation ratios with hydrophobicity on polymers

that made suitable for more various tissue engineering applications [22]. The PCL, in contrast, has been known to have a significantly lower biodegradability compared to the other polyester polymers mentioned earlier. The PCL is an FDA-approved biocompatible polymer that possesses high strength and low biodegradability [23]. It is used as a substitute for solid tissue replacement or as a reinforcing material for support of other soft biodegradable polymers [24]. However, overall polyester polymers, known for their high strength and plasticity, are not suitable for replacing tissues having low mechanical property [25]. In addition, there were decrease of cellular activity and migration correlated with increased immune responses in tissues when the polyesters degraded to monomers in wet environments [26-28]. For this reason, the synthetic polymer polyester, even with high water affinity, hardly applicable for soft tissue reconstruction which need functional cell proliferation that requiring physiological specialty originated from cell connectivity and signaling along with elastic tissue environments.

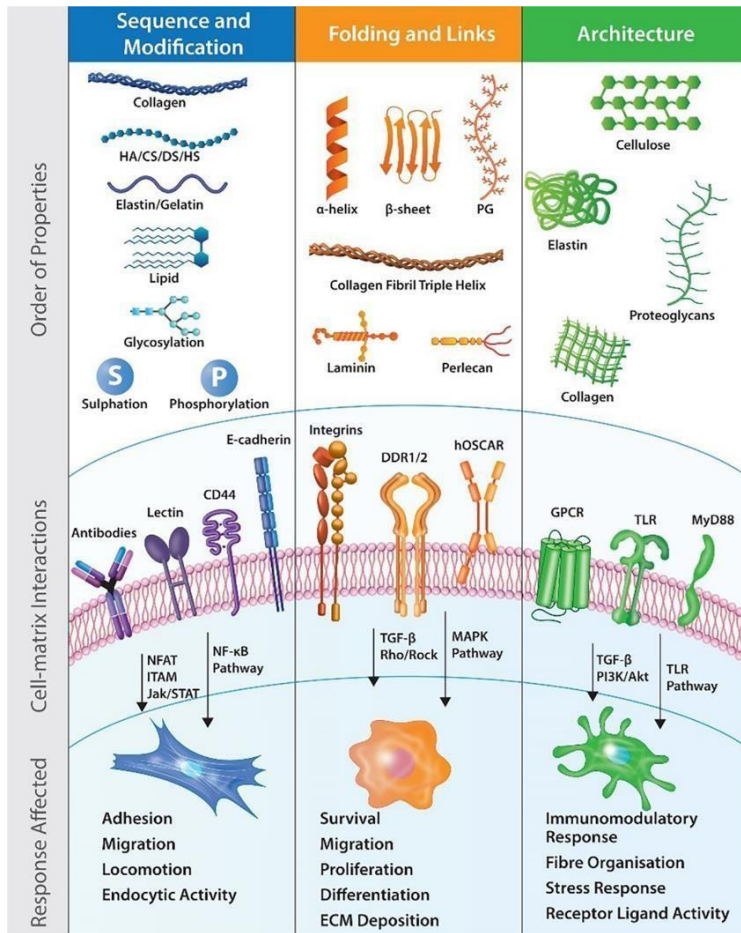


Figure 2.2 Natural derived polymers for tissue engineering and cell responsive abilities. Copy right (2021), springer nature

The use of soft hydrophilic three-dimensional structures has achieved the unique tissue formation and supply of cell culturing basements in various tissue engineering studies in the past [29]. The

naturally derived polymers were fabricated to the three-dimensional structure as tissue mimicking object that provided 3D tissue environment for tissue regeneration and applied by their functional characteristics (mechanical property, biochemical, cell binding) [30-32]. (Figure 2.2) To address these issues, research has been conducted using naturally derived polymers with high cell compatibility, such as gelatin, collagen, sulfated glycosaminoglycan (sGAG), chitosan, and hyaluronic acid (HA), for tissue regeneration showing mild immune response and tissue formation [33, 34]. Studies involving the formulation of three-dimensional networks with chemical modification of functional moieties in polymers, like the sGAG and the HA, have been actively progressed with carbon tubing and protein conjugation [35, 36]. However, polysaccharide-based polymers have difficulty inducing complete cell attachment, differentiation by own polymeric states without the incorporation of other cell compatible chemical moieties or cell attachment peptides [37]. To provide extremely cell compatible 3D network, protein-based polymers were studied that can provide cell reactive binding site. The Gelatin that fabricated with hydrolysis of collagen, in particular, has been widely used as a tissue engineering platform due to its easy modifying characteristics and innate cell binding

sites [38]. The collagen, as a major ECM component of tissues, has been extensively utilized in various regenerative medicine fields including vascular grafting and dermal tissue formations [39, 40]. It offers advantages such as high cell attachment, cell and tissue compatibility, and the ability to form stable three-dimensional structures like original tissue network [39]. The researches about utilizing collagen in tissue engineering have been actively ongoing to apply collagen as a base material for complex tissue formation. In addition, the collagens were also applied in combination with other polysaccharides or modification of chemically reactive residues to promote additional biophysical properties and more native tissue like complex ECM compositions [41, 42].

2.1.2 Decellularized ECM for tissue engineering

With development of natural polymer designing method, the researchers have been able to achieve the specific formation of the fundamental structure of tissues and organs, known as the extracellular matrix (ECM), resulting in effective tissue regeneration outcomes. The ECM serves as the base for tissue formation, which is the basic unit of

biological organization before cells come together to become organs [34]. The ECM provides physical and structural rigidity within tissues, facilitates multicellular organism formation and individual cell functionality through high cell attachment and topological capabilities, and creates an environment that enables physiological and biophysical signaling at the tissue level [43]. (Figure 2.3)

To replicate the composition, physical characteristics, and multicellular reactivity of native tissue, natural-derived polymers have been widely used as described above. However, artificially producing the unique microenvironment of primordial properties of tissues that inherent in mammal organs and specific physical structure and compositions are still challenging [44]. There were some trials to establish specific tissue like ECM for clinical investigations about activating of self-regeneration abilities of stem cells existing in host tissues with material inherent cues like stiffness, structure, degradability [45] and controlling of the immune system also with specific material contact, sensing of immune cells evasion, and adaptability in a comprehensive manner [46]. Artificially designed natural polymer derived biomaterials showed considerable tissue regeneration activity.

However, the existing methods still hard to provide ideal tissue environments in terms of controlling variables that contribute to specific tissue area regeneration and developing as customized concept [47, 48]. The ultimate goal of all these trials from biomaterial fabrication to regulation of cell physiology in tissue environments with extra material modification is to achieve the regenerative scaffold that having original tissue like physical structure and inducing endogenous regeneration of host tissues [49]. To address these challenges, a technique called decellularization has emerged. This technique involves extracting immunogenic generic material and preserving the polymers, protein components within the original tissue in highly complex compositions to create an ideal regenerative medicine for formal tissue regeneration.

The decellularized ECM (dECM) has known for one of the regenerative biomaterials for their mammalian tissue originated proteins and various structural polymeric molecules in one condensed batch [50]. In contrast to synthetic biomaterials, containing non-degradable components that can provoke immunological response but difficult to degrade by immune cells, the dECM is composed of collagens and polysaccharides that were gradually degradable with acute immune

response. This immune responsive degradation of dECM not only provided binding site for tissue interactive enzymes with uncover of fibrillar surface of biopolymers but also supplying spare rooms for newly generating tissues. The pro-inflammatory response derived dECM degradation also induced release of tissue inherit proteins from dECM, provoking regenerative cell activities in around tissues [51, 52].(Figure 2.4) The bulk implantation of dECM allow it to properly respond to the inherent immune response of the host. It activates appropriate defense mechanisms against foreign materials and promotes the release of regenerative factors (ECM, growth factor, etc) by dECM degradation that facilitate the regeneration process in the tissue, while simultaneously creating a regenerative niche [53]. Moreover, its property of being naturally degraded by the immune response in the body ensures that it does not impede the initial defense mechanisms and prevents long-term exposure of the tissue to the pro-inflammatory state, unlike synthetic materials [54, 55].

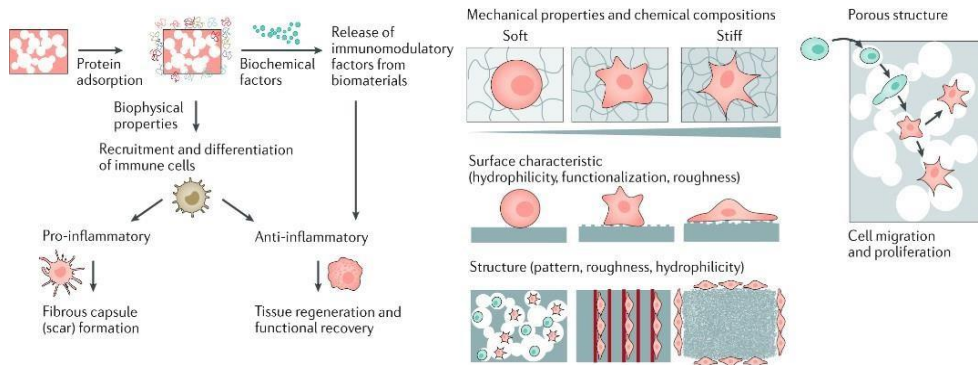
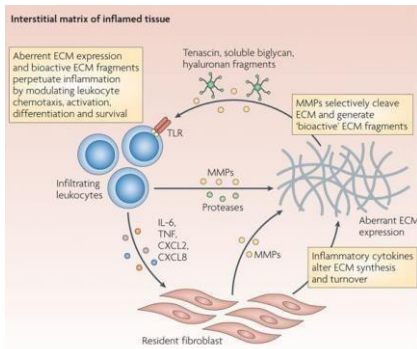


Figure 2.3 Scheme of 3D scaffold application to *in vivo*, cell environments by providing of chemical and physical cues. 3D scaffold implantation regulating immune response of host tissues that affect regeneration and endogenous cell priming. Mechanical property and surface modification of polymers affect cell fate and migration characteristics in intact situations.

A



B

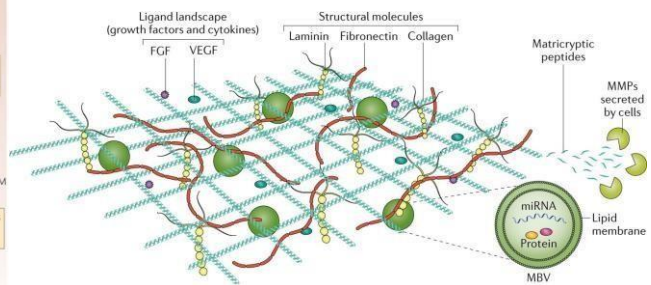


Figure 2.4 Description about host immune cell and ECM interaction in tissue environments (A) Immune cell and ECM interaction cycle resulting ECM degradation and fibroblast activation in inflamed tissue environments. (B) Representative microenvironments of decellularized ECM of intestinal tissue

2.1.3 Application of decellularization technique to tissue engineering

The dECM is ready to use biomaterial for cell and tissue regeneration as it contains beneficial biomolecules and a diverse array of structural polymers derived from mammalian tissues [56]. Its unique native tissue like properties make it highly suitable for use as a implantable biomaterial. Its regenerative effects are a result of the integration of various factors, such as tissue-specific regenerative molecules, polymeric materials, matrix-based molecular adsorption, and affinity which presented in complex polymeric environments [57]. Furthermore, these compositional characteristics can be designed by their biological sources that having different histological appearance and physiological feature of mammalian tissue environments [56]. Although this tissue dependent uniqueness of dECM limits its application to specific area that matched to the corresponding lost tissue type or similar origins [58, 59]. This tissue-to-tissue match strategy of using dECM has been set as a guideline in dECM applications to maximize their regeneration ability [60, 61].

The most commonly used form of dECM for biomaterial fabrication is the hydrogel, which is fabricated by crosslinking of polymers in it [62]. Hydrogels have a semi-solid structure containing moisture, resembling

the wet environments and properties of native tissues in the mammalian body. They can be refined to encapsulate water-soluble factors and allow free movement of cells and substances due to the fluidity of water[63]. When the dECM exposed to a specific temperature range, the dECM undergoes a phase transition, where the internal polymer components aggregate and physically crosslink to form a hydrogel state[64]. This semi-solid polymer form can be stably maintained within the body, enabling transplantation in fixed state. Moreover, during the transplantation process, it offers advantages such as ease of manufacturing and handling due to its consistent shape and volume.

Hydrogels derived from dECM provide an advantageous platform for tissue engineering and regenerative medicine as described above. They can be modified to rearrange the tissue environment, providing more hard structural support, promoting target cell adhesion and proliferation, and facilitating the engulf state of bioactive factors for proper tissue regeneration [65, 66]. Specifically, the dECM's ability to transform from a dissolved liquid to a hydrogel form, along with its hydrophilic nature, has led to ongoing efforts in processing and engineering dECM to incorporate additional factors or other polymers

needed for tissue regeneration process [67]. Various studies have focused on introducing cell-binding peptides or mixing them to enhance the regenerative effects. For example, cell adhesion moieties such as RGD peptide have been coded to dECM [68]. And the GRGDSPC peptide conjugated to decellularized tissue to promote the growth of endothelial cells or employed the REDV sequence for the formation of artificial micro vessels [69, 70]. To address the limited tensile strength and structural stability of thermally crosslinked hydrogels, strategies such as coating with gold (Au) nanoparticles or incorporating stiff materials like PCL have been explored to enhance the properties and develop hard tissue structures that could not be achieved with natural polymer-derived dECM solely [71, 72]. These dECM designs editing with extra material incorporation could provide selective tissue microenvironments that easily tunable. Ongoing research in this field aims to optimize the composition and newly added properties of dECM-based biohybrids for a wide range of tissue engineering applications. Those newly fabricated dECM based biomaterials should perform advanced regenerative potential with dECM and precise controlling of newly edited components in it.

The use of dECM has shown great potential in various areas of research and application, particularly in tissue engineering. Although the dECM have known for ideal materials for regenerative medicine but still need more investigations about fabricating method using dECM to atypical tissue structuring. One notable application is in the fabrication of unique 3D structures using a toolkit for processing dECM solutions to having specific architectures.

To create thin sheet-like dECM structures with cell compatibility and binding affinity, researchers have mixed dECM with materials such as PCL (polycaprolactone) and PVA (polyvinyl alcohol), which are suitable for electrospinning [73]. Electrospinning is a technique that uses an electric field to draw polymer materials into thin fiber states, enabling the production of thin films. By incorporating dECM into electrospun materials, it becomes possible to create thin, cell-compatible structures with specific alignment and mechanical properties [74]. The muscle dECM has also been used alone to create aligned scaffolds for muscular tissue formation [75, 76]. These scaffolds facilitate the bi-directional extension of muscular cells, allowing for the development of functional muscle tissue. This application is particularly valuable in tissue

engineering approaches aimed at repairing or replacing damaged muscle tissue. This fiber aligning method also applied to neural tissue engineering for fabricating of neuron cell guidance platform using dECM. This technique provided controllable cell outgrowth guiding basement that produced high cell migration and tissue regeneration in vivo [77].

Furthermore, dECM has been employed as a bioink in 3D printing tech, in combination with sacrificial or support materials [78]. This approach enables the structural and cellular reproduction of various tissues and multiple organs. By utilizing dECM as a bioink, researchers can recreate complex three-dimensional geometries and diverse cell distributions in sole structure, aiming to replicate tissues at the organ level [79, 80]. There was constructing results of cartilage tissue with dECM and PCL, alginate matrix with increased mechanical strength and fast 3D structuring of tissues [81]. Not only structural tissue, the endocrinal and hepatic tissues that have functional role in physiology also fabricated with 3D printing with dECM [82] [83].

The potential of dECM extends to the field of organ transplantation and artificial organs. Instead of simply digesting dECM into a solution,

researchers have developed methods to decellularize whole organs while preserving their macro native tissue structure [84]. These decellularized organs can then be transplanted intact into animals or recellularization study, with the aim of assessing whether functional cell groups can reform the tissues within the scaffold of the dECM. The perfusion-based methods have been developed to utilize whole tissue structure as regenerative biomaterials for organ replacements. These methods focus on keep preserve the microstructure of vessels which supply nutrients to tissue and organs and usually applied to highly vascularized tissues like kidney [85] [86] and heart [87]. These trials highlight the versatility of dECM as a biomaterial in regenerative medicine. Its ability to preserve the native tissue structure and recreate complex 3D architectures makes it a promising tool in tissue engineering, organ transplantation, and the development of functional artificial organs. Ongoing research continues to optimize dECM-based approaches and explore their potential for clinical applications.(Figure 2.5)

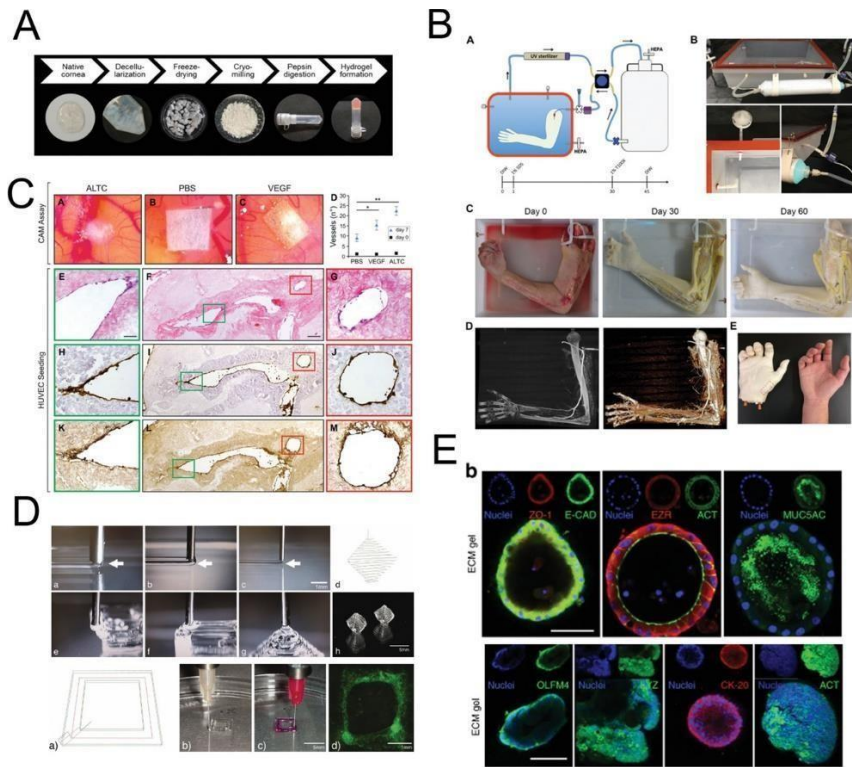


Figure 2.5 dECM applications in various tissue engineering strategies. (A) Standard process of decellularization and thermal crosslinking of dECM. (B) Whole organ decellularization method of extremities. (C) Vascularization of dECM with endothelial cell 3D culture (D) Utilization of dECM as bio ink for 3D printing method. (E) Organoid platform development with dECM

2.2 Decellularization principle and methods

2.2.1 Principle of decellularization process and traditional decellularization methods

Decellularization has emerged as a promising approach for creating acellular scaffolds that retain the native ECM architecture by removing only cellular components from native tissues, decellularized scaffolds provide an environment conducive to cell repopulation, tissue regeneration, and transplantation.

The decellularization protocol varied by their purposes of application and the characteristics of samples except one specific aim, removing generic materials [88].(Table 2.1) The physical stress methods including freeze-thaw cycle and direct physical agitation induced unnormal conditions for cell membrane disruption in tissues [89]. This repeated outer stress induces non-homeostasis of cell membrane and physical disruption to cell membranes and ECM. Due to their easy to control variables like temp and pressure, the decellularization with physical parameters could make reproducible process to samples but their harsh condition destroyed ECM structures [90]. The chemical based decellularization method have been applied for animal tissue process because of their convenience and fast removal of generic compound

within tissue. The chemical-based method using SDS, Triton-X100 used principle of surfactant that disrupting interactions among protein and lipids [91, 92]. SDS, ionic detergents, has more strong action of decellularization that made more quick process than other mild detergents. However, SDS treatment to mammalian tissues provoke the breakage of protein-protein interaction and dissolve of ECM components with DNA materials in detergent solutions [93]. This degradation procedure made lower dECM yields, tissues structure demolition and decreased matrixome in dECM [94]. Those tissue damages induced weaken structural support of ECM and lower cell response integrity that exert regeneration ability. For this reason, there were development of new kind of detergent presented high decellularization affinity but highly focus on lower tissue degradation. A sodium deoxycholates (SDC) treatment showed higher ECM preservation than SDS but still need extra enzymatic solution treatment to eliminate DNA fragments in tissues [95, 96]. Zwitterionic detergent have both characteristics of ionic and non-ionic detergents. This amphoteric characteristic made the detergent more stable and but still need additive DNA degradation treatments [97]. 3-[(3-cholamidopropyl) (dimethylammonio)-1-propane sulfonate(CHAPS) decellularizes tissues by disrupting lipid-protein and lipid-

lipid interactions but due to their lower tissue permeability it still needs further DNA degradation process after process also [98]. Sulfobetaine 10,16 (SB-10,16), one of the zwitterionic detergents were known for their apoptosis activity inducing cell removal but still need further post treatments for removal of DNA [99]. The chemical solution based decellularization method have been used with proper kind of detergents and concentrations depend on tissue types or sizes. The chemical based decellularization method is easy and quick process and had high reproducibility of product. However, the use of detergents in the decellularization process still has some disadvantages, including inefficient sequential solution exchange, tissue loss, and difficulties in removing residual detergents after decellularization [100, 101]. As described above, for now, the traditional decellularization methods using physical stress and chemicals have their own limitations to fabricate ideal biomaterial[102]. To minimize tissue degradation and non-homogeneous DNA removal in tissues, a newly programmed decellularization protocol is needed. This protocol should focus on achieving high permeabilization rate and mild conditions to decrease tissue damage during process. Furthermore, it should aim to use of non-cytotoxic solvents and easy to remove after decellularization process, to avoid potential side effects in

host tissues.

Table 2.1 Description about traditional decellularization methods. Chemical, enzymatic, physical decellularization process were investigated by their types, mechanisms and current limitations.

Methods	Types	Mechanism	Side Effects on the ECM
Chemicals	SDS, Triton, SDC, CHAPS, Acid/ Base	Solubilizes cytoplasmic components, disrupts nucleic acids, Liquefies the internal and external cell membranes, Disrupts protein–protein interactions	Damages collagen and GAG. Tends to denaturalize proteins and may induce nuclear and cytoplasmic waste in the remaining matrix.
Enzymes	Pepsin, Trypsin, Collagenase	Breaks cell adhesion to matrix. It targets peptide bounds	Can damage the proteins in the ECM, in particular laminin and GAG. Causes high damage in the ECM proteins if left for too long
Physical Stress	Force, Thermal shock, Vacuum assisted	Mechanical pressure can be enough to induce the lysis in some tissues, Crystals created in the freezing process destroy the cell membrane	The overall protein structure of the ECM may be compromised. Limited to tissues with hard structures, as it can greatly damage the ECM structure

2.2.2 Supercritical fluid-based decellularization

Supercritical fluid-based technology is a cutting-edge field of research and development that has gained significant attention in various scientific disciplines. It offers a unique and versatile approach for numerous applications, ranging from pharmaceuticals and materials science to environmental and energy sectors [103].

At its core, supercritical fluids refer to substances that are heated and pressurized to a state beyond their critical points, where they exhibit exceptional properties that combine the characteristics of both liquids and gases. This state occurs when the temperature and pressure reach a specific threshold, resulting in a supercritical fluid that possesses a high density, low viscosity, and remarkable solvating power.

Supercritical fluid-based technology utilizes these distinctive properties to perform a wide range of processes, such as extraction, purification, particle formation, and synthesis [104]. The choice of the supercritical fluid depends on the targeted application, with carbon dioxide (CO₂) being the most commonly employed due to its low toxicity, low cost, and environmentally friendly nature. However, other

supercritical fluids like water, ethane, and propane can also be utilized based on the specific requirements of the process [105].

One of the key advantages of supercritical fluid-based technology is its ability to extract valuable compounds from natural sources with high efficiency [106]. Supercritical fluid extraction (SFE) has been extensively used in industries such as pharmaceuticals, nutraceuticals, and food processing to extract essential oils, flavors, fragrances, and bioactive compounds from various botanical sources [107, 108]. The process offers several benefits over traditional methods, including reduced solvent consumption, minimal thermal degradation, and the ability to selectively extract specific components.

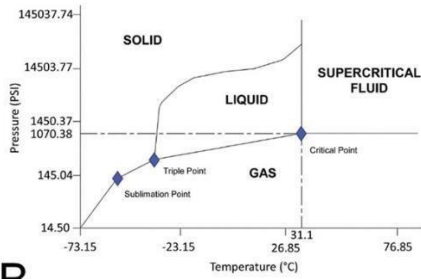
Moreover, supercritical fluid-based technology finds applications in materials science, particularly in the fabrication of nanoparticles and composite materials. Supercritical fluid technology allows precise control over particle size, morphology, and composition, enabling the production of advanced materials with enhanced properties [109, 110].

The supercritical process were designed to controllable with regulation of various parameters during process. The temperature of supercritical state solvents plays a critical role in the supercritical process.

The substance must be heated above its critical temperature to transition into the supercritical state. Higher temperatures generally increase the solubility and diffusivity of substances, affecting extraction efficiency and reaction rates [111]. Pressure is another crucial factor in the supercritical process. The substance must be pressurized above its critical pressure to reach the supercritical state. Increasing the pressure enhances the density and solvating power of the supercritical fluid, impacting its ability to dissolve and interact with other materials [112]. Supercritical fluid solvent should be considered depends on the materials or target aim for their direct chemical reaction that trigger the extraction and dissolving. Carbon dioxide (CO₂) is the most commonly used raw material for extraction as described above. And other supercritical fluids like water, ethane, and propane may be selected based on their specific properties and compatibility with the target compounds [113]. The flow rate of the supercritical fluid through the system affects the efficiency of the process. Appropriate flow rates ensure sufficient contact between the supercritical fluid and the target substances, facilitating extraction, reaction, or enough particle formation [114]. In some cases, co-solvents can be added to the supercritical fluid to enhance solubility and improve the extraction or reaction efficiency. These co-solvents can modify the

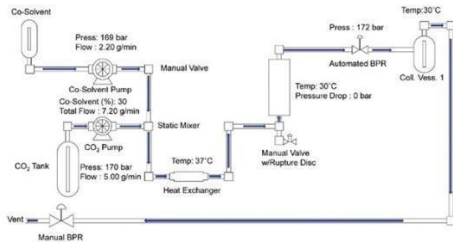
properties of the supercritical fluid, such as its polarity and viscosity, to better match the requirements of the process [115]. Not only depend on machinery compartment, but properties of the target compounds also one of the most important coefficients of super critical process, such as their solubility, volatility, and stability, should be considered when designing a supercritical process. Understanding the behavior of the target compounds in supercritical conditions helps optimize the process parameters for efficient extraction or reaction.

A



Factors	Area of action
Temperature	Over critical point
Pressure	Over critical point and depressurization
Sample condition	Particleization, polarity
Solvent composition	Co-solvent %(v/v), density

B



C

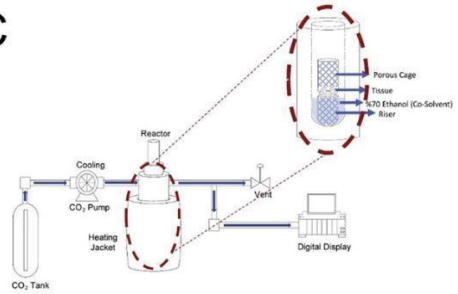


Figure 2.6 Basic information of super critical flow process. (A) Description of supercritical state of carbon dioxide and parameters of supercritical flow process which controlled by purpose. (B), (C) Flow charts of supercritical process.

Super critical fluid process has been used for decellularization protocol to minimize protein degradation and extra ECM loss that occurred when tissue decellularization were processed with detergent based methods. The principle of decellularization with supercritical fluid with CO₂ quite simple to flush out generic material by using their solubility. This technology incorporated supercritical state of CO₂ which have both features of liquid and gas states. This multiple characteristics of supercritical state CO₂ enable to change the CO₂ features to having high solubility like a liquid and deep infiltration to microstructure of samples like a gas state [116]. Furthermore, the CO₂ have non polarized characteristics which stand for having higher solubility to hydrophobic molecules more than hydrophilic polymers. This selective solubility makes the efficient decellularization process that can eliminate cell membrane, phospholipid bilayer, and expose the generic material to outer environments easily [117]. However, the cell membrane comprised of many types of phosphor molecules and glycoproteins, giant polar proteins, cholesterol that have complex polar characteristics also that hard to dissolved in non-polar solvents [118]. These complex compounds need other solutions that support supercritical fluid extraction process which can solubilize polar materials that hardly soluble in CO₂. For this

reason, in supercritical decellularization process the ethanol, water like polar reagents used as co solvent in process for more efficient elimination of generic materials from tissues [119].

Supercritical process for decellularization can be amended with solvent composition and pressure, temperature and even with treating times like generic application conditions [120, 121]. The controllable parameters should be increased depend on tissue state like wet/dry, size, original mechanical property of samples. The higher mechanical strength of tissue and larger size of tissue particles make the supercritical process harsher and taking more time to proceed ideal decellularization protocol. There were some experimental results that showed the efficiency of supercritical process increased with common pre-treatment before supercritical decellularization process with enzymatic solution, acid/base solutions even with detergent chemicals [121, 122]. Those pre-conditioning made tissues softer and easier to penetrate and accessible of supercritical state of CO₂ and co solvents for optimal decellularization process. The various conditions of supercritical fluid-based decellularization processes were described (Table 2.2).

Table 2.2 Supercritical fluid based decellularization with various parameter conditions and tissue sources.

Tissue source	Solvent composition	Process time (hours)	Pressure, temperature/ Pre -treatment condition
Optic nerve (bovine)	70%(v/v) ethanol, CO ₂	4hours	1071.8 psi, 38-40 °C / 10 mM Tris, 0.5% EDTA solution (pH 8)
Myocardium (bovine)	70%(v/v) ethanol, CO ₂	1hours	2500 psi, 37 °C/ 1.5 M NaCl in 0.05 M Tris-HCl (pH 7.6)
Cartilage (porcine)	75%(v/v) ethanol, CO ₂	0.6hours	100-350bar/ -
Cornea, aorta (bovine)	70%(v/v) ethanol, CO ₂	1hours	2500, 4500 psi, 37 °C/ Isotonic saline solution (Polifarma, Turkey)
Aortic leaf, wall (ovine)	95%(v/v) ethanol, CO ₂	1hours, 3hours	10,15,25 MPa, 37 °C/ 1 M NaOH, 0.8 M Na ₂ SO ₄ , 0.5%(w/v) SDS, SD
Adipose tissue (porcine)	CO ₂	0.5hours	10 MPa-30 MPa, 30-40 °C/ 0.05% of Trypsin-EDTA and 0.032 M of Deoxycholic acid
Cartilage (bovine), skin (human), tendon (horse)	CO ₂	1hours	25MPa/ LS-54, 0.05% Trypsin-EDTA, hypertonic buffer solution
Bone (bovine)	CO ₂	0.5hours	30 MPa, 50 °C/ EDTA 0.1%(v/v), 0.1%(W/V) SDS
Aorta (porcine)	CO ₂ , Pure ethanol, water, Ls-54	1hours	10.3,27.6 MPa, 10-37 °C/ 0.1 % (v/v) SDS, 0.2 mg/ml DNase, 0.02 mg/ml RNase

CHAPTER THREE:

FABRICATION OF NGF RELEASING CRYOGEL WITH BRAIN DECELLULARIZED ECM FOR TRAUMATIC BRAIN INJURY TREATMENT

3.1 Introduction

Traumatic brain injury (TBI) is a disruption in normal brain function caused by sudden traumatic damage resulting in tissue destruction and cerebral parenchymal damage [123]. TBI, arising from traumatic events or external forces, leads to critical physiological dysfunction, including acute contusions, hematoma, and axonal injury [124]. These severe symptoms induce secondary brain damage, characterized by vascular disruption and excitotoxicity, ultimately leading to tissue necrosis [125]. Regenerating neuronal tissue in the damaged area represents the most challenging aspect of TBI treatment. Instead of the desired volumetric regeneration of brain tissue, consisting of highly interconnected neuronal and glial cells, TBI leads to the formation of fibrotic scar tissue, which impedes proper neuron cell growth. Fibrotic tissue formation in the

central nervous system (CNS) is triggered by vessel disruption, allowing infiltration of hemostasis-related proteins and other hematogenous cells [126]. Hence, we hypothesize that implanting a three-dimensional (3D) structure that mimics the extracellular matrix (ECM) composition of brain tissue holds promise as a strategy to promote neural tissue regeneration while preventing fibrotic tissue infiltration at the injury site. This biomimetic 3D structure aims to facilitate the formation of functional neural tissue by providing mechanical support, spatial guidance, and biochemical cues that emulate the natural brain tissue environment.

Recapitulating 3D microenvironments in traumatic brain injury (TBI) has been implemented using brain-mimetic biomaterials in conjunction with neuronal recruitment. These approaches have shown potential to provide structural neuron binding moieties and reconstruct ECM microenvironments. Recently, decellularization of native ECM (dECM) has emerged as a promising strategy for regenerating damaged tissues. The process of tissue decellularization eliminates cellular and genetic components, such as cells, DNA, and RNA, using chemicals (acidic, basic, detergents) or physical stimulation. This preserves the original

ECM components and functional protein extracts derived from native tissues [127]. The utilization of brain dECM has demonstrated characteristics compatible with neuronal cells, promoting selective differentiation of neuronal stem cells by providing cell binding ECM basement and cell reactive proteins in dECM [128]. Furthermore, extracted dECM materials have been applied in tissue and organ regeneration using thermally cross-linked hydrogel forms to address tissue loss and degenerative neuronal diseases [62, 129, 130]. However, the current thermal cross-linking method for pure brain dECM still requires further investigation to achieve a more practical state. This involves improving structural strength, enhancing cell infiltration ratio, and optimizing the concentration of biological supplements due to limitations in ECM availability, preservation of functional protein ratios, and inadequate structural enforcement and homogeneity for long-term applications [131].

Cryogel, characterized by its high porosity and interconnectivity resulting from chemical crosslinking, holds potential for achieving a high cell infiltration ratio and providing robust reinforcement when implanted in tissue environments [132]. The substantial cell infiltration

into the porous structure can promote increased cellular activity and facilitate cell-cell interactions, thereby accelerating tissue formation. Moreover, the 3D high porous structure of cryogels lends itself to drug-delivery strategies, allowing for the incorporation of drug-dissolved liquid solutions to achieve controlled release profiles [133]. Heparin sulfate, a member of the glycosaminoglycan family found in the ECM, has been extensively employed in the fabrication of protein-releasing 3D scaffolds due to its ability to bind proteins based on charge interactions, enabling control over the release amount from the material [134]. In practical applications, heparin-incorporated cryogels have been utilized in drug sustain release applications involving neuron growth factor (NGF) to induce neuronal re-connections. We hypothesize that brain dECM-based cryogels incorporated with heparin sulfate can provide structural and biochemical cues to regenerate functional volumetric brain tissue.

In this study, decellularized ECM and heparin sulfate based cryogels were fabricated with NGF encapsulated form for regeneration of neuronal tissues in the brain TBI model. The cryogels were capable of sustain releasing of NGF and providing brain tissue like ECM for formal neural tissue formations. The neuronal cell outgrowth was controlled

with NGF that released from cryogels by regulating heparin concentrations and polymer network density. In animal model, the NGF releasing cryogel showed host tissue reformation with accelerated neuronal tissue regeneration in defect areas and increased neuronal cell infiltration to cryogel scaffold.

3.2 Materials and method

3.2.1 Decellularization of brain tissue

Brains from bovine were purchased from domestic slaughterhouse. The brain tissue was washed with deionized water and incubated for 24 hrs in 4°C. After that brain tissues were minced in 2x2x2 cm³ size and incubated with trypsin-EDTA (0.025%) for 1h 30min in 37°C. after the trypsin-EDTA solution treatment the brain tissues were incubated with 0.3%(w/v) sodium dodecyl sulfate (SDS) solutions for 48 hours in room temperature. The SDS solution changed every 24 hours. Wash two times with deionized water, the brain tissues were stirred in 0.1%(v/v) peracetic acid in 4%(v/v) ethanol solutions. After that the decellularized brain were freeze dried. The brain decellularized ECM (dECM) solutions

were prepared by dissolving for 24hrs with pepsin(sigma) digestion as 10:1 weight ratio to the ECM.

3.2.2 Paraffin sectioning of brain tissues

Native brain tissues and decellularized tissues were fixed with Paraformaldehyde (4 % w/v) at 4°C for 24 hrs. Fixed tissues were transferred to ethanol solution (50 % v/v) at 25°C for 30min. The brain tissues transferred to higher concentration of ethanol solutions for 20min (70, 90, 100 %, 100% v/v). After that the brain tissues were transferred to xylene solution twice for 1hrs. And the brain tissues were incubated 60 °C in paraffin solutions for 24 hrs. The paraffinized brain tissue blocks were transferred into microtome (Leica) and sectioned for 10 µm thickness.

3.2.2.1 H&E staining of brain tissues

Dehydrated brain tissues were rehydrated with two xylene solution change and transferred to gradation of ethanol solution change (100%, 100%, 90%, 70%, 50% v/v) for 10 min. After that tissue slices transferred to deionized water. Washed tissue slides were incubated with hematoxylin solution (Vector) for 1min 30s. The tissue slides were

dipped in acidic ethanol (0.3% v/v HCl in ethanol solution) and washed in running tap water for 20 min. Tissue slides were stained with eosin Y (0.25% v/v) in acetic acid (0.2% v/v). Stained tissue slides were dehydrated with changes of different concentrations of alcohols (75%, 95%, 100 % v/v) and xylene solutions. And dehydrated slides were mounted with DPX mounting solutions.

3.2.2.2 Trichrome staining of brain tissues

Trichrome stain protocol followed by manufacturers protocol (abcam, ab150686). Briefly, rehydrated brain tissues were immersed in purified water 3 times for 5 minutes. The tissue slides were incubated in preheated Bouin's Fluid for 60min and cool for 10 min. After rinsing with purified water, tissue slides were incubated in weigert's Iron solutions for 5min. Tissue slides were washed with purified water. And incubated with Biebrich Scarlet/ Acid Fuchsin solutions for 15 min. Tissue slides were washed with purified water. And tissue slides were differentiated in phosphomolybdic/ Phosphotungstic acid solution for 15 min. Without rinsing, tissue slides were incubated in Aniline Blue solution for 5 min. After rinsing with purified water, tissue slides were

incubated in acetic acid solution (1% v/v) for 5min. Stained tissue slides were dehydrated with changes of alcohols (75%, 95%, 100 % v/v) and xylene solutions. And dehydrated slides were mounted with DPX mounting solutions.

3.2.2.3 Safranin-O staining

Rehydrated tissues were stained with hematoxylin for 1 min and incubated in running tap water for 30min. and tissue slices were stained 0.05%(w/v) fast green solution for 5 min. After rinsed with 1% (v/v) acetic acid the nerve slices were stained with 0.1% of safranin -O solution for 5 min. Stained tissue slices were dehydrated with different concentrations of alcohols (75%, 95%, 100 % v/v) and xylene solutions. Slides were mounted with DPX solutions.

3.2.2.4 DNA quantification in brain tissues

Papain enzyme solutions (3% v/v, Worthington 3120) were prepared with PBE-cys buffer (100mM Phosphate, 10mM EDTA, 0.10M L-cysteine, pH 6.5). Brain tissues were incubated at 60°C for 24hrs with diluted papain enzyme solutions until tissues were fully digested. DNA quantification of brain tissues were followed by manufactures protocol Quant-iT Pico Green dsDNA Assay kits (Invitrogen). Briefly, Pico green dyes were 20-fold diluted in TE buffer (10mM Tris-HCL, 1mM EDTA,

pH 7.5) and mixed with digested tissue solution (1:1 volume ratios). Fluorescence of dyes were measured with microplate reader (Tecan) at excitation 480 nm, emission 520nm wavelength. Standard line for calculation of relate DNA contents in brain tissue were made with Quant-iT Pico Green dsDNA stock.

3.2.2.5 Hydroxy proline quantification in brain tissues

Papain enzyme solutions (3% w/v) were prepared with PBE-cys buffer (100mM Phosphate, 10mM EDTA, 0.10M L-cysteine, pH 6.5). The prepared brain tissue solutions were hydrolyzed with 10N sodium hydroxide in 100°C for 16hrs (total 1%(w/v) dECM). After that, 100µl of chloramine T solution (0.056M in 50% v/v isopropanol) were transferred to 300ul of hydrolyzed sample and oxidation processes were allowed for 25 min in room temperature. After that 100µl of echrlich's aldehyde reagent (1M p-dimethylaminobenzal aldehyde in 30% HCl / 70% isopropanol) was added to each sample and incubated at 60°C for 20 min. Absorbance were measured by microplate reader (Tecan) at 550nm wavelength. Standard line for calculation of relate Hydroxy proline contents in brain tissue were made with hydroxy proline. The hydroxy proline solution samples were processed with same conditions of assay protocols. All reagents of this protocol were diluted in acetate citrate

buffer (0.5mM sodium acetate, 0.1mM citric acid, 0.1mM acetic acid, 0.5mM NaCl, pH 6.5).

3.2.2.6 DMMB assays for quantifications of sGAG

Papain enzyme solutions (3% w/v, Worthington 3120) were prepared with PBE-cys buffer (100mM Phosphate, 10mM EDTA, 0.10M L-cysteine, pH 6.5). Brain tissues were digested at 60°C for 24hrs with diluted papain enzyme solutions. And the tissue solutions were transferred 96-well plate (SPL life sciences) after then DMMB solutions (40.5 mM glycine, 40.5mM NaCl, 50µM DMMB, pH 3.5) were transferred to well plate and mixed with tissue solutions (1:1 volume ratios). Absorbance were measured by microplate reader (Tecan) at 525nm wavelength. Standard line for calculation of relate sGAG contents in brain tissue were made with chondroitin sulfate sodium salt.

3.2.3 Characterization of brain dECM and heparin derived cryogels

3.2.3.1 Preparation of brain dECM and heparin derived cryogel

PDMS mold were prepared for cryogel fabrication by mixing pre-PDMS solution and linker with 10 :1 weight ratio. After 4hour crosslinking in 60°C, the PDMS mold were punched with 6mm diameter biopsy punch. Brain derived decellularized ECM(B-dECM) pre-cryogel solution were prepared by dissolving B-dECM in 0.1M hydrochloric acid to 1%, 2% (w/v) concentration with 10:1 weight ratio of pepsin to tissue mass. Heparin sulfate were dissolved to 0.2%, 0.6%, 1%(w/v) concentration in deionized water. B-dECM solution and heparin sulfate solution were mixed by 1:1 ratio. And DMTMM were also dissolved to 30mM concentration in pre-cryogel solution for cross-linking. Pre-cryogel solution were cross-linked in -20°C for 24hrs.

3.2.3.2 Reaction efficiency calculation

The crosslinked cryogel incubated with 300ul deionized water. The 100ul of deionized water collected and the dECM contents and heparin sulfate were measured with BCA (thermo fisher scientific kit. 23227) and DMMB assay to calculate unreacted polymers after cross linking.

3.2.3.3 FTIR analysis of cryogel

The cryogel were fabricated by 6mm diameter, 2mm height size with PDMS mold and freeze dried before analysis. Chemical component of cross-linking mechanism was characterized with FTIR (PerkinElmer Frontier). All samples were scanned 64times with resolution of 8cm^{-1} and wavenumber range 500 to 4000 cm^{-1} . And brain dECM and heparin sulfate were also characterized with same conditions for control.

3.2.3.4 Microstructure analysis of cryogel

For scanning electron microscopic (SEM) images, each cryogel was freeze dried before imaging. The cryogels were fixed with carbon tape onto the stubs and coated with platinum scatter. The microstructure of the cryogels were imaged at 10 kV with a microscope (JSM-7800F Prime, JEOL Ltd, Japan). The area of pores was quantified by ImageJ.

3.2.3.5 Swelling ratio calculation of cryogel

First, weight of lyophilized cryogels were weighed (W_d) and after swelled for 24 hrs with deionized water the swelled cryogel were weighed (W_s). The swelling ratios cryogels were calculated by the following equation: $\text{Swelling ratio} = (W_s - W_d)/W_d$.

3.2.4 Mechanical property characterization of cryogel

3.2.4.1 Compressive modulus measurements of cryogels

The cryogel were fabricated by 6mm diameter, 2mm height size with PDMS mold. Elastic modulus was characterized with using a universal-testing-machine (Shimadzu EZ-SX, Japan). Compression test were performed with 1mm/min velocity of zig and the elastic modulus were calculated by slope measuring of strain-stress curve.

3.2.4.2 Rheological property characterization of cryogels

The rheological characteristics of cryogels were tested in anton parr using rheometer (MCR 302, Measuring cell: P-PTD & H-PTD 200, Measuring System: PP 25, Anton-Paar, Austria). Briefly, all the cryogels were prepared in 8mm diameter and 2.5mm thickness. Amplitude sweep test was conducted with 0.01~100% range of amplitude with constant 1Hz frequency. Frequency sweep test were conducted with 0.01~10Hz with 0.2% constant strain. Continuous step strain tests were conducted by alternating 0.2% and 25% of strain to cryogels for 50s each. This experiment conducted for 250s total.

3.2.4.3 Cryogel injectability test

All the cryogels were fabricated in 6mm diameter 2mm thickness. The injection test of cryogels was proceeded by 17G needle injection to 60pi dish. The remaining weight of cryogels were calculated after injection.

3.2.5 Heparin mediated protein sustain release kinetics measurement.

For the observation of heparin-mediated sustained release of NGF, 30µl of 50 ng/mL NGF solutions (Sigma Aldrich, N2513) were transferred to freeze dried cryogels. After 30 min, 300 µL of PBS was added to the cryogels and the PBS was collected at each time point. The amount of released NGF was measured by NGF Elisa kit assay (My bio source). The BCA release kinetics also characterized with 1mg/ml solution with same volume and incubation time with BCA assay (thermo fisher scientific).

3.2.6 PC12 cells culture and differentiation

3.2.6.1 PC12 differentiation with cryogel encapsulated NGF

PC12 cells were proliferated in 100pi dish for 5days cultured with growth medium (5% fetal bovine serum, 5% v/v horse serum, 1% v/v

penicillin streptomycin). And the PC12 cells transferred to 48 well plates in 30,000 cells per well. The cryogels were fabricated with 8mm diameter and 2mm thickness. 50ul of 50ng/ml NGF solutions were treated and incubated for 30min. After that, cryogels were incubated with PC12 differentiation medium (1% v/v horse serum, 1% v/v penicillin streptomycin) for 3days (30000 cells per well).

3.2.6.2 PC12 culture on the cryogel

The cryogels were prepared in 6mm diameter and 2mm thickness. 50ul of 50ng/ml NGF solutions were treated to cryogel and incubated for 30min and the cryogels were freeze dried. The PC12 cells were seeded to freeze dried cryogel in 250,000 cells per ml densities for 20days. The PC12 cultured on cryogels were imaged with confocal microscope (Zeiss LSM 700).

3.2.6.3 β -3tubluin staining of PC12 cells

The PC12 cells were fixed with 4% (v/v) PFA for 15 min. after that cells were permeabilized with triton X-100 0.3%(v/v). After that, samples were incubated with 5%(v/v) normal goat serum in PBS. The cells incubated with β -3tubluin 1st antibody (abcam,300:1 ab18207) for

24hrs overnight in 4°. The cells then incubated with 2nd antibody (500:1 Alexa fluoro 488 ab150077). The cells were counter stain with DAPI and imaged with confocal microscope (Zeiss LSM 700)

3.2.7 Regeneration of TBI animal model with cryogel

3.2.7.1 Brain defect model design and cryogel application in vivo

To remove soft tissue of brain cortex of mouse, the 4mm diameter cranial defects were made before brain tissue removal with micro drill. And 3mm diameter, 3mm depth cortex defects were made with 3mm punch. The removed tissues were weighed to confirm reproducibility of brain defect model. The De1.0HS0.3 cryogel groups were chosen to apply to brain defect model and 3mm diameter and 3mm depth cryogels were implanted to the brain defect. The 20ul of 50ng/ml NGF solutions were treated to cryogels before apply to *in vivo* with same method described above. And the samples were collected in 1week, 2weeks, 4weeks time points.

3.2.7.2 Fluorescence staining of brain tissues

The brain tissues were dehydrated with same method described above and sectioned in 10um thickness. The samples were autoclaved in 97° with citrate buffer (pH 6.0) for 1min 30s to retrieve antigens and permeabilized with triton X-100 0.3%(v/v). after that, samples were

incubated with 5%(v/v) normal goat serum in triton X-100 0.1%(v/v). the samples were incubated with 1st antibody for 24hrs in 4° and incubated 2nd antibody for 1hrs. the tissue samples were mounted with DAPI mount medium and imaged. 1st antibody : anti collagen III from rabbit (abcam, 300:1, ab7778), anti collagen IV from rabbit (abcam, 300:1, ab6586) anti GLUT-1 from rabbit (abcam, 300:1,epr3915), anti PDGFR-β from rabbit(abcam, 300:1,Y92),anti-double cortin from rabbit (abcam, 300:1,ab18723), anti-MAP-2 from rabbit (abcam, 10000:1,EPR19691), anti GFAP from mouse (abcam, 500:1, ab279289), anti Iba1 from rabbit (abcam, 300:1, ab5076). 2nd antibody (500:1 alexa fluoro 488, 594 ab150077, ab150080).

3.2.8 Statistics analysis

All data were processed with Graph pad prism 5.0 and tow-tailed t-test and one-way ANOVA statistics calculation were performed. P-value = * p < 0.05, ** p < 0.01, *** p < 0.005. # p < 0.05, ## p < 0.01, ### p < 0.005. * statistics symbol compared control group versus experimental group. # statistics symbol compared scaffold only group

versus scaffold + growth NGF group.

3.3 Results

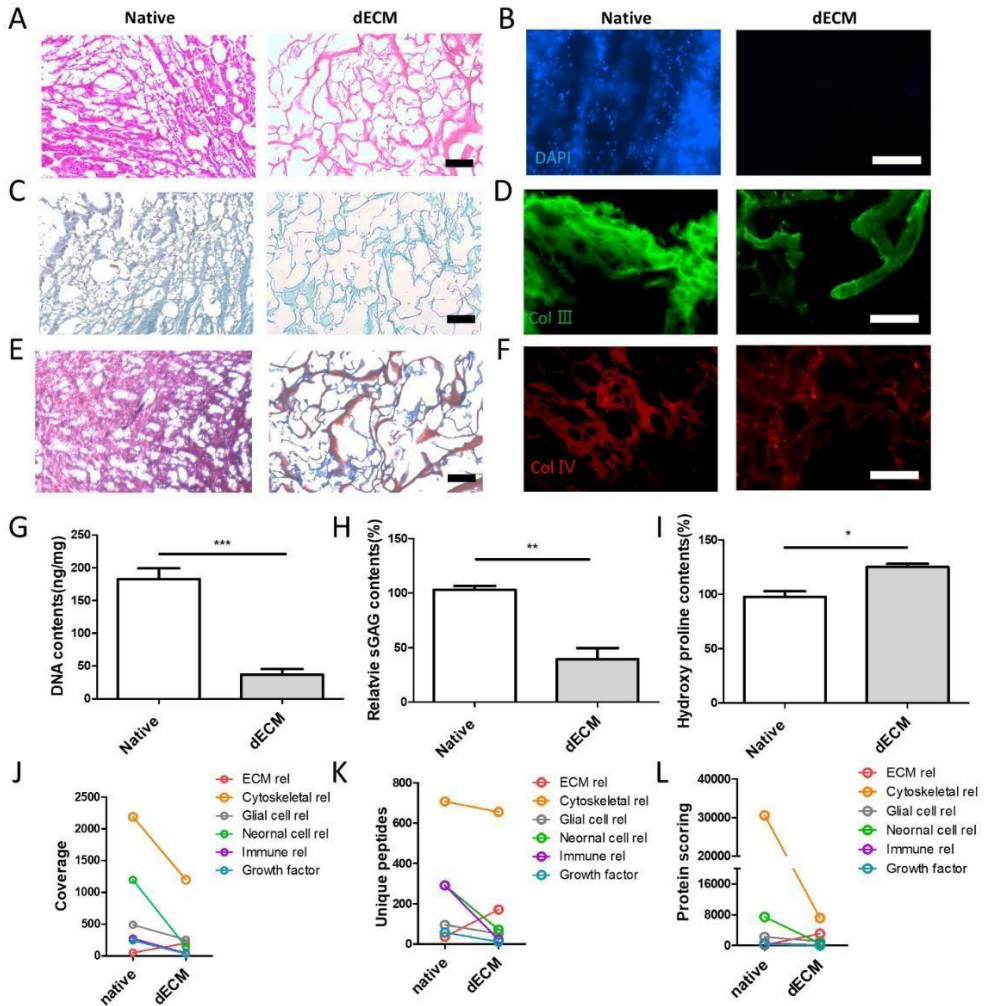


Figure 3.1 ECM structure analysis and quantification in native and decellularized brain tissues (dECM). (A) Hematoxylin & Eosin staining of native and dECM tissues. (B) DAPI staining of native and dECM tissues to confirm DNA elimination after decellularization. (C) Safranin-O staining of native and dECM tissues for staining of sGAG in tissues. (D) Collagen type III fluorescence image of native and dECM tissues. (E) MCT staining of native and dECM tissues. (F) Collagen type IV fluorescence image of native and dECM tissues (All histologic images scale bar=100μm). (G) DNA contents quantification in native and dECM tissues. (H) DMMB assay for sGAG quantification of native and dECM tissues. (I) Hydroxy proline quantification of native and dECM to quantify relative collagen contents in tissues (J), (K), (L) Proteomic analysis of native and dECM. Error bars indicate SD. P-value = * $p < 0.05$, ** $p < 0.01$, *** $p < 0.005$. # $p < 0.05$, ## $p < 0.01$, ### $p < 0.005$.

3.3.1 Decellularization of the brain tissue and component characterization native tissue and brain dECM.

The structural characteristics and ECM composition of the decellularized ECM were assessed using histological evaluation and quantitative assays (Figure 3.1). The preservation of polysaccharides and proteins in the decellularized tissue after the chemical process was compared to native tissues. The effectiveness of the decellularization protocol in removing cellular components was confirmed through H&E staining and DAPI nucleus staining (Figure 3.1 A, B). Quantification of DNA concentration revealed a significant reduction in DNA content after the decellularization protocol (Figure 3.1 G; 23.55 ± 12.08 ng/mg). Measurement of sGAG content using the DMMB assay demonstrated a 50% decrease compared to native tissues (Figure 3.1 H). Safranin-O staining indicated a reduction in red-stained sGAG areas in the decellularized ECM tissues compared to native tissues (Figure 3.1 E). Fluorescence staining of Col III and Col IV in brain tissues confirmed the preservation of collagen components in the decellularized ECM (Figure 3.1 D, F). Quantification of hydroxyproline, the main amino acid in collagen, showed a relative increase in collagen content after decellularization (native: 103.87 ± 10.37 ; dECM: 136.24 ± 18.26)

(Figure 3.1 I). Proteomic analysis using LC-MS characterized the remaining functional protein components in the dECM (Figure 3.1 J-L). The results indicated the preservation of ECM components and the presence of other cellular and growth factors in soluble form in the dECM.

	De0.5 cryogels			De1.0 cryogels		
Sample name	De0.5HS0.1	De0.5HS0.3	De0.5HS0.5	De1.0HS0.1	De1.0HS0.3	De1.0HS0.5
dECM %(w/v)	0.5	0.5	0.5	1	1	1
Heparan sulfate %(w/v)	0.1	0.3	0.5	0.1	0.3	0.5

Table 3.1 Decellularized ECM and heparin sulfate concentrations in each cryogel group

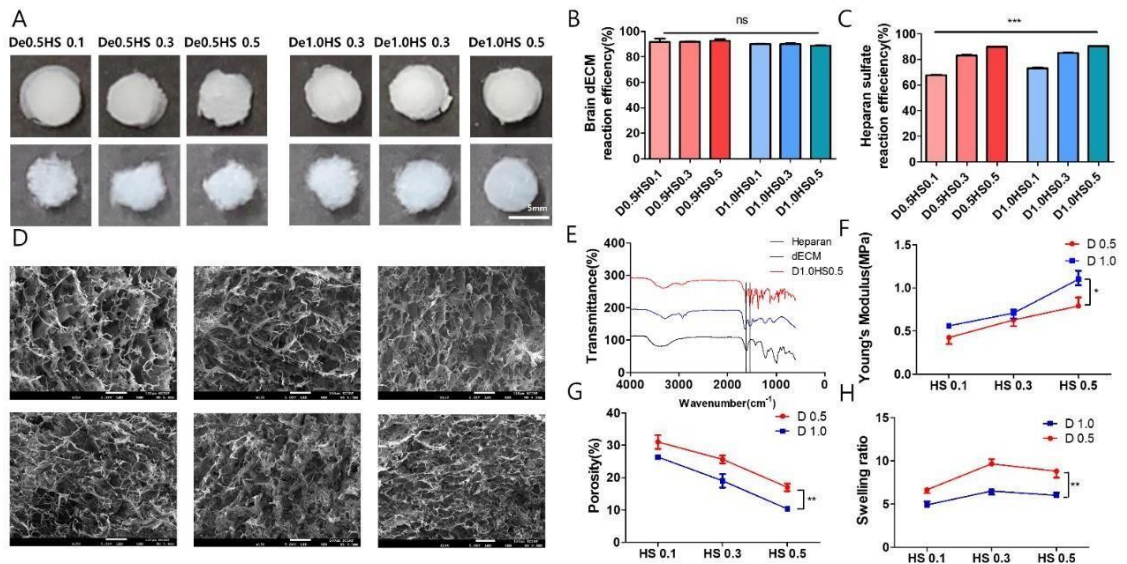


Figure 3. 2 Characterization of cryogel scaffold about crosslinking and microstructure formations. (A) Representative images of the cryogels with various polymer concentrations. (B) Remained dECM quantification after crosslinking process to characterize reaction efficiency of crosslinking system. (C) Remained heparin sulfate quantification after crosslinking process to characterize reaction efficiency of crosslinking system. (D) Microstructure analysis with SEM images of cryogels (E)FT-IR transmittance analysis of cryogels crosslinking. (F) Compressive modulus measurements of the cryogels (G) Porosity characterization of cryogels (H) Swelling ratio measurements of the cryogels. Error bars indicate SD. P-value = * p < 0.05, ** p < 0.01, *** p < 0.005.

3.3.2 Fabrication and characterization of brain dECM based cryogel.

The brain dECM-based cryogel was fabricated using DMTMM chemistry to facilitate the cross-linking of carboxyl acid in heparin sulfate and amine in dECM polymers. A 300 mM DMTMM solution was diluted to a total concentration of 30 mM to achieve homogeneous cross-linking networks in the dECM and heparin mixed solutions (Figure 3.2 A). The different compositions of cryogels were described in Table 3.1. The reaction efficiency of the cryogels was assessed by measuring the unreacted heparin and dECM released from the cryogels after cross-linking. The reaction efficiency of dECM was found to be above 85% in all groups, with no significant difference observed among the six different combinations (Figure 3.2 B; $88 \pm 11.23\%$). The reaction efficiency of heparin sulfate gradually increased with higher concentrations of heparin sulfate in the cryogel, indicating that the DMTMM chemistry was more effective (Figure 3.2 C; De0.5HS0.1: $67 \pm 0.65\%$, De0.5HS0.3: $82 \pm 0.46\%$, De0.5HS0.5: $89 \pm 0.98\%$, De1.0HS0.1: $72 \pm 1.11\%$, De1.0HS0.3: $85 \pm 0.72\%$, De1.0HS0.5: $90 \pm 2.33\%$).

The cross-linking of dECM and heparin was confirmed by FTIR spectra measurements. The FTIR transmittance peaks at around 1550 and 1650 cm^{-1} corresponded to amide II for N-H bending and C=O stretching of amide I, respectively. These peaks in the cryogel FTIR data confirmed that the two different polymers (dECM and heparin sulfate) were fully cross-linked in the DMTMM cross-linking system. The microstructure of the cryogels was characterized using SEM imaging, and their porosity was calculated using ImageJ software (Figure 3.2 D, G). The porosity of the cryogels decreased as the polymer content increased in the cryogel solutions, indicating a higher density of polymer network formation. This trend also influenced the compressive mechanical properties of the cryogels, which increased with higher polymer concentrations (Figure 3.2 F). The swelling ratio data showed that the cryogel group containing HS0.1 had lower swelling ratios compared to cryogels with higher concentrations of heparin (Figure 3.2 H; De0.5HS0.1: 4.95 ± 1.11 , De0.5HS0.3: 9.23 ± 1.53 , De0.5HS0.5: 7.36 ± 1.84 , De1.0HS0.1: 4.98 ± 0.32 , De1.0HS0.3: 6.58 ± 0.82 ,

De1.0HS0.5: $5.33 \pm 1.48\%$).

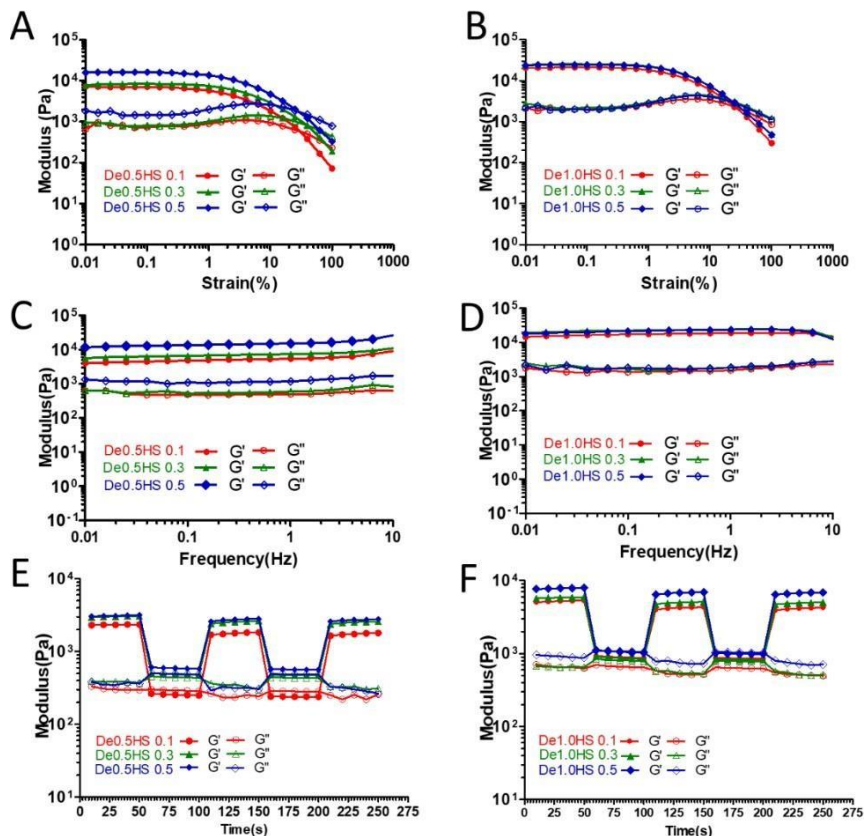


Figure 3.3 Rheological characteristics measurements of the cryogels. (A) Strain sweep test results of the cryogels with 0.5% of dECM and 0.1, 0.3, 0.5 % of heparin sulfate (B) Strain sweep test results of the cryogels with 1% of dECM and 0.1, 0.3, 0.5 % of heparin sulfate (C) Frequency sweep test results of the cryogels with 0.5% of dECM and 0.1, 0.3, 0.5 % of heparin sulfate. (D) Frequency sweep test results of the cryogels with 1% of dECM and of 0.1, 0.3, 0.5 % heparin sulfate (E) Continuous step strain test results of cryogels with 0.5% of dECM and 0.1, 0.3, 0.5 % of heparin sulfate. (F) Continuous step strain test results of cryogels with 1% of dECM and 0.1, 0.3, 0.5 % of heparin sulfate.

3.3.3 Rheological property characterization of fabricated brain dECM derived cryogel

The rheological properties of the cryogels were evaluated using strain sweep, frequency sweep, and continuous strain sweep tests (Figure 3). The rheological moduli (G' : storage modulus, G'' : loss modulus) were measured during each test, with varying variables. The moduli of the cryogels increased with higher concentrations of heparin sulfate in the cryogels. The cryogels containing a total of 1% (w/v) dECM exhibited a similar trend to the 0.5% dECM group, where the modulus increased with increasing heparin polymer concentration. However, there was no distinct increase in modulus observed among the 1% dECM groups, as seen in the 0.5% dECM groups (Figure 3.3 B, D, F). The ultimate strength of the cryogels was recorded at around 40% strain in the 0.5% dECM groups (Figure 3.3 A). The crack points decreased to 25% in the 1% dECM group (Figure 3.3 B). Continuous step strain tests were conducted for each cryogel group to assess their recovery efficiency from consecutive strain changes. Both the 0.5% dECM and 1.0% dECM groups showed changes in modulus without cryogel fractionation when subjected to strain variations during the tests (Figure 3.3 E, F).

3.3.4 Characterization of injectability of fabricated cryogels.

The shape and micro-porous structure sustainability of the cryogels were characterized using physical pressing and injection tests (Figure 3.4). The cryogels maintained their structure in wet environments and under stress-inducing conditions in each group (Figure 3.4 A). The remaining weight ratio after injection of the cryogels using a 17G needle was calculated to assess material stability under shear-thinning stress (Figure 3.4 C). The remaining weight ratios decreased with lower dECM concentrations in the cryogels (De0.5HS0.5: $83.32 \pm 13.95\%$, De1.0HS0.5: $91.32 \pm 6.37\%$). The concentration of heparin also affected the weight loss in the injection test, but the injectability of the cryogels decreased with increased dECM content (De0.5HS0.1: 76.25 ± 22.11 , De0.5HS0.3: 82.77 ± 0.93 , De1.0HS0.1: 90.66 ± 10.84 , De1.0HS0.3: $90.58 \pm 5.82\%$).

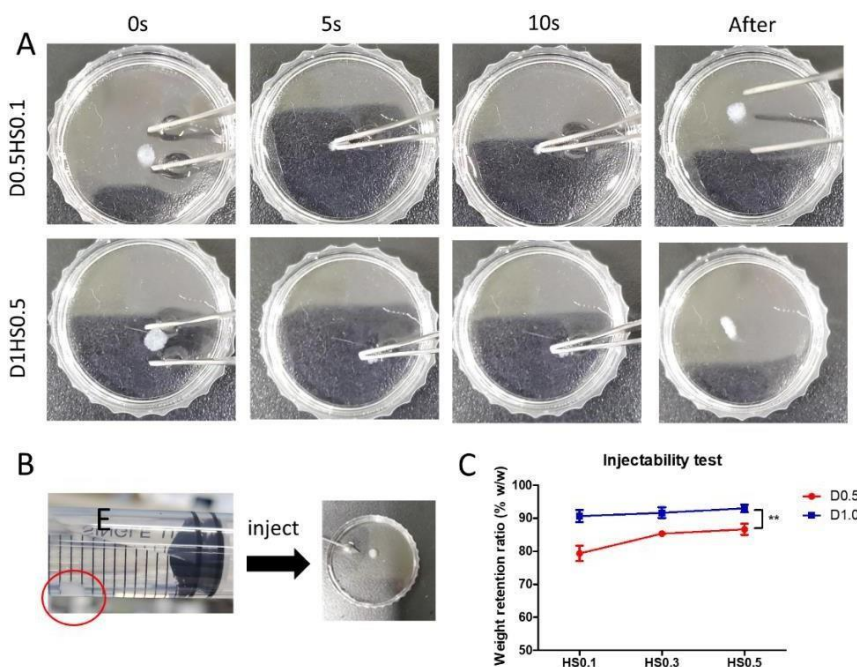


Figure 3.4 Injectability characterization of the cryogels. (A) The representative images for confirmation of shape sustainment of the cryogels versus outer stress. (B) The images of injection capability of the cryogels through 17G needle. (C) The remaining weight ratio of the cryogels after injection versus weight of cryogels before injection. Error bars indicate SD. P-value = * $p < 0.05$, ** $p < 0.01$, *** $p < 0.005$.

.

To investigate the protein-releasing ability of the cryogels, BSA and NGF were encapsulated in the cryogels respectively, and the release of proteins over time was quantified. It was observed that the number of released BSA from the cryogels was directly proportional to the concentration of heparin sulfate (Figure 3.5 A). Additionally, the groups containing 1% (w/v) dECM released more proteins compared to the groups with lower dECM concentrations but the same heparin sulfate concentrations. Based on these findings, the group using 1% (w/v) dECM, which exhibited a higher protein release, was selected for the NGF sustained release test. The results demonstrated that the amount of released NGF increased with higher concentrations of heparin sulfate in the cryogels (Figure 3.5 B).

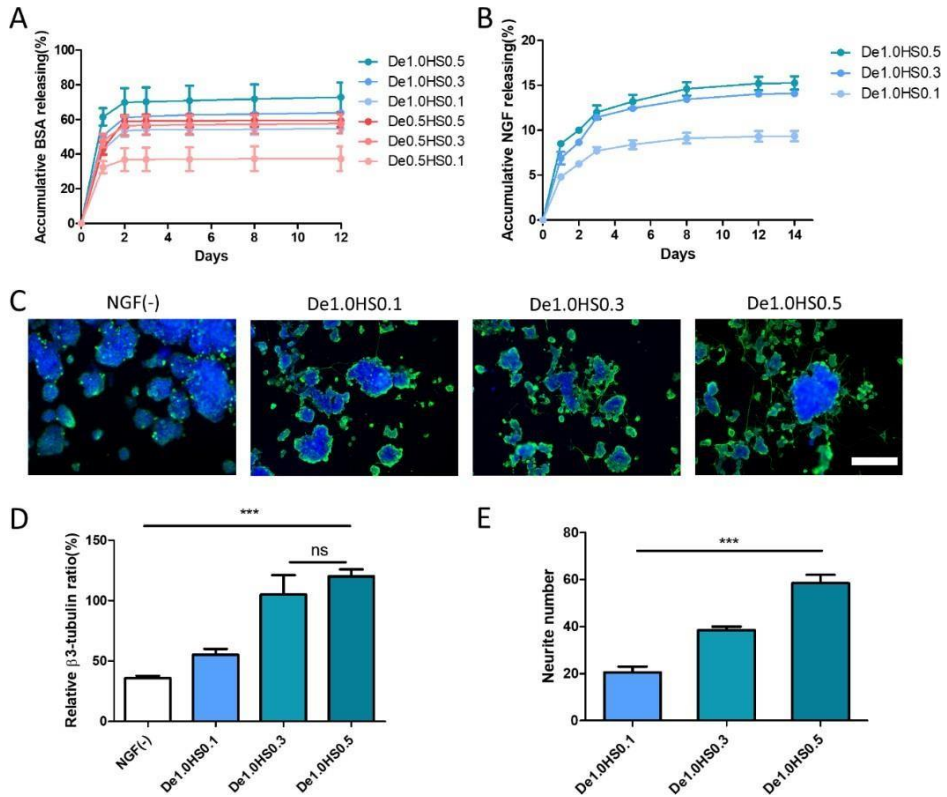


Figure 3.5 Sustain release profile of the proteins and characterization of neuronal cell differentiation ability followed by releasing of NGF from cryogels. (A) Sustain release of BSA amounts measurements for 12 days after cryogel encapsulation. (B) Sustain release of NGF amounts measurements for 14 days after cryogel encapsulation. (C) The representative images of PC12 cells culturing with NGF encapsulated cryogels (D) The β -3 tubulin signal measurements of PC12 cells after differentiation. (E) Characterization of neurite numbers of PC12 cells after differentiation. (scale bar= 100 μ m). Error bars indicate SD. P-value = * $p < 0.05$, ** $p < 0.01$, *** $p < 0.005$. # $p < 0.05$, ## $p < 0.01$, ### $p < 0.005$.

3.3.5 Heparin dependent protein loading efficiency of cryogels and NGF correlated PC12 cell differentiation ratio characterization

The sustained release of NGF from the cryogels directly influenced the differentiation of PC12 cells cultured with the cryogels (Figure 3.5 C). The β -3tubulin signal and neurite outgrowth were enhanced with higher heparin sulfate concentrations, which correlated with the quantity of NGF delivered (Figure 3.5 D: NGF (-) 36.28 ± 3.02 , De1.0HS0.1 53.28 ± 6.55 , De1.0HS0.3 112.18 ± 18.54 , De1.0HS0.5 $121.05\pm 11.37\%$; Figure 5E: De1.0HS0.1 67.11 ± 6.25 , De1.0HS0.3 65 ± 5.18 , De1.0HS0.5 116.42 ± 6.37 μm ; Figure 3.5 E: De1.0HS0.1 21.51 ± 3.42 , De1.0HS0.3 38.75 ± 1.26 , De1.0HS0.5 58.06 ± 3.09 neurite numbers).

The sustained release ability of the cryogels, attributed to the presence of heparin sulfate, increased proportionally with the concentration of heparin. This indicates that precise control of protein delivery can be achieved by regulating the heparin sulfate content in the scaffolds. Furthermore, the encapsulated NGF in the cryogels maintained its active state during the cell culture period, even after direct contact with charged materials and dECM proteins in the cryogels. In order to identify the most suitable combination for culturing adherent cells and

achieving sustained release of NGF from the cryogels, PC12 cells were cultured and differentiated in NGF-encapsulated cryogels. This experiment focus about characterization of cell differentiation ratio increase depends on NGF releasing and remaining amounts. In addition, the charge derived neuronal outgrowth obstruction also reflected. The results revealed that cells cultured in the De1.0HS0.3 group exhibited better differentiation compared to the other two groups (Figure 3.6 A: De1.0HS0.1, De1.0HS0.5). The De1.0HS0.3 group showed the longest neurites and strong β -3tubulin signals in the culture environment (Figure 3.6 F: De1.0HS0.1: $10.52 \pm 5.29 \mu\text{m}$, De1.0HS0.3: $97.51 \pm 14.35 \mu\text{m}$, De1.0HS0.5: $47.22 \pm 8.06 \mu\text{m}$).

3.3.6 PC12 culture and differentiation on the NGF loaded cryogels

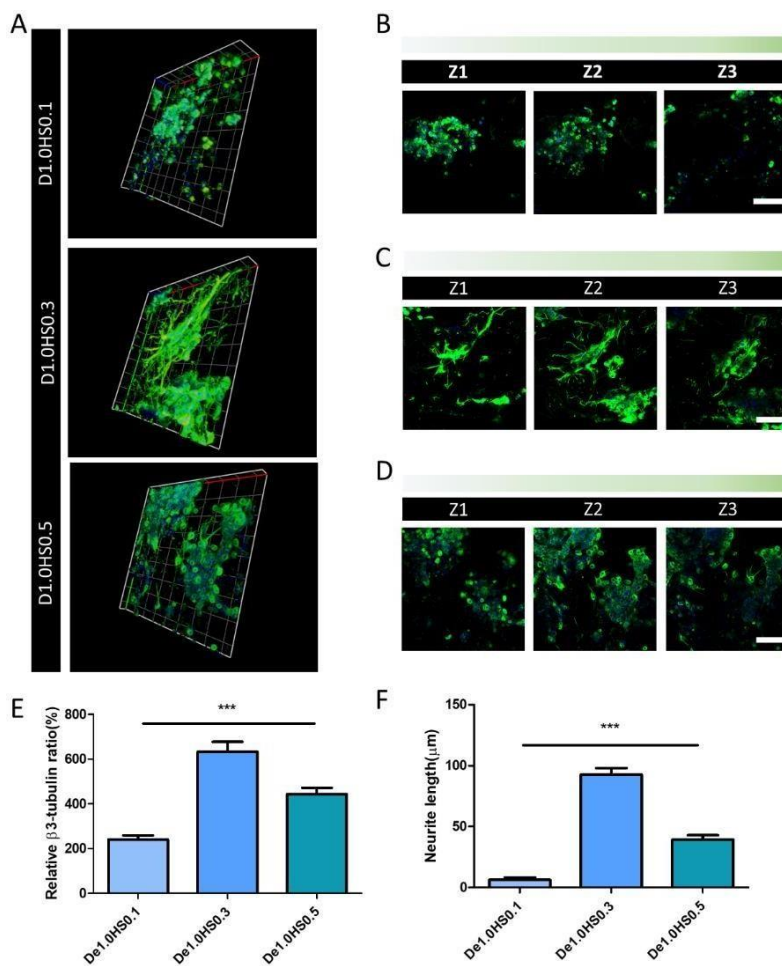


Figure 3.6 3D culture of PC12 cells on NGF encapsulated cryogels for 21 days (A) Representative images of differentiated PC12 cells with NGF encapsulated cryogels (B) Representative Z-stack images of PC12 cells on De1.0HS0.1 cryogel (C) Representative Z-stack images of PC12 cells on De1.0HS0.3 cryogel (D) Representative Z-stack images of PC12 cells on De1.0HS0.5 cryogel (E) The β -3 tubulin signal measurements of PC 12 cells on each cryogel groups (F) Axon length measurements of PC12 cells on each cryogel groups. (scale bar = 100 μ m) Error bars indicate SD. P-value = * p < 0.05, ** p < 0.01, *** p < 0.005. # p < 0.05, ## p < 0.01, ### p < 0.005.

3.3.7 *In vivo* application of cryogel (De1.0HS0.3) and characterization of vessel formation

Subsequently, to confirm the neuronal tissue regeneration ability of the cryogel, the fabricated cryogel was implanted into a mouse brain model of traumatic brain injury (TBI). This *in vivo* characterization procedure focused on maintaining the blood-brain barrier (BBB) structure after stroke and activating the immune response in the early phase of TBI. Furthermore, the formation of neuronal tissue in the tissue defect and the infiltration of neuron cells into the cryogel area were investigated over time following the release of NGF and direct supply of porous ECM. Tissue defects with a diameter and depth of 3 mm were created in the brain tissues, and a cryogel from the De1.0HS0.3 group was transplanted into the defects (Figure 3.7 A). The cortical areas of the brain tissue were removed, and the reproducibility of the removal process was confirmed by weighing the removed tissue from the rodent brain (Figure 3.7 B).

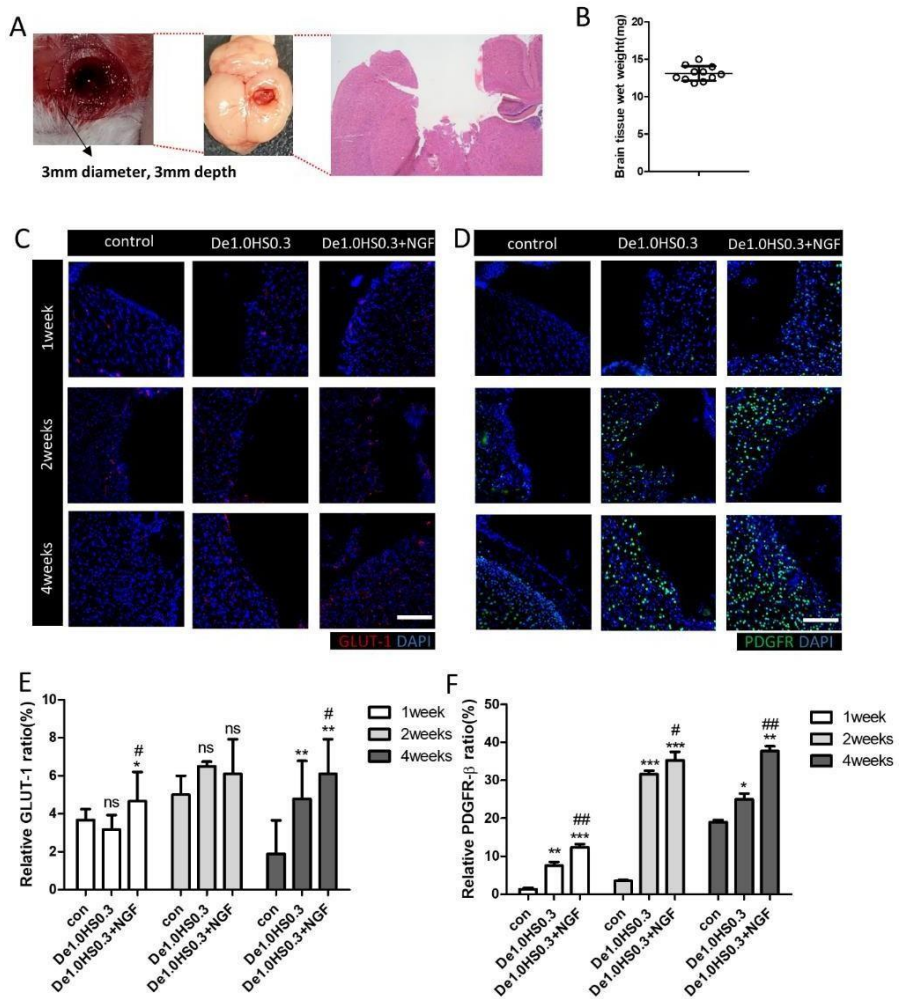


Figure 3.7 In vivo brain defect model development and assessments of vascularization of brain tissues. (A) Brain defect model characterization with macro images and staining. (B) Measurement of weight of removed brain tissues. (C) Representative fluorescent images of GLUT-1 in brain tissues (D) Representative fluorescent images of PDGFR in brain tissues. (E) Relative GLUT-1 signal measurements on brain tissues (F) Relative PDGFR signal measurements on brain tissues. (control : no treatment, De1.0HS0.3 : cyrogel only De1.0HS0.3 + NGF : NGF encapsulated cyrogel treatments, scale bar = 100 μ m). Error bars indicate SD. P-value = * $p < 0.05$, ** $p < 0.01$, *** $p < 0.005$. # $p < 0.05$, ## $p < 0.01$, ### $p < 0.005$.

At first, we examined the response of immune cells in the brain to the implanted De1.0HS0.3 using Iba-1 staining. We confirmed that Iba-1 was highly expressed around the implanted De1.0HS0.3 in the early phase of implantation. The Iba microglia signals decreased over time, and no significant difference in signals was found with NGF encapsulation in the scaffold (Sup Figure 3.2). (Iba-1 at 1 week: De1.0HS0.3: 38.33 ± 15.22 , De1.0HS0.3 +NGF: 32.38 ± 6.25). (Iba-1 at 4 weeks: De1.0HS0.3: 15.13 ± 4.12 , De1.0HS0.3 +NGF: 13.28 ± 6.85).

To determine whether the initial tissue regeneration was influenced by the NGF-releasing dECM scaffold, the expression of GLUT-1 and PDGFR in the tissue was evaluated using fluorescent immunostaining. The results showed that the expression of GLUT-1 increased in the group where the NGF-releasing scaffolds were implanted compared to the control group and the De1.0HS0.3-only group at week 1 (Figure 3.7 E: con: 4.03 ± 1.58 , De1.0HS0.3: 3.88 ± 1.82 , De1.0HS0.3 +NGF: 5.75 ± 2.74). This trend was maintained after 4 weeks, and it was also observed that vascular recovery occurred in the De1.0HS0.3 group compared to the control group that did not receive any treatment (Figure 3.7 E: con: 3.23 ± 2.28 , De1.0HS0.3: 6.18 ± 3.55 , De1.0HS0.3 +NGF:

7.78±3.04). Similarly, the expression of PDGFR increased in the same manner at week 4 (Figure 3.7 F: con: 19.88±1.33, De1.0HS0.3: 26.54±7.17, De1.0HS0.3 +NGF: 37.91±11.42) as observed in the GLUT-1 signal results.

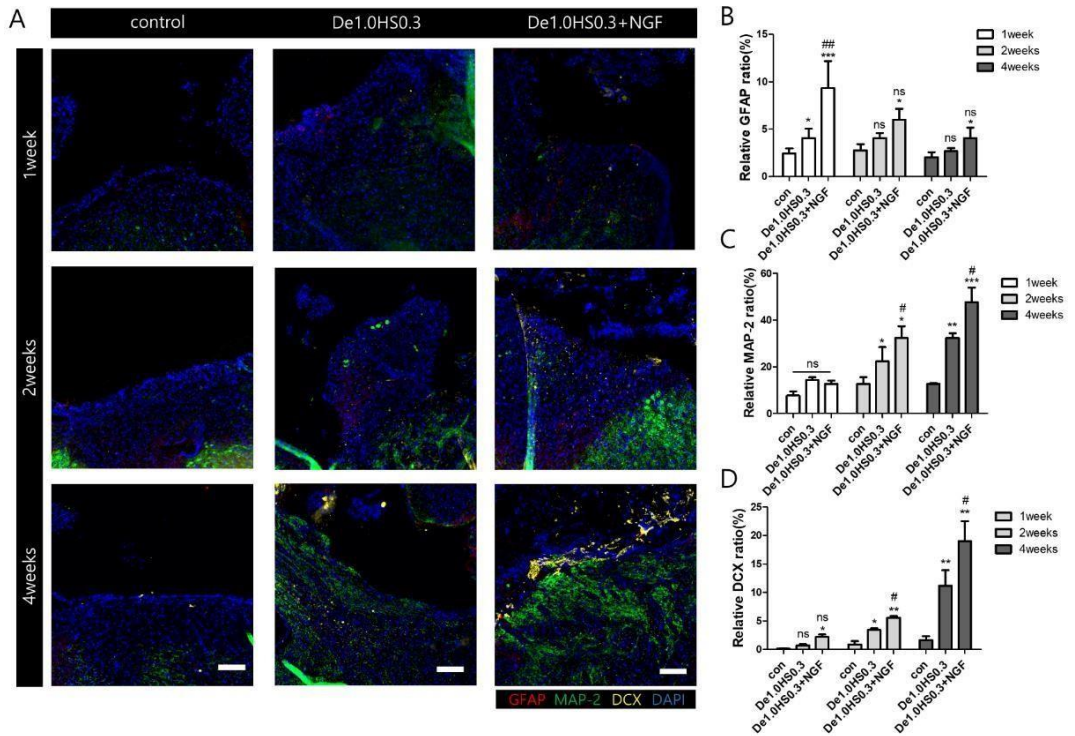


Figure 3.8 Neuronal tissue regeneration assessment post implantation of cryogels in infarct area of host tissues. (A) Representative fluorescent images of GFAP(Red), MAP-2(Green) and DCX(Yellow) images. (B) Relative GFAP signal measurements. (C) Relative MAP-2 signal measurements. (D) Relative DCX signal measurements. (control: no treatment, De1.0HS0.3: cryogel only De1.0HS0.3 + NGF: NGF encapsulated cryogel treatments, scale bar = 100µm). Error bars indicate SD. P-value = * p < 0.05, ** p < 0.01, *** p < 0.005. # p < 0.05, ## p < 0.01, ### p < 0.005.

3.3.8 *In vivo* application of cryogel (De1.0HS0.3) and characterization of neuronal cell migration in host tissues

It was confirmed that NGF and dECM are effective in vascular tissue regeneration in the brain infarct areas. Additionally, the nerve regeneration effects of the NGF-releasing cryogels were investigated using nerve cell-related proteins and nerve cell-supporting astrocyte markers in brain tissue (GFAP, MAP-2, DCX). It was observed that NGF had a significant effect on GFAP expression in the first week (Figure 3.8 B: con: 3.03 ± 0.88 , De1.0HS0.3: 4.74 ± 2.08 , De1.0HS0.3 +NGF: 12.31 ± 7.35). However, as time passed, there was not a significant increase in GFAP signal in the tissue defect areas. Nonetheless, in the group where NGF was encapsulated, a slightly higher level of expression was observed compared to the other two groups at each time point (Figure 3.8 B: con: 3.25 ± 1.02 , De1.0HS0.3: 4.45 ± 1.27 , De1.0HS0.3 +NGF: 6.41 ± 2.15 / con: 2.68 ± 0.48 , De1.0HS0.3: 3.14 ± 1.20 , De1.0HS0.3 +NGF: 4.88 ± 1.97). In the first week, the results of MAP-2 staining showed that the nerves did not progress into the defect area, but from the second week, some nerve expression was observed in the De1.0HS0.3 and De1.0HS0.3 +NGF groups (Figure 3.8 C: De1.0HS0.3:

26.34±9.28, De1.0HS0.3 +NGF: 37.21±11.85). After 4 weeks of implantation, the group with NGF showed a significant increase in MAP-2 expression compared to the other two groups (Figure 3.8 C: control 13.35±0.88, De1.0HS0.3: 34.84±6.05, De1.0HS0.3 +NGF: 51.01±16.15). DCX, which is involved in the migration of nerve cells in neural tissue and the connection between neurons, was observed to significantly increase due to NGF after 4 weeks. The dECM also showed its neuronal cell regeneration ability by relatively increased DCX signals in infarct areas after 4 weeks post-implantation (De1.0HS0.3 group), but the NGF-releasing group showed approximately twice the level of DCX signals compared to the De1.0HS0.3-only applied group in the tissue infarct area (Figure 3.8 D: control 3.13±0.18, De1.0HS0.3: 13.24±5.05, De1.0HS0.3 +NGF: 22.06±6.85).

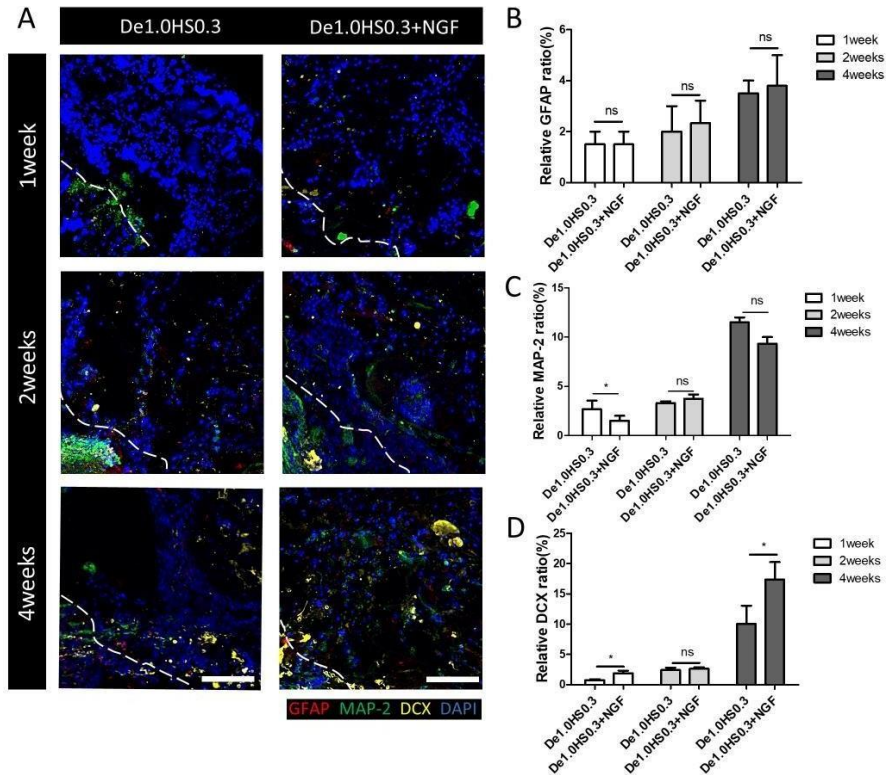


Figure 3.9 Neuronal tissue regeneration assessment post implantation in implanted crygel areas. (A) Representative fluorescent images of GFAP(Red), MAP- 2(Green) and DCX(Yellow) images infiltrated to implanted De1.0HS0.3 cryogels. (B) Relative GFAP signal measurements. (C) Relative MAP-2 signal measurements. (D) Relative DCX signal measurements. (De1.0HS0.3: cryogel only De1.0HS0.3 + NGF: NGF encapsulated cryogel treatments, scale bar = 100 μ m. Error bars indicate SD. P-value = * p < 0.05, ** p < 0.01, *** p < 0.005. # p < 0.05, ## p < 0.01, ### p < 0.005.

3.3.9 *In vivo* application of cryogel (De1.0HS0.3) and characterization of neuronal cell recruitment in to the cryogel network

To investigate whether neural tissue can grow within the De1.0HS0.3 scaffold, we examined the migration of neural and glial cells within the De1.0HS0.3 scaffold. In the first week, there was no significant activity of astrocytes and neural cells that infiltrated the scaffolds. In the second week, although DCX signals increased compared to the first week, the signal expression level remained around 3%. After the fourth week, higher DCX, MAP2, and neural cell markers were observed in the De1.0HS0.3 scaffold network (Figure 3.9 C : MAP2: De1.0HS0.3: 12.11 ± 2.45 , De1.0HS0.3 +NGF: 9.16 ± 3.82), (Figure 3.9 D : DCX: De1.0HS0.3: 13.92 ± 6.25 , De1.0HS0.3 +NGF: 18.26 ± 4.66).

3.4 Discussion

In the brain tissue, the extracellular matrix (ECM) plays a crucial role in providing a physicochemical structure, promoting neuronal connectivity, and maintaining brain function. The brain ECM consists of hyaluronan in the core, with the lectican family, which includes chondroitin sulfate proteoglycans (CSPGs), attached to the side of the hyaluronan backbone. It has been demonstrated that this lectican family maintains synaptic plasticity and affects axonal guidance, which is essential for neuronal connectivity. However, following traumatic brain injury (TBI), the composition of the brain ECM undergoes significant changes, even after tissue remodeling processes with fibrotic tissue formation. For example, CSPGs are overexpressed at the injury site, inhibiting neuronal migration and axonal growth, leading to malfunction of regenerated brain tissue. To address this challenge in TBI, it is important to recapitulate the brain ECM to reconstruct normal physiological brain tissue. In this study, we used decellularized brain ECM to mimic the brain ECM environment and synthesized NGF-incorporated dECM-based porous cryogels to promote neuronal migration at the injury site and regenerate brain tissue.

The decellularization process is widely used in tissue reconstruction to obtain biomaterials by removing DNA within the original tissue, preserving only the tissue ECM and structural molecules [92]. We employed decellularization protocols using bovine brains and surfactants such as sodium dodecyl sulfate (SDS). The main objective of tissue decellularization is to remove cellular components such as DNA while preserving ECM and structural molecules. Following SDS-based decellularization, we successfully eliminated DNA to below 50 ng/mg, which indicates the avoidance of adverse immune responses. The amount of sulfated glycosaminoglycan (sGAG) in the dECM decreased compared to native tissue. Previous studies have shown that most detergents can cause the removal of sGAG in dECM, which may lead to a decrease in the viscoelastic properties of the dECM-based scaffold [135]. To address this, we incorporated heparin sulfate in the dECM-based cryogels to supplement the sGAG components and increase the rheological properties. Collagen is the main component of animal tissues, providing a cell binding base and 3D structural support. Collagen components were still found in brain dECM, with an increased concentration compared to native tissues [136]. This suggests that the relative decrease in tissue mass resulting from the decellularization

process led to a higher proportion of collagen remaining in the decellularized brain tissues. Furthermore, the proteomic analysis showed that the types and scoring of ECM-related proteins were upregulated in the dECM compared to native tissues (Figure 3.1 L). These results are expected to promote higher neuron cell migration to fabricated cryogels with increased collagen and sGAG degradation in the dECM [137, 138].

When designing a scaffold for traumatic brain injury (TBI) models, it is crucial to ensure that it possesses a suitable porous structure capable of attracting endogenous cells. Cryogels based on biomaterials have been extensively studied as scaffolds in TBI models because they provide an environment that supports endogenous neurons, promotes neuronal connectivity, and facilitates tissue remodeling. Furthermore, incorporating biological cues such as growth factors into the scaffold can enhance neuronal migration. In this study, we developed cryogels based on decellularized extracellular matrix (dECM) and heparin sulfate, with the inclusion of nerve growth factor (NGF) factors within the cross-linking networks. The DMTMM crosslinking system was chosen for fabricating these cryogels due to its simplicity and high yields. By utilizing the DMTMM chemistry, we successfully crosslinked the brain

dECM with heparin sulfates to form a three-dimensional (3D) structure, facilitated by the amide bonds formed between the amine groups of dECM and the carboxyl groups of heparin sulfate (Figure 3.2 A). The use of DMTMM chemistry not only enabled the formation of a structurally sound brain dECM-based cryogel but also endowed it with the ability to swell [139, 140]. The higher concentration of heparin sulfate used during the reaction resulted in a higher cross-linking density, as evidenced by the lower levels of unreacted heparin sulfate detected in the cryogel after cross-linking (Figure 3.1 C).

To assess the rheological properties of the cross-linked cryogels, three different rheological analyses were conducted for each group. It was observed that the modulus of fully cross-linked cryogels increased as the polymer concentration in each cryogel increased. The results indicated that the modulus characteristics were enhanced with higher concentrations of heparin sulfate under external forces such as frequency and strain sweeps. Notably, it was found that the properties increased in proportion not only to the heparin sulfate concentration but also to the dECM content in the cryogels. The rheology data for the groups using 1% (w/v) dECM demonstrated a tendency of low modulus increase with

higher heparin sulfate concentration. This suggests that dECM has a greater impact on changes in physical properties compared to the influence of heparin sulfate (Figure 3.3).

Various tests were performed to evaluate the physical properties of the cross-linking networks under different external force conditions. The results revealed that dECM played a more significant role in property changes within the cross-linking systems compared to heparin. Subsequently, injectability was assessed to determine whether the chemically cross-linked scaffold could maintain its shape and structure under shear-thinning stress conditions [141]. When the cryogel was injected using a 17G needle, the group with a higher heparin concentration exhibited greater resistance to shear thinning stress in the 0.5% (w/v) dECM groups. In the 1.0% (w/v) dECM group, the remaining weight ratio increased compared to the 0.5% dECM groups during the shear thinning injection process. This result indicated that the structural stability, which contributed to the formation of the 3D structure, increased with dECM and heparin concentrations.

The binding and release properties of heparin sulfate, which can induce sustained protein release, were investigated by varying the

concentration of heparin sulfate in the cryogel. Heparin sulfate is commonly used in protein release systems due to its negative charge, which allows for temporary attachment or fixation with positively charged protein components[142, 143]. In the sustained release experiment using bovine serum albumin (BSA), it was observed that the amount of released BSA increased with the concentration of heparin sulfate and cross-linking density (Figure 3.5 A). This phenomenon is believed to occur because the higher density of the cross-linking network with heparin sulfate provides a more stable protein binding environment and enhances the binding efficiency of a larger amount of proteins. Therefore, only the groups containing higher concentrations of dECM were selected for the NGF release kinetics experiments. The profiles of NGF release were found to be influenced by the amount of heparin sulfate in the cryogels (Figure 3.5 B). Even under the same protein loading conditions in the release experiments, there were differences in the encapsulation efficiency between BSA and NGF. These differences arise from the distinct net charge of proteins, which can be altered by pH, amino acid compositions, and 3D structural characteristics [144, 145].

NGF in the cryogels serves two distinct biological functions. The

first function is the recruitment of endogenous neuronal cells near the cryogels through the controlled release of NGF. The second function is the promotion of proliferation and neuronal connectivity of migrated cells within the cryogels. To evaluate the first hypothesis, PC12 cells were cultured with NGF-incorporated cryogels. The released NGF successfully differentiated PC12 cells, indicating that NGF in the cryogels maintains its biological activity without deformation even when encapsulated (Figure 3.5 C). The differentiation efficiency was characterized by the ratio of β -tubulin signal and neurite outgrowth. The β -tubulin signal and neurite length increased with heparin concentration, indicating a higher quantity of NGF released in the cell culture environment and the maintenance of an active state of NGF release in all cryogel groups.

Next, we conducted experiments where PC12 cells were encapsulated in NGF-incorporated cryogels. In the De1.0HS0.1 group, short neurite formation was observed in the 3D cell culture systems, suggesting that the cells did not fully differentiate due to limited NGF binding in the initial binding states. This is likely due to an insufficient concentration of NGF, possibly caused by the low concentration of

heparin sulfate, which was unable to provide an adequate NGF concentration for differentiation in the 3D environment compared to 2D cultures. On the other hand, the De1.0HS0.3 group exhibited better neurite formation compared to the De1.0HS0.5 group, despite the latter having a higher heparin concentration and thus more NGF content. This can be attributed to the De1.0HS0.3 group containing a sufficient amount of NGF to support PC12 differentiation in the 3D culture conditions, while the presence of heparin components did not interfere with the behavior or attachment of nerve cells. In contrast, in the group containing 0.5% (w/v) heparin sulfate, NGF was adequately contained and released to promote neurite outgrowth, but excessive heparin sulfates hindered the full growth and extension of neurites in the 3D culture systems (Figure 3.6 A). Although cryogels capable of sustained protein release were successfully fabricated using negatively charged materials, it is known that these charge characteristics can act as negative factors that potentially impede cell migration and adhesion[146, 147]. Through in vitro studies, it was demonstrated that dECM-based cryogels can provide the necessary structure and biochemical cues to support the proliferation of PC12 cells. Furthermore, the controlled release of NGF by heparin sulfate can induce neuronal migration and differentiation both within and

outside PC12 cells within the cryogels.

Based on *in vitro* experiments, the De1.0HS0.3 group was identified as the most suitable for neuronal regeneration, as it resulted in neuronal cell differentiation states with a sufficient amount of NGF release and proper heparin sulfate concentrations that inhibited neurite growth. To validate brain tissue regeneration in an *in vivo* setting, we implanted cryogels in a mouse model of traumatic brain injury (TBI) induced by cortex defects created with a biopsy punch. We evaluated functional brain tissue regeneration from four perspectives: (1) the host response to dECM-based cryogels by endogenous glial cells to assess any immune response evoked by dECM, (2) the reconstruction of an effective blood-brain barrier (BBB) and neo-vascularization near the defect area, (3) the recruitment of endogenous neuronal cells through the sustained release of NGF, and (4) neuronal migration and connectivity within the cryogels. The immune cell response following biomaterial implantation in brain tissue defects was characterized using the Iba-1 marker, which represents microglial cells in the brain [148]. Microglia cells have a role in downregulating neuronal cell function under normal conditions, but they can adopt a neuroprotective phenotype in response to specific cytokines

or signals [149]. In the results, the presence of Iba-1 markers was barely observed in the infarct area of the brain, but their signals increased in the vicinity of the implanted De1.0HS0.3 scaffold (Sup Figure 3.2, 3.3). Upon initial implantation of the De1.0HS0.3 material, an increased population of microglia was observed in the surrounding tissue at the one-week time point. However, as time elapsed, the microglia population gradually decreased. The activation and infiltration of microglia toward the biomaterial can be attributed to their role in defending the tissue environment. [150]. This cellular activation and infiltration likely occur in response to the degradation of the dECM cryogel, which may trigger the release of regenerative molecules from the dECM, thereby promoting tissue remodeling processes [151]. Overall, these findings indicate that microglia play a dynamic role in the response to biomaterial implantation, initially responding to the presence of the material and subsequently contributing to the tissue remodeling process by interacting with the degraded dECM and facilitating the release of regenerative molecules [152, 153].

Next, we employed immunostaining techniques to investigate the formation of vascular tissue by detecting markers such as GLUT-1 and

PDGFR. GLUT-1 is a member of the glucose transporter family that is selectively expressed in brain tissue, particularly in the blood-brain barrier (BBB), facilitating the transfer of glucose to the brain tissue environment [154]. GLUT-1 is abundantly expressed in endothelial cells of the BBB, enabling the transfer of glucose from blood vessels to neuronal and glial cells by overcoming tight junction barriers [155]. This endothelial cell marker is highly associated with neurogenesis in the surrounding tissues and can be upregulated by BDNF protein supplementation, which is an archetype of neurotrophins derived from the same pro-neurotrophin family as NGF but undergoes different cleavage mechanisms to mature [156-158]. Regarding GLUT-1, we observed an increase in signaling in the infarct area during the first week due to NGF treatment. After 4 weeks post-implantation of De1.0HS0.3, the De1.0HS0.3 + NGF group still exhibited modest improvements in regeneration compared to the control and De1.0HS0.3-only treated groups. However, there was no significant improvement in the population of GLUT-1 positive tissue compared to the early timepoints in each group (Figure 3.7F). These results suggest that GLUT-1 is expressed in the early stages, and the temporal maturation of the BBB is facilitated by De1.0HS0.3 + NGF treatment. However, further

investigation is needed to understand the latency of these effects and their development in a hypoxic state, along with other related markers of cellular response [159]. PDGFR, a marker for pericytes, interacts with microvascular tissues in the brain and correlates with GLUT-1 expression on endothelial cells [160]. PDGFR is predominantly expressed in pericytes and is known to induce vascular leakage and brain tissue deformations when downregulated [161, 162]. The results of PDGFR signaling showed that both dECM and NGF treatments exhibited advanced regenerative effects compared to the control group, and this effect significantly increased over time. Even in the control group, there was an increase in PDGFR signaling at 4 weeks compared to the early phase of defect creation, likely due to feedback physiology in a hypoxic environment [163]. As the results demonstrated, both GLUT-1 and PDGFR were increased with NGF encapsulation in the cryogel, even in the absence of NGF. This could be attributed to the charge-receptor interaction of heparin sulfate, which binds to angiogenesis inhibitors and pro-angiogenic receptors, inducing angiogenic signals through material-receptor interactions [164, 165]. Moreover, the dECM derived from the brain, which contains various cytokines and growth factors in soluble form, may also contribute to this

effective therapeutic approach [166, 167]. Furthermore, studies on NGF-related vascular regeneration have been conducted on brain endothelial cells and the peripheral bone vascularization system, providing insights into NGF-mediated vascular tissue regeneration in brain defects [168, 169].

Then, we proceeded to analyze the recruitment of endogenous neuronal cells using NGF-incorporated cryogels. MAP-2 is a molecule involved in the reconstruction of neuronal networks and the recovery of brain tissue function. Its expression is downregulated in the ischemic state of the brain but increases upon treatment in clinical trials [170]. NGF has been utilized in repair strategies for the central nervous system (CNS), ranging from recombinant proteins to cellular vesicles, and has been shown to promote neuronal cell recovery [171, 172]. NGF treatment has been found to delay the degradation of MAP-2, an elongation protein in neuronal axons, in brain tissue ischemia [173]. In our results, MAP-2 signals increased with cryogel treatment alone and further advanced with NGF treatments, indicating the regenerative capabilities of the biopolymer and growth factor combination (Figure 8). Similarly, the neuroregenerative factor doublecortin (DCX) also

exhibited an increasing trend with cryogel and NGF treatments [174]. DCX expression is closely associated with NGF, and it increases with NGF treatment in hypoxic-ischemic brain injury [175]. In a brain stroke model, DCX also increased with dECM treatment in the absence of NGF, and in vivo results demonstrated that other axonal markers of neuronal cells also increased with DCX [176, 177]. These findings support the notion that the dECM, a complex mixture of biopolymers and proteins, can promote tissue-specific regeneration in the brain, and when engineered with growth factors, it can significantly induce the recruitment of neuronal cells near the site of defects. Neuronal cells infiltrated the tissue defect area through the dECM polymers and the regeneration process mediated by NGF. The presence of highly populated neuronal markers and signals related to neuron cell migration was observed in the tissue defect area treated with the De1.0HS0.3 scaffold and NGF additions.

Furthermore, the markers MAP-2 and DCX showed increased expression in the De1.0HS0.3 scaffold area, indicating the infiltration of neuronal cells into the 3D porous structure, promoting the formation of brain tissues. However, the ratio of neuronal cell infiltration was not

significantly higher in the De1.0HS0.3 + NGF group compared to the group treated with the scaffold alone and the host tissues under the same in vivo conditions. It appears that as immune cells and fibroblasts also migrated to the scaffold structure, the higher density of neuronal and glial cells on the surface of the host tissues treated with De1.0HS0.3 + NGF had a competitive advantage in migrating to the scaffold area compared to the NGF-absent group [178]. These findings indicate that after the tissue remodeling process, endogenous neuronal cells could effectively migrate into the cryogels, supported by the upregulation of DCX expression.

3.5 Conclusion

The brain-decellularized ECM-based cryogel, with its 3D porous structure, exhibited improved efficiency in releasing NGF, particularly when combined with heparin. This combination enhanced the sustained release of NGF, which is advantageous for promoting brain regeneration and providing a supportive 3D structure. The manuscript further investigated the effect of heparin concentration on the inhibition of neuronal cell migration. By studying the inhibitory effect of charge on

neuronal cell outgrowth, an optimal heparin concentration for neural cell culture was determined. In the context of traumatic brain injury (TBI), the brain-decellularized ECM-based cryogel was applied, resulting in the stabilization of the blood-brain barrier (BBB) and the formation of neural tissue in the defect area. This demonstrates the potential of the cryogel for TBI treatment and brain tissue repair through the recruitment of neural cells. The migration of neural cells within the cryogel scaffold was also observed. However, it was observed that the incorporation of immune cells and fibroblasts within the scaffold hindered the migration of neuronal cells into the interconnected network. Therefore, further investigation is recommended to understand this phenomenon, including studying the impact of immune cell-derived scaffold degradation or employing immune regulation strategies to create more favorable environments for neuronal cell migration.

In summary, this study highlights the promising potential of the brain-decellularized ECM-based cryogel combined with heparin sulfate and NGF for brain regeneration. However, it also emphasizes the need for further research to address challenges related to the incorporation of immune cells and fibroblasts and their impact on neuronal cell migration

within the 3D scaffold.

3.6 Supplementary figure

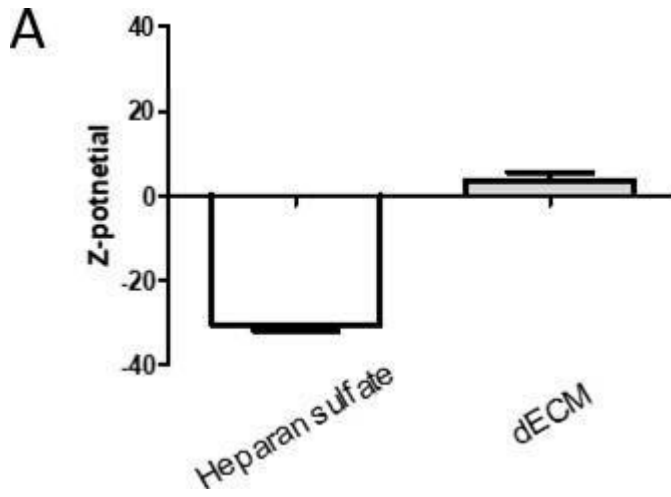


Figure S3.1 Zeta potential of heparin sulfate and decellularized brain ECM

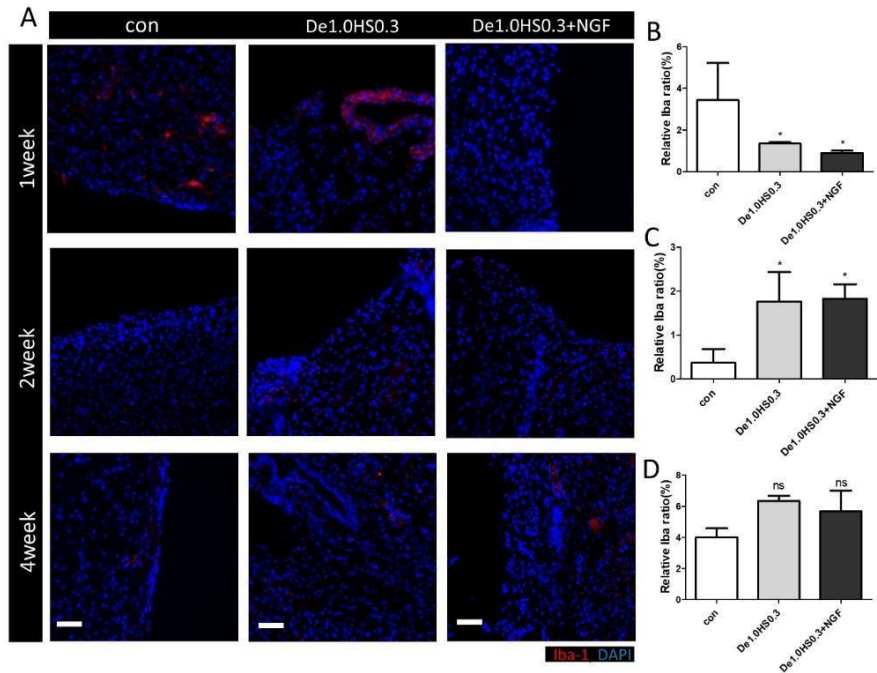


Figure S3.2 Figure. S3.2 Immune cell population of infarct area after surgery A) Representative images of Iba-1 images in infarct area of host tissues. (B) Relative Iba-1 signal measurements at 1 week. (C) Relative Iba-1 signal measurements at 2 weeks. (D) Relative Iba-1 signal measurements at 4 weeks. (control: no treatment, De1.0HS0.3: cyrogel only De1.0HS0.3 + NGF: NGF encapsulated cyrogel treatments, scale bar = 100 μ m). Error bars indicate SD. P-value = * $p < 0.05$, ** $p < 0.01$, *** $p < 0.005$. # $p < 0.05$, ## $p < 0.01$, ### $p < 0.005$.

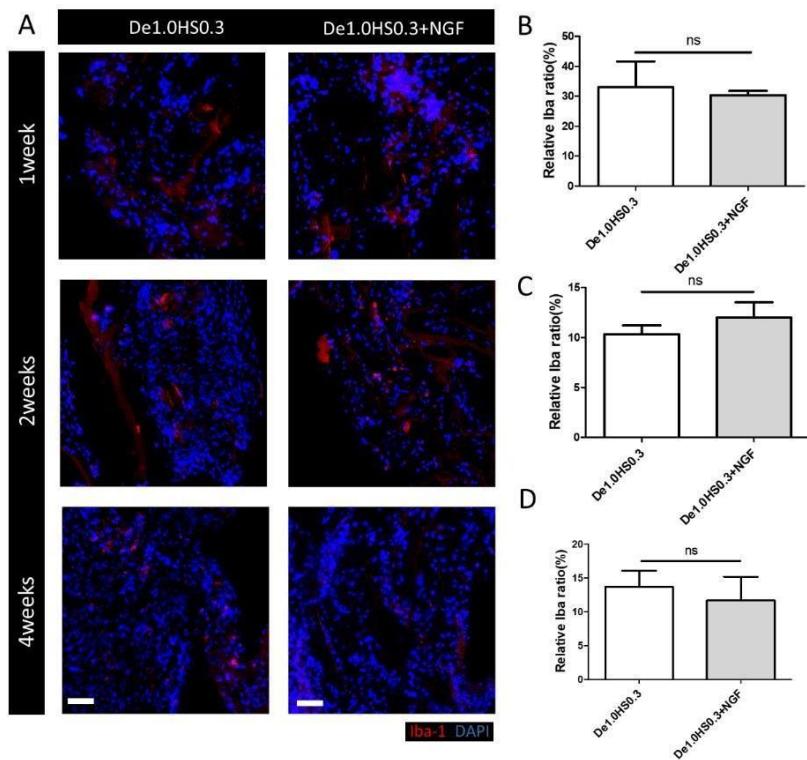


Figure S3.3 Immune cell population in implanted cryogel area. A) Representative images of Iba-1 images interacted with cryogels post implantation. (B) Relative Iba-1 signal measurements at 1 week. (C) Relative Iba-1 signal measurements at 2 weeks. (D) Relative Iba-1 signal measurements at 4 weeks. (De1.0HS0.3: cryogel only De1.0HS0.3 + NGF: NGF encapsulated cryogel treatments, scale bar = 100 μ m). Error bars indicate SD. P-value = * $p < 0.05$, ** $p < 0.01$, *** $p < 0.005$. # $p < 0.05$, ## $p < 0.01$, ### $p < 0.005$.

CHAPTER FOUR:

COMPARATIVE STUDY OF CHEMICAL AND SUPER-CRITICAL FLUID DECELLULARIZATION FOR FABRICATION OF PERIPHERAL NERVE SCAFFOLD

4.1 Introduction

Peripheral nerve injury (PNI) is a traumatic disease that can occur in all parts of the nervous system, except the brain and spinal cord. Traumatic PNI casualties were recorded over 80% of all nerve injuries in upper extremities category [179]. The cost of PNI treatments is estimated to be about 50,000 USD, and over 0.5 million casualties were reported for traumatic PNI cases in the USA [180].

To treat PNI, stem cell therapies have been actively investigated for peripheral nerve regeneration, given their intrinsic growth function of peripheral neurons in response to injuries, different from central nervous system [181]. Studies have reported that mesenchymal stem cells can transdifferentiate into Schwann cells and assist neuronal tissue

regeneration and remyelination of injury sites *in vivo* [182, 183]. However, these cell-based therapies were hard to maintain their self-renewal and differentiation ability in injected or implanted sites [184]. Implanted stem cells are expected to contribute partial neuro regeneration by promoting Schwann cell function and axon growth but it is difficult to recapitulate the cylindrical nerve structure to bridge the distal and proximal ends of the injured gap [185].

To bridge neuronal tissue, polymeric scaffolds were fabricated with biocompatible materials with high mechanical properties. Polyester family of polymers (PVA, PGA, PLGA, PCL and their copolymers) has been used for nerve conduit fabrication because of their easy handling and hydrolyzing affinity, which degrade easily in specific circumstances [186, 187]. But these synthetic materials lack cell binding moieties or cell compatible polysaccharide and proteins which are essential to attract cell migration as the first step of tissue formation. To overcome these limitations, simple blending of synthetic materials with native tissue-derived collagen or cell binding arginyl-glycyl-aspartic acid (RGD) peptide have been implemented in nerve tissue regeneration studies [188, 189]. However, the polymeric material mixture and cell responsive

protein conjugation strategies which commonly introduced were not enough to replace complex living tissue compositions comprised of proteins and extracellular matrix (ECM).

For this reason, autologous nerve transplantation is the most preferable treatment of nerve defects, which shows good regenerative potential without host rejection, but is limited by tissue-dependent neuroma and size variation of donated tissues in same body [190]. To alleviate issues related to nerve tissue surgery, the U.S. Food and Drug Administration (FDA) has approved the use of hollow polymeric scaffold as nerve conduits for clinical application [191], however, these simple bridging shapes are hard to replace 3D tissue structure and volumetric tissue formation in implanted sites [192, 193]. To fabricate biocompatible, nerve tissue responsive, volumetric bridging available nerve conduit, chemical decellularization technology using Triton X-100, sodium deoxycholate (SDS), or sulfo betaine (SB) was developed to fabricate decellularized ECM (dECM) from native animal tissues [194, 195].

Chemical decellularization technology extracts ECM from specific tissue with detergents to eliminate immunogenic genetic materials (*ie.*

DNA and RNA) from native tissue ECM while preserving cell responsive polysaccharides and proteins [52, 127]. For this controllable elimination process, the decellularized tissues were applied to biomedical applications and clinical research works offering ideal tissue microenvironment without risk of immune rejection or inflammation between the native tissue and implanted biomaterial [196]. However, chemical decellularization technique also has its limitation, including material loss and damage to structural integrity as a result of harsh chemical processing. Common detergents used in decellularization process have been reported to degrade ECM in tissues, which consequently decreases biological response and regenerative potential of decellularized tissues [197].

To decrease ECM material loss during the decellularization process, stable and non-ionic solvents, such as supercritical CO₂, are utilized in tissue decellularization process [198]. Supercritical CO₂ sustains mild operating conditions (10.3 to 27.6 MPa, 10 to 37 °C) during process and also have low reactivity with polar proteins and ECM materials in tissues [199]. Supercritical phase CO₂ has liquid and gas-like characteristics that make the supercritical state CO₂ diffuse instantaneously into solid

structures and solubilize chemicals efficiently [200]. Thus, supercritical fluid-based decellularization method is expected to eliminate DNA materials more selectively and better preserve ECM components in the native tissue than chemical-based methods.

In this study, we have conducted detergent(chemical)-based and supercritical state CO₂-based decellularization methods on nerve tissues, comparing their decellularization efficiency, tissue-cell response and therapeutic potential. We hypothesized that supercritical method can maintain ECM components and structural, mechanical characteristics of tissues after decellularization more stable than detergent-based method. The polymeric components degradation were characterized with biochemical assays. Mechanical and structural changes were quantified via measuring modulus of ECM. ECM distribution change and their effect on cellular microenvironment were evaluated via *in vitro* neuronal outgrowth tests and *in vivo* sciatic nerve injury recovery.

4.2 Material & methods

Reagents

Sodium Dodecyl sulfate (Biorad, USA, 1610302), papain

(Worthington, USA, 9001-73-4), sGAG (Biosynth Carbosynth, England, YC31458), 4% paraformaldehyde (PFA; Biosesang, Republic of Korea, BP031a), chloramine T (MP, USA, 7080-50-4), p-dimethylaminobenzaldehyde (MP, USA, 100-10-7), Bovine serum albumin (Gen depot, USA, A0100-005), Triton X-100 (Sigma Aldrich, USA, 9036-19-5).

Phosphate buffered saline (PBS, Thermo fisher scientific, USA, 10010023), Trypsin-EDTA (Thermo fisher scientific, USA, 27250018), Normal goat serum (Thermo fisher, USA, 31872), RIPA lysis buffer (Thermo fisher, USA, 89901) were purchased from Thermo fisher scientific.

sucrose (Sigma Aldrich, USA, S0389), DMMB (Sigma Aldrich, USA, 341088), cysteine (Sigma Aldrich, USA, C7352), hydroxy-proline (Sigma Aldrich, USA, 51-35-4), Canada balsam (Sigma Aldrich, USA, 8007-47-4), Proteinase K (Sigma Aldrich, USA, 3115887001) were purchased from Thermo fisher scientific.

4.2.1 Isolation and decellularization of sciatic nerve tissues

Sciatic nerves were isolated from porcine biceps femoris after elimination of fat and skin. Isolated sciatic nerves were cleaned with PBS and treated with different concentrations of detergent solution (0.1, 0.5,

1% w/v of sodium dodecyl sulphate, SDS) at 37°C for 36 h with gentle mixing. The nerve tissues were collected and stored at -80°C until further use. The native porcine nerve tissues were prepared as described above. Tissues were then transferred to medical container in supercritical fluid devices. 50 ml of pure ethanol was added to container as co-solvents. CO₂ fluid was injected into medical container at 200-400 bar. After 3 h of treatment, decellularized tissue was washed with PBS and stored in -80°C freezer. DOF Inc, Korea conducted the supercritical fluid-based decellularization process and provided the processed samples.

4.2.2 Histological assessment of sciatic nerve tissues.

4.2.2.1 Paraffin sectioning of nerve tissues

Native nerve tissues and decellularized tissues were fixed with PFA (4% v/v) at 4°C for 24 h. Fixed tissues were then moved to ethanol solution (50% v/v) and incubated at 25°C for 30 min. From the first dehydration step with ethanol the nerve tissues transferred to higher concentration of ethanol solutions for 30 min (70, 90, 100, 100% v/v). After that the nerve tissues were immersed in xylene solution twice for 1 h. And the nerve tissues were incubated 60°C in paraffin solutions for 24 h. Nerve tissue paraffin blocks were sectioned at 10 μ m thickness using

microtome (Leica).

4.2.2.2 H&E staining of nerve tissues

Nerve tissue sections were deparaffinized and rehydrated with two changes of xylene and transferred to consecutive ethanol change (100, 100, 90, 70, 50% v/v) for 5 min. After that tissue slices transferred to deionized water. Deparaffinized nerve tissues were immersed in purified water 2 times for 5 minutes. Washed tissue slides were incubated with hematoxylin solution (Vector) for 1min. And tissue slides were washes in running tap water for 30 min. Tissue slides were stained with eosin Y (0.25% v/v) in acetic acid (0.2% v/v). Stained tissue slides were dehydrated with changes of different concentrations of alcohols (75, 95, 100 % v/v) and xylene solutions. And dehydrated slides were mounted with Canada balsam mounting solutions.

4.2.2.3 Trichrome staining of nerve tissues

Trichrome stain protocol followed by manufacturers protocol (abcam, ab150686). Briefly, rehydrated nerve tissues were immersed in purified water 3 times for 5 minutes. The tissue slides were incubated in preheated Bouin's Fluid for 60min and cool for 10 min. After rinsing with purified water, tissue slides were incubated in weigert's Iron solutions for 5min. Tissue slides were washed with purified water. And

incubated with Biebrich Scarlet/ Acid Fuchsin solutions for 15 min. Tissue slides were washed with purified water. And tissue slides were differentiated in phosphomolybdic/ Phosphotungstic acid solution for 15 min. Without rinsing, tissue slides were incubated in Aniline Blue solution for 5 min. After rinsing with purified water, tissue slides were incubated in acetic acid solution (1% v/v) for 5 min. Stained tissue slides were dehydrated with changes of different concentrations of alcohols (75, 95, 100% v/v) and xylene solutions. And dehydrated slides were mounted with Canada balsam mounting solutions.

4.2.2.4 Safranin-O staining

Deparaffinized nerve slice samples were washed with deionized water two times for 5 min each. And tissues were stained hematoxylin for 1 min and incubated in running tap water for 30 min. and tissue slices were stained fast green solution (0.05% w/v) for 5 min. after rinsed with 1% (v/v) acetic acid the nerve slices were stained with safranin -O solution (0.1% w/v) for 5 min. Stained tissue slices were dehydrated with different concentrations of alcohols (75, 95, 100 % v/v) and xylene solutions. Slides were mounted with Canada balsam solution.

4.2.3 ECM characterization in nerve tissues

4.2.3.1 DMMB assay for quantifications of sGAG

Papain enzyme solutions (3% v/v) were prepared with PBE-cys buffer (100mM Phosphate, 10mM EDTA, 0.10M L-cysteine, pH 6.5). Nerve tissues were incubated at 60°C for 24h with diluted papain enzyme solutions until tissues were fully digested. And the tissue solutions were transferred 96-well plate (SPL life sciences) after then DMMB solutions (40.5 mM glycine, 40.5mM NaCl, 50µM DMMB, pH 3.5) were transferred to well plate and mixed with tissue solutions (1:1 volume ratios). Absorbance were measured by microplate reader (Tecan, Switzerland, Infinite 200) at 525nm wavelength. Standard line for calculation of relate sGAG contents in nerve tissue were made with chondroitin sulfate sodium salt.

4.2.3.2 DNA quantification in nerve tissues

Papain enzyme solution (3% v/v) was prepared with PBE-cysteine buffer (100 mM phosphate, 10 mM EDTA, 0.10 M L-cysteine, pH 6.5). Nerve tissues were incubated at 60°C for 24 h with diluted papain enzyme solutions until tissues were fully digested. DNA quantification of nerve tissues were followed by manufactures protocol Quant-iT Pico Green dsDNA Assay kits (Invitrogen, P7589). Briefly, Pico green dyes

were 20-fold diluted in TE buffer (10 mM Tris-HCL, 1mM EDTA, pH7.5) and mixed with digested tissue solution (1:1 volume ratio). Fluorescence of dyes were measured with microplate reader (Tecan) at excitation 480 nm, emission 520nm wavelength. Standard line for calculation of relate DNA contents in nerve tissue were made with Quant-iT Pico Green dsDNA stock.

4.2.3.3 Hydroxyproline quantification in nerve tissues

Papain enzyme solution (3% w/v) was prepared with PBE-cys buffer (100mM Phosphate, 10mM EDTA, 0.10M L-cysteine, pH 6.5). Nerve tissues were incubated at 60°C for 24h with diluted papain enzyme solutions until tissues were fully digested. 100µl of samples were hydrolyzed with 5N sodium hydroxide in 100°C for 16 h. After that, 100µl of chloramine T solution (0.056M in 50% v/v isopropanol) were transferred to hydrolyzed sample and oxidation processes were allowed for 25 min in room temperature. 100 µl of echrlich's aldehyde reagent (1M p-dimethylaminobenzal aldehyde in 30% HCl / 70% isopropanol) was added to each sample and incubated at 60°C for 20 min. Absorbance were measured by microplate reader (Tecan) at 550 nm wavelength. Standard line for calculation of relate hydroxyproline contents in nerve tissue were made with hydroxyproline. Hydroxyproline solution samples

were processed with same conditions of assay protocols. All reagents of this protocol were diluted in acetate citrate buffer (0.5 mM sodium acetate, 0.1 mM citric acid, 0.1 mM acetic acid, 0.5 mM NaCl, pH 6.5)

4.2.3.4 Proteomic evaluation of tissue samples

The nerve tissues were incubated in RIPA buffer for 10 min in 4°C. and tissues were mechanically dissociated with tissue pestle. After quantification of protein contents with BCA assay kit (Pierce BCA assay kit, Thermo fisher), sample solutions were purified with consecutive 8M urea wash with filter centrifuge (14,000g for 60min). And 100 µl 0.05M iodoacetamide in 8M urea were treated to purified protein solution for 25 min at room temperature. And 50mM ammonium bicarbonate (pH 8.0) were added to protein samples and centrifuged (14,000 for 20 min) for three times. After trypsin digestion (20 ng/ml) at 37°C overnight and the samples were vacuum dried. The dried samples were dissolved in trichloro acetic acid and transferred to LC/MS (Orbitrap Exploris 240, Thermo fisher scientific) the proteomic data were processed by National Instrumentation Center for Environment Management mass spectrometer research department. Total protein contents, Coverage, Unique peptides, Proteomic scoring raw data were extracted and used for characterization of proteomic analysis.

4.2.4 Mechanical property characterization of nerve tissues

4.2.4.1 Extension force test of nerve tissues

Nerve tissues were thawed in 4°C for 1 h and incubated in PBS solutions until measurements. 1.5cm length, 4mm thickness of nerve tissues were fixed in universal tensile machine (Shidmazu, Japan, Ez-sx) and extended with 1mm/min velocity until nerve tissues were separated from machine zig. Compressive stress and critical strength were calculated.

4.2.4.2 Compression force test

Nerve tissues were thawed in 4°C for 1h and incubated in PBS solutions until measurements. 0.5cm length, 4mm thickness of nerve tissues were fixed at bottom plate of universal tensile machine zig. Consecutive compression was applied to nerve tissues (10 cycles, 1mm/min velocity). Compressive modulus was calculated in loading and unloading sites at each cycle. Blunt tip (22G) were used for cyclic compression test tip.

4.2.5 Neuronal cell culture

4.2.5.1 PC12 cell cultures for proliferation and differentiation

PC12 cells were cultured with growth medium (5% horse serum, 5%

FBS, 1% penicillin streptomycin v/v) for proliferation in 100 pi dish. PC12 cells were differentiated with differentiation medium (1% horse serum, 1% penicillin streptomycin, 100ng/ml Nerve growth factor). Cell culture medium were changed with every other day.

4.2.5.2 PC12 cell differentiation on nerve tissues

4-mm diameter of nerve tissue slices were prepared with vibratome (series 3000, Sectioning system) as 300 μm thickness. The PC12 cells were cultured for 3, 7, 21 days on nerve tissue slices with 30,000 cells per slices and differentiated with nerve growth factor-containing (NGF; 100 ng/ml) differentiation medium as described above.

4.2.5.3 PC12 cell imaging with confocal microscopy

The PC12 cells on ECM slices were fixed with paraformaldehyde 4%(v/v) for 24h in 4°C. And tissue slices were incubated with proteinase K for 20 min. after that tissues were incubated with 5% (w/v) normal goat serum for 2 h in room temperature. Tissue slices were washed twice and incubated with primary antibody staining for Class III β -tubulin(300:1, abcam ab75810). Primary antibody solution washed with buffer and incubated with 2nd antibody (500:1 alexa fluoro 488). The stained tissue slices were imaged with Zeiss 700 (Zeiss, Germany,

LSM780)

4.2.6 Surface image of decellularized ECM with SEM

The decellularized nerve tissues were fixed with 2.5% (w/v) glutaraldehyde and 2% perform aldehyde for 16 h. and fixed samples were transferred to 1% (v/v) osmium tetroxide solution and incubated for 1h in 4°C. After washing with deionized water 3 times for 5 min each dehydrated with different concentration of ethanol (50%, 70%, 80%, 90%, 100%, 100% w/v) and specimens were dried with critical-point dryer (Thermo) and stored in vacuum state until imaging with SEM. Dried tissue samples were fixed with carbon tape on the SEM mount and coated with Pt sputter for 1min. the coated samples were imaged with Mini SEM(JCM-6000)

4.2.7 In vivo experiment and characterization of regeneration of tissues

4.2.7.1 Nerve tissue implants to subcutaneous area for immune reaction characterization

The sciatic nerve tissues and dECM, decellularized with SDS and supercritical flow-based method, were implanted in subcutaneous area of mouse for 4weeks. The immune cells infiltrated to sciatic nerves were

stained with CD68 antibody (300:1, abcam ab283654) and imaged with microscopy (EVOS 3000).

4.2.7.2 dECM implantation in sciatic nerve defect model

The animal study was approved by IACUC of Seoul National University (SNU-210604-3-1), 8 weeks old CD (Sprague Dawley) rats (Raon bio, Republic of Korea) were prepared for sciatic nerve defect injury model. The rats were anesthetized with isoflurane, after hair remove, the skin of left biceps and biceps femoris were incised to exposure sciatic nerves. The 1 cm of nerve defects were made in sciatic nerve tissues of rats by dissecting 1cm of sciatic nerves. After rid of dissected nerve tissues, the dECM materials (decellularized with 0.5% SDS and supercritical fluid CO²) were directly sutured to distal, proximal site of host nerve tissues with 8-0 suture. Negative control groups were not treated after nerve dissection. The incised skins and muscle tissues were sutured with 6-0 needle.

4.2.7.3 Gait analysis of sciatic nerve defect model

Sciatic functional index was calculated with following equation (1).

$$\text{SFI} = -38.3(\text{EPL}-\text{NPL})/\text{NPL} + 109.5(\text{ETS}-\text{NTS})/\text{NTS} + 13.3(\text{EIT}-\text{NIT})/\text{NIT} - 8.8 \quad \text{Eq. (1)}$$

(PL= print length, TS=toe spread, IT= intermediary toe spread / E is experimental, N is normal)

The variables were measured with ImageJ analysis measure tools by recording video of stride pattern of each rat for 8 weeks.

4.2.7.4 Evaluation of muscular tissue regeneration

Muscular tissues regeneration was evaluated with muscle weight and histological methods. Wet weights of gastrocnemius muscular tissue from experimental group and non-treated normal side of muscles were measured for calculation of muscle weight ratio with following equation (2)

$$\text{Muscle weight ratio} = (\text{weight of (E)} / \text{weight of (N)}) \text{ E Eq. (2)}$$

(E is experimental, N is normal)

And muscular tissues (gastrocnemius) were stained with Hematoxylin & Eosin to measure muscle fiber diameter and muscle fiber areas (whole 2D area of fibers). The quantification was performed with ImageJ software.

4.2.7.5 Histological assessment of sciatic nerve tissues

Paraffinized tissue were rehydrated as described above. And nerve

tissue slices were incubated with proteinase K for 20 min. after that tissues were incubated with 5% (w/v) normal goat serum for 2h in room temperature. Tissue slices were washed twice and incubated with 1st antibody staining for GAP-43 (500:1, abcam ab75810) and S 100 (500:1, abcam ab52642) for 16 h in 4°C. 1st antibody solution washed with buffer and incubated with 2nd antibody (500:1 alexa fluoro 488, 594 ab150077, ab150080). The stained tissue slices were imaged with Ti2 Eclipse microscope (Nikon, Japan, Eclipse Ti2)

4.2.7.6 Luxol fast blue staining of regenerated nerve tissues

After deparaffinization of tissue slices with incubation in two steps of xylene and two steps of 100 % (v/v) ethanol, 90 % (v/v), 70 (v/v), 50% (v/v) for 10 min each. The tissue samples were incubated in 0.1% (w/v) of luxol fast blue (Sigma Aldrich, USA, S3382) staining solution for 16h in 65°C. after that tissues were rinsed with 95% (v/v) ethanol solution for 5second and transferred to deionized water. Tissue samples were differentiated with 0.05% (w/v) lithium carbonate solution and 70% (v/v) ethanol consecutively. After wash with deionized water the tissue samples were dehydrated and mounted with DPX solutions.

4.2.8 Statistics analysis

All data were processed with Graph pad prism 5.0 and tow-tailed t-

test and one-way ANOVA statistics calculation were performed. P-value
= * $p < 0.05$, ** $p < 0.01$, *** $p < 0.005$. # $p < 0.05$, ## $p < 0.01$, ###
 $p < 0.005$. * statistics symbol compared control group versus SDS 0.5,
SC groups. # statistics symbol compared SDS0.5 group versus SCgroups.

4.3 Results

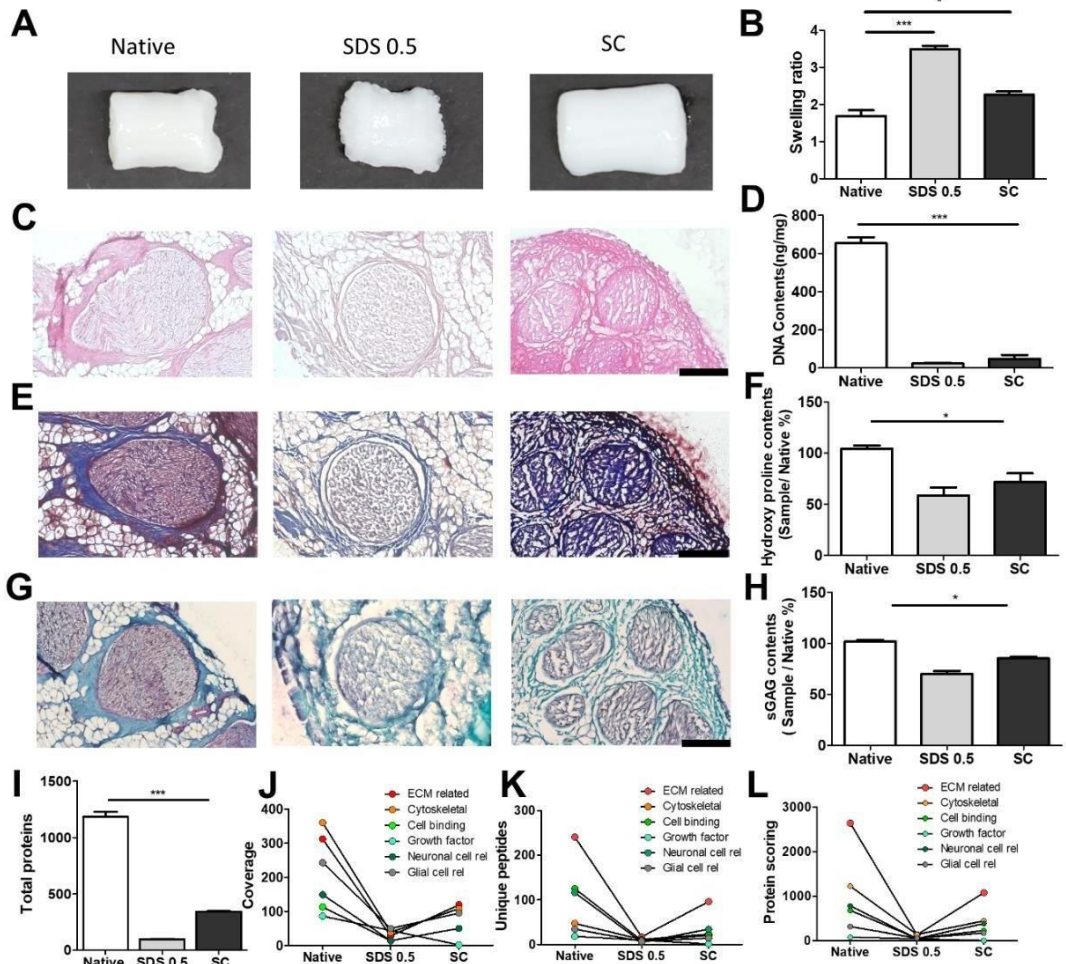


Figure 4.1 Composition analysis of native tissue and decellularized tissues processed with different decellularization methods. (A) Representative images of native and decellularized nerve tissues. (B) Swelling ratio, (C) H&E staining, (D) DNA content, (E) MTC staining, (F) Hydroxyproline content, (G) Safranin-O staining, (H) sGAG content, and (I) total protein content of native tissue and decellularized nerve tissues. (J-L) Proteomic analysis data of proteins in native and decellularized tissues. (Scale bar = 200 μ m). Error bars indicate SD. n = 3. * $p < 0.05$, ** $p < 0.01$, *** $p < 0.005$

4.3.1. Decellularized ECM scaffold fabrication and characterization of ECM

We have produced decellularized ECM scaffolds using two different decellularization methods to remove genetic elements from animal tissues that may trigger immune reactions upon transplantation. We compared a conventional decellularization technique using a chemical (SDS) and a novel technique using a supercritical fluid (CO₂), in terms of effective DNA removal while preserving protein and ECM contents of native tissues. To determine optimal SDS concentration, porcine nerve tissues were treated with different concentrations of SDS solutions. Tissue deformation occurred from the outer surface of nerve tissues (Figure 4.1A) and the extent of deformation increased with SDS concentration (Sup Figure 4.1A). The swelling ratio stand for higher water contents in polymeric network with lower crosslinking density were characterized to describe about tissue deformation and increased swelling ratio that occurred by SDS treatments. The swelling ratio of tissues were increased with SDS treatment as compared with native tissues and SC samples (Figure 4.1B). In SDS-based decellularization process, we confirmed that the concentration of immunogenic DNA in

the tissue decreased to less than 50 ng/mg when SDS concentration was maintained at or above 0.5% (w/v) (Figure 1D). DNA remnants were not observed in H&E staining in for groups treated with over 0.5% SDS (Figure 4.1C). Tissue structure degradation and deformation were further characterized with MTC, Safranin-O staining and ECM-quantifying assays (Hydroxyproline : SDS 0.5 : 52.21 ± 3.32 , SC : 67.39 ± 4.23), (sGAG: SDS 0.5 : 68.33 ± 6.03 , SC : 82.09 ± 8.11 %), (Figure 1E,F,G,H). It seems the ECM content generally decreased with increase in SDS concentration, while ECM content of SC group remained relatively intact correlated with surface image of nerve tissues (Figure 4.1A). Therefore, we optimized the SDS concentration to 0.5% (w/v), which can fulfill both requirements of <50 ng/ml DNA content and >50% of native tissue ECM content. So, in further experiments, the 0.5% (w/v) SDS-treated group were directly compared with SC group. Total protein content quantification and proteomic analysis were conducted. While total protein contents decreased in both decellularization method compared to Native (1098 ± 125.12), SC group (345 ± 48.23) showed higher preservation of protein contents after decellularization than SDS group (103 ± 22.38) (Figure 4.1I). Even same kind of proteins in tissues were decreased in decellularized tissues (Figure 4.1J-L). ECM-related

proteins were most abundant protein type in decellularized nerve tissues, followed by cytoskeletal proteins. Other cell-responsive and neuronal, glial cell related proteins were also observed. Proteomic scoring recorded that both decellularizing method recorded decreased protein contents than native tissues, post-process (Figure 4.1L). But still higher portion of proteins were preserved in SC samples.

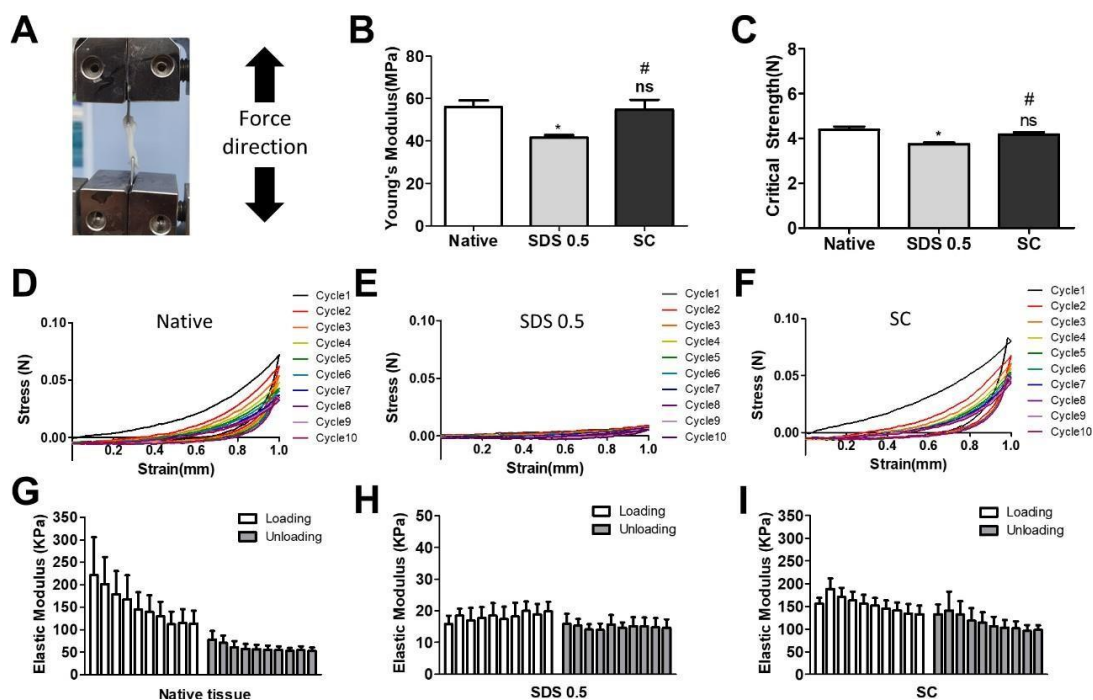


Figure 4.2 Mechanical characterization of native and decellularized tissues. (A) Representative image of extension test method of wet tissue. (B) Young's modulus and (C) Critical strength of native and decellularized tissues. (D-I) Cyclic compression test and elastic modulus of (D,G) native tissues, (E,H) 0.5% SDS-decellularized tissues, and (F,I) decellularized tissues with supercritical fluid. Error bars indicate SD. P-value = * $p < 0.05$, ** $p < 0.01$, *** $p < 0.005$. # $p < 0.05$, ## $p < 0.01$, ### $p < 0.005$.

4.3.2 Mechanical characterization of decellularized tissue samples

It has been previously confirmed that the surface and microstructure of tissue can be damaged by SDS treatment, which affects its mechanical property. To measure mechanical property of decellularized and native

tissues, extension test was performed with bidirectional extension method (Figure 4.2A). The mechanical property of decellularized tissues was characterized with Young's modulus and critical tension strength (Figure 4.2 B-C). The SC group had relatively higher modulus compared to the SDS 0.5 group (SDS 0.5: 42 ± 3.5 , SC: 57 ± 5.3 MPa). The critical strength of SC group was higher than that of SDS 0.5 group (SDS 0.5: 3.64 ± 0.89 , SC: 4.13 ± 0.46 N). To investigate repeated external forces-derived tissue deformation, a repeated indentation test was conducted following the extension test. The strain-stress curve showed that SDS group has significantly lower properties than the native or SC groups (Figure 2D-F). As the number of cycles increased, the sequentially measured modulus gradually decreased in the tissues. There was a larger modulus decrease in native tissue than that of the SC group as indentation cycle increased. The sequential modulus data of SC group showed that it can maintain stable modulus even with repeated indentation procedure.

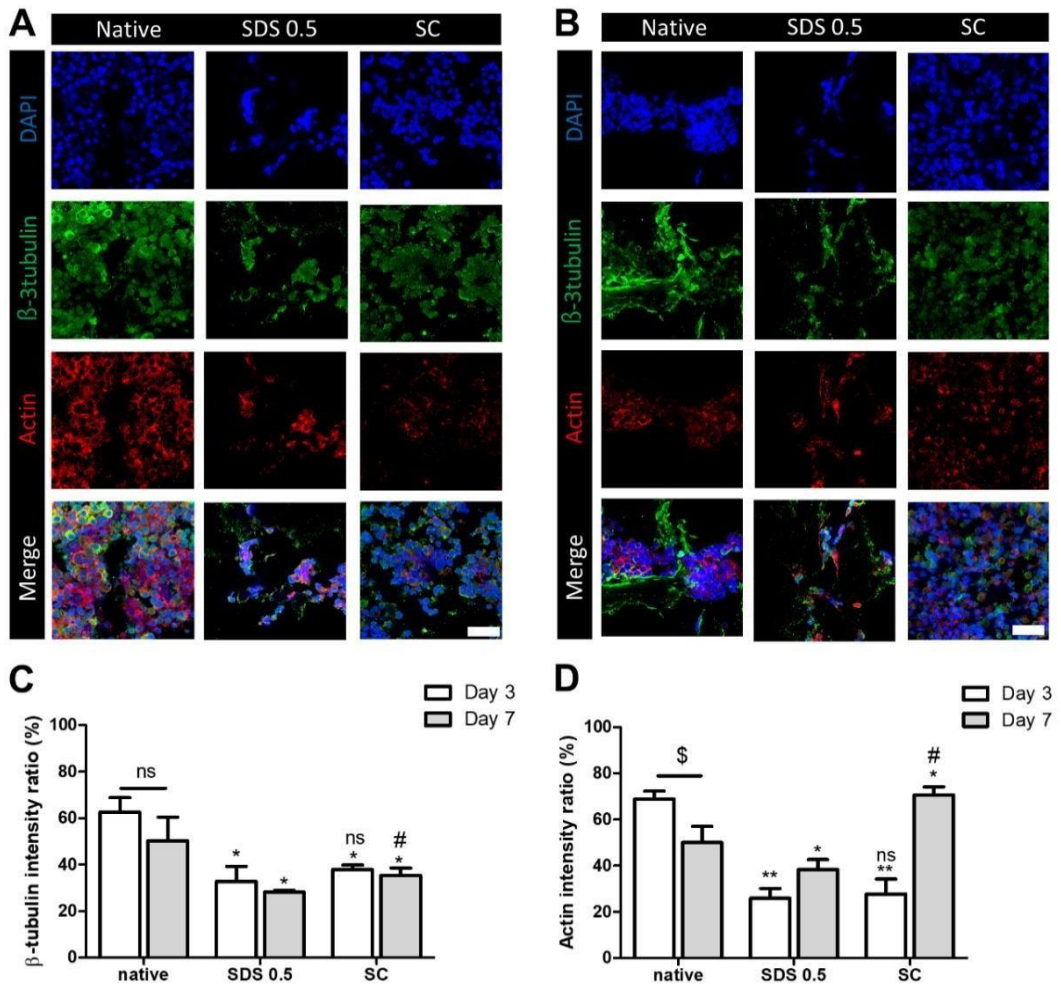


Figure 4. 3 PC12 cell culture and differentiation on nerve tissue slices. (A-B) Class III β -tubulin and actin staining of PC12 cell cultured on native and decellularized tissues on (A) day 3 and (B) day 7. (C-D) Relative fluorescence data of (C) Class III β -tubulin and (D) actin staining. (scale bar = $50\mu\text{m}$). Error bars indicate SD. P-value = * $p < 0.05$, ** $p < 0.01$, *** $p < 0.005$. # $p < 0.05$, ## $p < 0.01$, ### $p < 0.005$.

4.3.3 PC12 differentiation on native and decellularized tissue slice samples

In order to investigate the cellular reactivity of decellularized tissues, PC12 cells were cultured on the tissue slices. After PC12 differentiation, the amount of microfilament attachment to the tissue and the degree of differentiation were assessed through Class III β -tubulin and actin staining (Figure 4.3A-B). The value of Class III β -tubulin signal, which stands for neuronal microtubule formation, was significantly increased in the supercritical decellularized tissue compared to the SDS-treated tissue (SDS 0.5: 28 ± 1.56 , SC: $37 \pm 2.33\%$). But the microtubule signal of SC group was lower than that of native group (native: 48 ± 6.92 , SC: $37 \pm 2.33\%$) (Figure 4.3C). The actin signals were also measured after PC12 differentiation on nerve tissue slices. Higher actin signal was observed in the SC group than in SDS 0.5 and native groups (native: 42 ± 4.32 , SDS 0.5: 37 ± 9.88 , SC: $72 \pm 20.65\%$) (Figure 4.3D). To measure the neurite extension and outgrowth of differentiated PC12 cells, long-term cell culture was conducted on the tissue slices for 21 days using the same culture conditions of short-term culture (Figure 4.4A). As a result, the signal of Class III β -tubulin was highest in the SC group (native:

175±21.71, SDS 0.5: 183± 7.36, SC: 224±37.65 %) (Figure 4.4B). Neurite length of PC12 cells measured to confirm the most efficient microenvironment conditions for neuronal cell culture (Figure 4.4C). As anticipated, the native group showed the longest neurites after neural differentiation of PC12 cells. SC group exhibited neurites slightly shorter than the native group, but longer than SDS 0.5 group (native: 84±11.28, SDS 0.5: 43± 3.36, SC: 74±18.35 %).

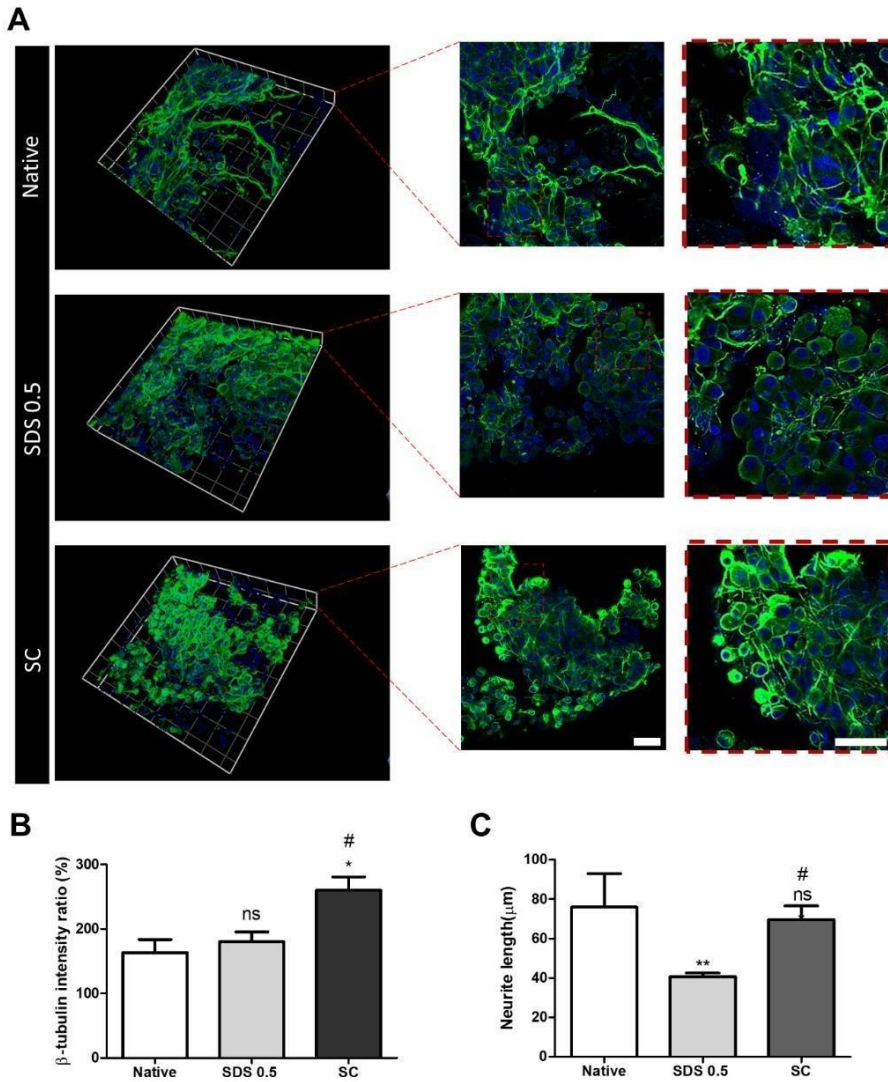


Figure 4.4 PC12 cell culture and differentiation on nerve tissue slices for a long-term period. (A) PC12 cell differentiation on nerve tissues for 21 days (B) Relative fluorescence data of PC12 cells (β 3-tubulin). (C) Neurite length measurement of differentiated PC12 cells. (scale bar = $50\mu\text{m}$). Error bars indicate SD. P-value = * $p < 0.05$, ** $p < 0.01$, *** $p < 0.005$. # $p < 0.05$, ## $p < 0.01$, ### $p < 0.005$.

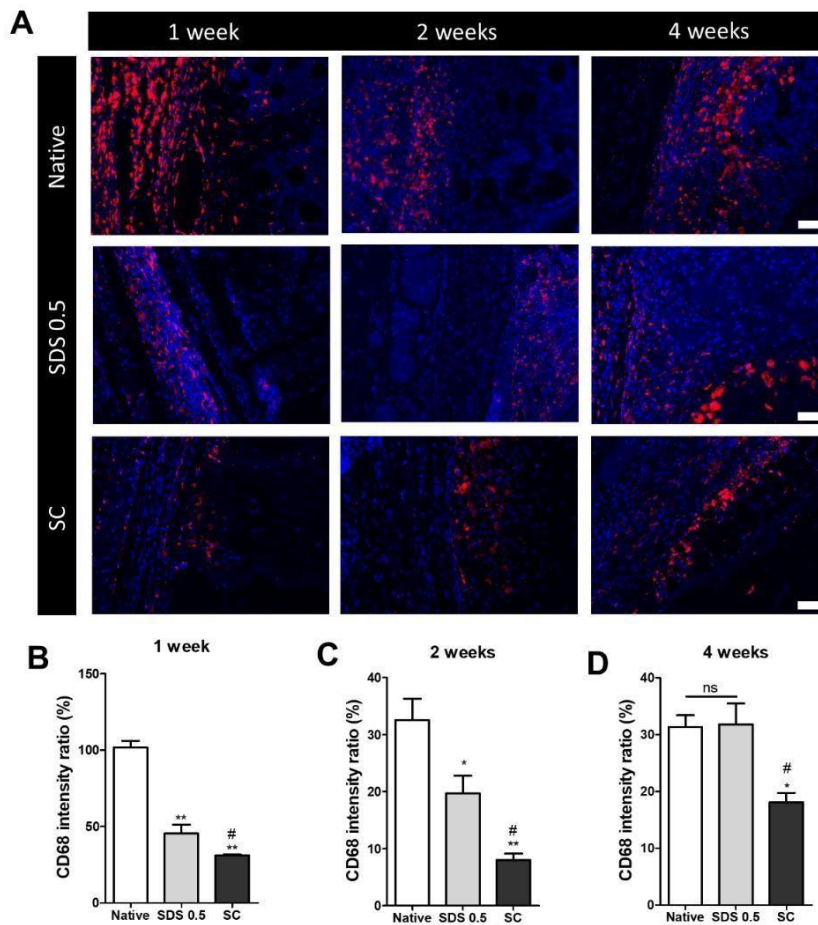


Figure 4.5 Immune cell infiltration ratio characterization of native tissues and dECM after implantation to skin area. (A) CD68 marker images of tissue implanted area (B) Relative fluorescence data of CD68 at 1 week (C) Relative fluorescence data of CD68 at 2 weeks. (D) Relative fluorescence data of CD68 at 4 weeks. (scale bar = 50 μ m) Error bars indicate SD. P-value = * $p < 0.05$, ** $p < 0.01$, *** $p < 0.005$. # $p < 0.05$, ## $p < 0.01$, ### $p < 0.005$.

4.3.4 Immune cell infiltration of implanted tissue samples

The decellularized and native tissue samples were subcutaneously implanted to verify decrease of host immune reaction to implanted decellularized tissue compared to native one (Figure 4.5). In the first week, the ratio of immune cells was much higher in the native tissue group than other decellularized samples (native: 103.36 ± 5.28 , SDS 0.5 : 48.29 ± 3.36 , SC: 31.65 ± 8.12 %) (Figure 4.5B). At week 2 of implantation, the immune reactions were decreased all experimental groups than one-week time point of implantation. The highest population of immune cells was found in native tissue implanted group (native: $34.65.11 \pm 2.15$, SDS 0.5 : 23.75 ± 8.26 , SC: 8.65 ± 3.95 %) (Figure 4.5C). After 4 weeks of implantation of tissues, immune reaction was maintained at a similarly high level as week 2 for the native group (native : 32.13 ± 4.32 %), while increased in SDS 0.5 group and SC group (SDS 0.5 : 33.65 ± 11.36 , SC : 16.29 ± 4.60 %). The lowest immune response was recorded in SC group at week 4.

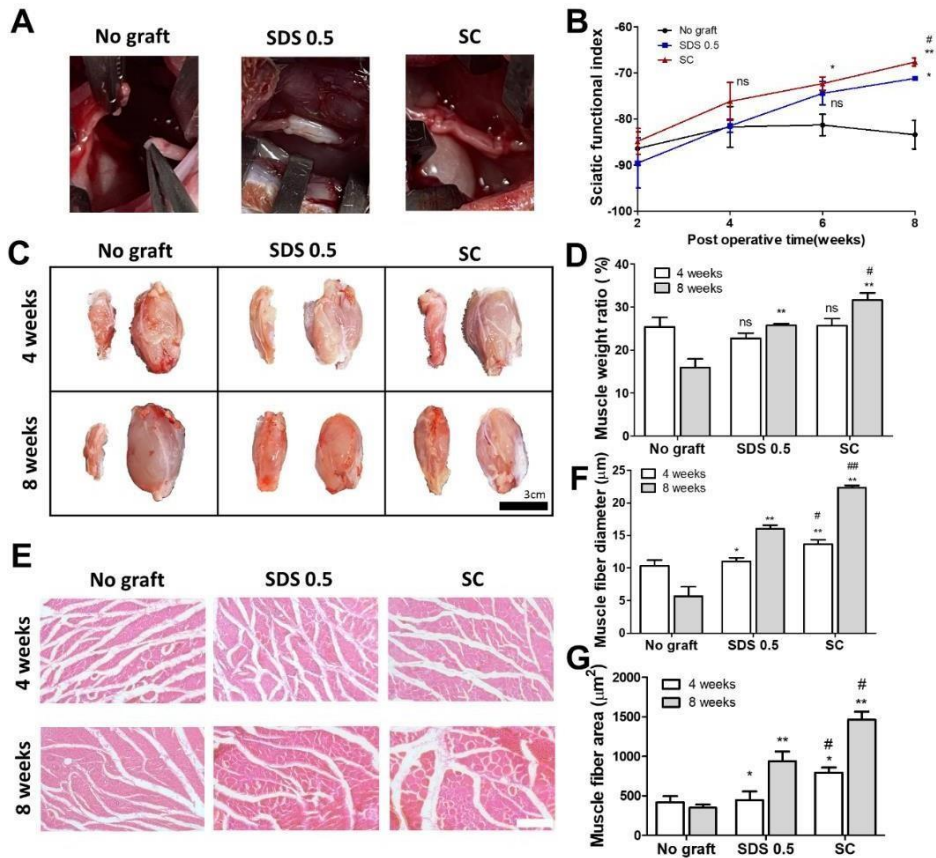


Figure 4. 6 Muscular regeneration and motor function recovery *in vivo*. (A) Nerve tissue implantation at nerve gap defects (B) Sciatic functional index characterization after 8 weeks nerve tissue implantation. (C) Representative images of rat gastrocnemius muscle after 4,8 weeks implantation (scale bar = 50 μm) (D) Weight ratio of experimental muscle normalized by weight of normal muscle(opposite limb). (E) H&E staining of gastrocnemius muscle. (scale bar = 100 μm) (F-G) Muscle fiber diameter (F) and area (G) of gastrocnemius muscle. Error bars indicate SD. P-value = * $p < 0.05$, ** $p < 0.01$, *** $p < 0.005$. # $p < 0.05$, ## $p < 0.01$, ### $p < 0.005$.

4.3.5 Motor function and muscular tissue regeneration after implantation *in vivo*

To assess regenerative potential of nerve tissue in animals, each decellularized tissue samples (SDS 0.5, SC) were transplanted into rat nerve defect model for 8 weeks. The decellularized tissues were transplanted and directly sutured to host nerve tissues after 1cm medial nerve elimination of rats. No graft group (control) was made with same defect of above experimental groups without any treatments. Motor function recovery was characterized with sciatic functional index test (Figure 4.6B). The index was increased in all groups until 4 weeks. But the functional recovery ratio was decreased in no graft group at 6, 8weeks. Motor functional recovery was occurred in SC group more efficiently than in SDS 0.5 group at 8 weeks (SDS 0.5: -70.69 ± 3.36 , SC: -66.79 ± 5.33). The muscle size of surgery leg(left) were decreased and the opposite muscle (right), in same anatomical area, were increased (Figure 4.6C). The muscle volume of SDS 0.5 group and SC group were restored more than No graft groups. the muscle weight ratios were calculated to characterize muscle restoration after surgery. The muscle weight ratio of surgery legs was recorded higher in SC groups than SDS

0.5 and control at 8 weeks after implantation (No graft: 16.36 ± 4.88 , SDS 0.5: 25.33 ± 1.32 , SC: 31.11 ± 4.33 %) (Figure 4.6D). Muscle fiber diameter and area was quantified using histological images (Figure 4.6E- G). Muscle fiber diameter was the highest in SC group at 4 weeks after implantation (No graft: 10.12 ± 1.33 , SDS 0.5: 11.39 ± 1.32 , SC: 14.11 ± 4.33 μm) (Figure 4.6F). Muscle fiber diameter of no graft group were decreased in 8 weeks compared to 4 weeks. The muscle diameter was increased as time elapsed in SDS 0.5 and SC group (No graft: 6.80 ± 2.36 , SDS 0.5: 16.11 ± 5.31 , SC: 22.09 ± 3.98 μm) (Figure 4.6F). Muscle fiber area were highest in SC group at 4 weeks after implantation (Figure 4. 6G). There was no significant difference between SDS 0.5 group and control at 4 weeks (No graft : 388.59 ± 73.67 , SDS 0.5: 423 ± 62.20 , SC: 796 ± 106.66 μm^2) (Figure 4.6F). Muscle fiber area was also highest in SC group at 8 weeks after implantation (No graft : 313 ± 68.36 , SDS 0.5 : 815 ± 121.22 , SC: 1496 ± 134.52 μm^2) (Figure 6G).

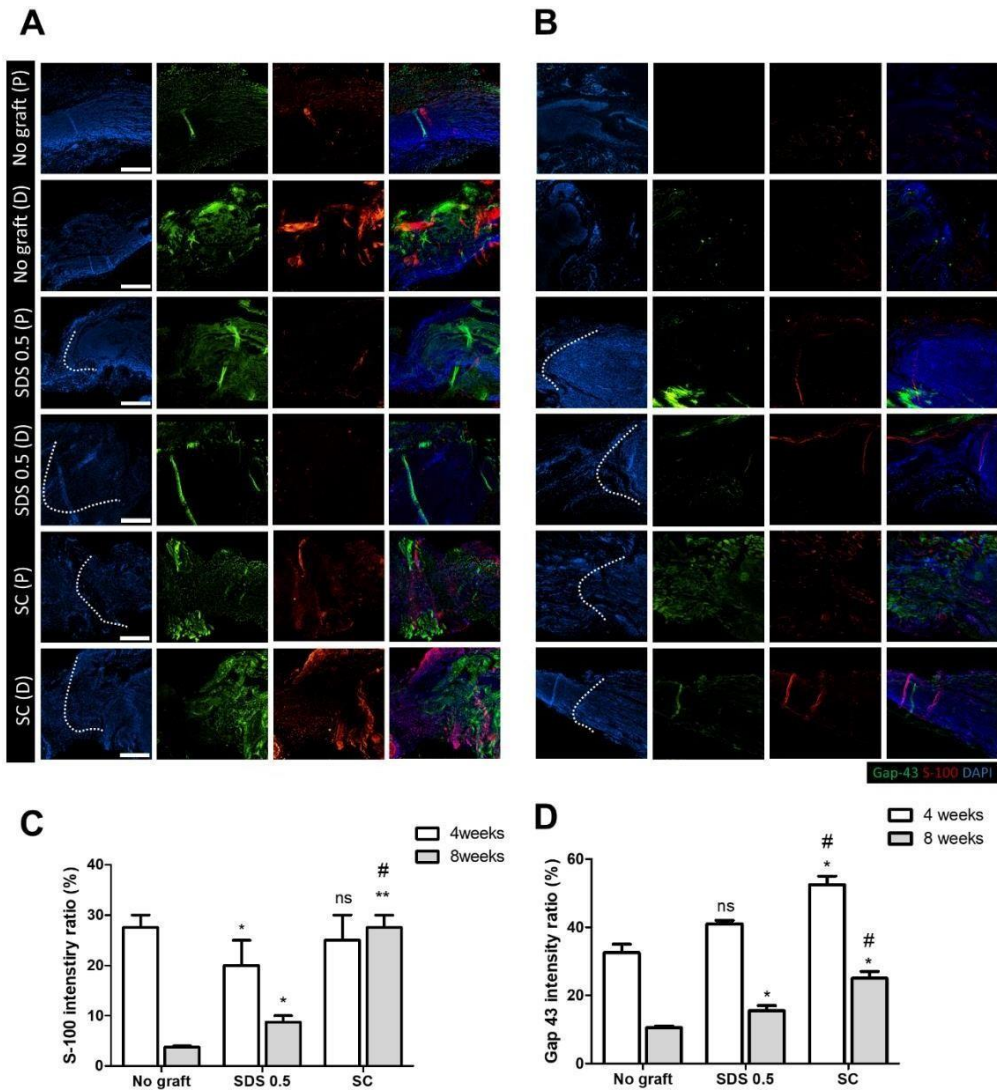


Figure 4. 7 Gap-43 and S-100 fluorescence staining of sciatic nerves post-implantation at 4,8 weeks (P: proximal, D: distal). (A) Gap-43 and S-100 fluorescence staining of sciatic nerves after regeneration after 4 weeks. (B) Gap-43 and S-100 fluorescence staining of sciatic nerves after regeneration after 8 weeks. (C) S-100 intensities characterization of regenerated sciatic nerves. (D) Gap-43 intensities characterization of regenerated sciatic nerves. (scale bar = 400 μ m). Error bars indicate SD. P-value = * $p < 0.05$, ** $p < 0.01$, *** $p < 0.005$. # $p < 0.05$, ## $p < 0.01$, ### $p < 0.005$.

4.3.6 Nerve tissue regeneration assessment after tissue implantation *in vivo*

To evaluate whether the neural tissue was properly connected and regenerated, fluorescence staining was performed to confirm the presence of Schwann cell marker (S100) and neuronal synaptic marker (GAP-43). Staining and analysis were performed by dividing the transplant site into distal and proximal sections to determine whether both sides of the neural junction were properly connected with implanted tissue after defect were made. The S-100 intensity of nerve implanted area were recorded with no significant difference at 4 weeks after implantation (No graft: 27.58 ± 3.88 , SDS 0.5: 22.62 ± 5.32 , SC: 28.11 ± 4.03 %) (Figure 4.7C). At 8 weeks, the S-100 expression was decreased in No graft group and SDS 0.5 group but sustained in SC group compared to that of week 4 (No graft: 5.21 ± 1.38 , SDS 0.5: 8.69 ± 3.09 , SC: 28.55 ± 6.83 %) (Figure 4.7B). The Gap 43 intensity was the highest in SC group at 4 weeks (No graft: 36.79 ± 9.31 , SDS 0.5: 41.64 ± 2.71 , SC: 53.85 ± 13.23 %) (Figure 4.7D). The Gap 43 were decreased at 8 weeks in all groups compared to 4-week time point but intensity trend was not changed. The highest intensity was observed in SC group and

still notable intensity of Gap 43 were also observed in SDS 0.54 group also (No graft: 11.01 ± 2.11 , SDS 0.5: 16.26 ± 4.44 , SC: 24.92 ± 4.13 %) (Figure 7D).

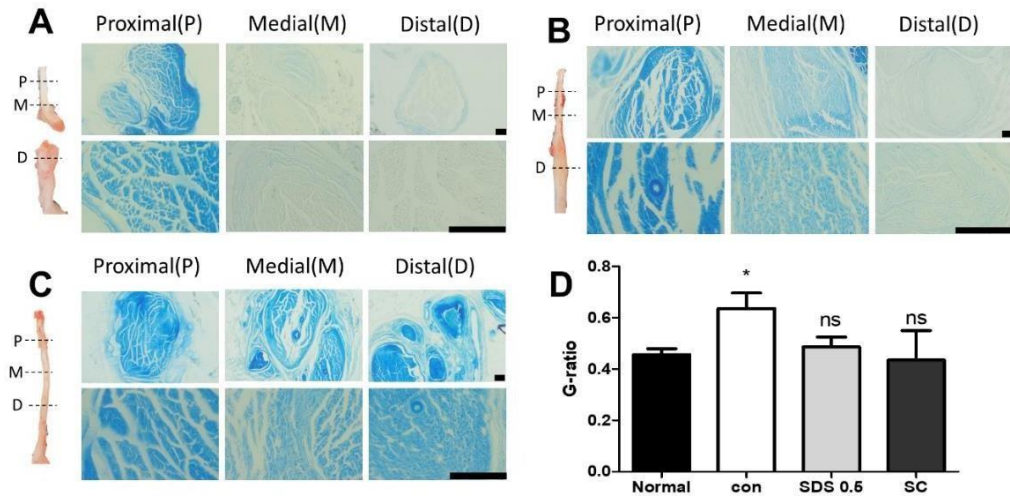


Figure 4. 8 Luxol fast blue staining of cross sectioned regenerated nerves after 8weeks. (A) Luxol blue staining of regenerated nerves (no material implant / proximal, medial, distal areas) (B) Luxol blue staining of regenerated nerves (SDS 0.5% decellularized ECM implant / proximal, medial, distal areas) (C) Luxol blue staining of regenerated nerves (SC decellularized ECM implant/ proximal, medial, distal areas) (D) G-ratio calculation of proximal area of experimental groups. . (scale bar = $50\mu\text{m}$) Error bars indicate SD. $n = 3$. * $p < 0.05$, ** $p < 0.01$, *** $p < 0.005$. *indicates statistical analysis about comparing no graft group versus SDS 0.5 and SC

To confirm whether the transplanted decellularized tissues were

connected to the host nerves and form the myelinated nerve fibers in the scaffolds, luxol fast blue staining was performed (Figure 4.8). In the control group, bulk fibrotic tissue was observed around the nerve, and weak myelin staining were observed in the medial and distal area (Figure 4.8A). In the SDS group, nerve bundles were well observed up to the medial part, but non-myelinated nerves were observed in the distal part of the transplanted scaffold (Figure 4.8B). In the SC group, well-formed neural tissue was observed in all three anatomical sections of the nerves (Figure 4.8C). The axons in proximal area were quantified for a G-ratio calculation. The G-ratio of control (no defect) were not significantly different with SDS 0.5 and SC group. But the No graft group were recorded higher G-ratio calculation versus other groups (No graft: 0.42 ± 0.05 , SDS 0.5: 0.47 ± 0.03 , SC: 0.49 ± 0.03) (Figure 8D).

4.4 Discussion

ECM components and DNA quantity have been quantified since preservation of major ECM components and effective removal of genetic component are important criteria for decellularization. The polymeric

material contents of native and decellularized nerve tissues were characterized by histological assessment and biochemical assays (Figure 4.1). The elimination process of genetic components was performed on sciatic nerve tissues to extract ECM selectively from native tissues. DNA concentration is a standard parameter of decellularization used to optimize decellularization processes. Successful decellularization is considered to contain 50 ng/ml of DNA [201]. Sciatic nerve tissues were treated with various concentrations of chemical solution to find out the decellularization conditions at which DNA is effectively eliminated and biological activity is preserved. DNA concentration of below 50 ng/ml was recorded in 0.5%, 1% (w/v) SDS conditions (SDS 0.5: 26.26 ± 10.06 , SDS 1.0: 18.15 ± 7.81 , SC: 38.07 ± 16.88). However, considerable tissue surface degradation and polymeric content loss was also observed in 1% SDS condition, which is why we chose SDS concentration (0.5% w/v) as the optimal concentration for chemical decellularization using harsh ionic detergent protocol inducing partial degradation of tissues [202]. Although both decellularization process (SDS, supercritical CO₂-based) process cannot completely preserve all protein found in native tissues, supercritical-based decellularization group showed higher preservation of proteins than chemical-based decellularization group (Figure 1I). The

total protein decreasing tendency in the decreasing order of native, SC, SDS0.5 groups seem correlated with protein scorings in proteomic data (Figure 4.1 J-L).

Both SDS and supercritical fluid-based decellularization processes can remove genetic material from the native tissues, accompanied by an inevitable loss in protein and the ECM contents. However, the extent of decrease was greater in the group treated with SDS compared to the group decellularized using supercritical fluid. The reduction in these components affected tissue mechanical properties, as shown by relatively higher compressive and tensile properties of SC group compared to SDS 0.5 group (Figure 4.2B-C). During the repeated indentation experiment, after 10 cycles, SDS 0.5 group recorded approximately 10 times weaker elastic modulus than the native tissue and SC groups. These results demonstrate that the decrease in tissue mechanical properties is proportional to the amount of tissue loss, suggesting that the decellularization method that best preserves ECM content helps maintain compositional and structural integrity of processed tissues.

Next, biological activity of dECM were investigated by culturing

PC12 cells *in vitro* on tissue slices to assess nerve cell migration, elongation capacity. Until day 3, relatively high levels of actin and Class III β -tubulin were detected in PC12 cells cultured on native group (Figure 4.3). However, in the SDS 0.5 group, the cells were found to not adhere as much as in the other groups (native, SC), possibly due to the loss of proteins during decellularization. Although the expression level of Class III β -tubulin was found to be higher in the native group than in both decellularized groups on Day 3 and Day 7, the signal of actin actually increased in the decellularized group on Day 7 compared to the native group (Figure 4.3D). It was reported that the expression of actin at the neurite tip relatively increased on growth cones of sprouting neurons [203], and even during differentiation portion of actin proteins moved to neurite tips from cytoplasm areas [204]. This implied a correlation between the expression level increase of Class III β -tubulin and actin level decrease in cytoplasm of differentiating PC12 cells in native group, where the same tendency was observed in the SC group (Figure 4.3C-D).

Differentiation of PC12 cells was observed in the outgrowth of neurites in long term culture conditions (Day 21). In 3D culture system,

the fully differentiated PC12 cells were hardly found in short term culture period (~Day7) which were set as standard differentiation condition with 2D culture method (Sup Figure 4.3). Specifically, proper outgrowth of neurites was not observed in the 3D culture by day 7, potentially due to the unique culture conditions associated with 3D scaffolds and ECM surface that are different from those used in 2D TCP culture [205, 206]. In addition, a minimum cell density required for cell-cell interaction is increased in 3D platform due to the formation of a volume, rather than simply along single z-axis like 2D system [207-209]. Additionally, the three-dimensional nature of the scaffold may slow cell migration and tubulin formation because of their structural turbulences [210]. Analysis of Class III β -tubulin signaling over a prolonged culture period (~Day21) revealed that the SC group exhibited the strongest signal of β 3-tubulin, with no significant difference observed between native and SDS groups. However, the longest neurites were observed in the native tissues, followed by the SC and then SDS 0.5 groups. This may be attributed to the preservation of the ECM components and cell responsive proteins in the native and SC groups, providing an environment conducive to neuronal growth [211]. The SDS 0.5 group still exhibited high Class III β -tubulin signals but showed relatively

lower neurite outgrowth than other groups. The SDS group exhibited tubulin signals primarily concentrated around the cell nucleus, and the increased cytoplasm size compared to the other two groups cultured in same conditions (Figure 4.4A). This means the tubulin proteins were still synthesized in cells by NGF signals but couldn't progress to designated directions and captured in cytoplasm. The condensed tubulin signals in nucleus made high internal Class III β -tubulin which present relatively higher tubulin portions in cell cytoplasm not in neurites. This is hypothesized to be due to the inability of neurites to extend, resulting in clustering around the nucleus and increased signal intensity of tubulin proteins [212].

In order to achieve the ultimate goal of neural regeneration, it is necessary to transplant decellularized tissue with minimal host immune response in implanted area. Immune reactions that occur during material transplantation are mainly mediated by monocytes and macrophages, unlike B and T cells that are mediated by adaptive immunity [213, 214]. Appropriate immune responses play a role in defense against external substances and in preventing fibrosis, but excessive immune reactions associated with foreign materials can potentially accelerate the

disintegration of transplanted tissues and provide a non-homogeneous environment for surrounding normal tissues, which can hinder tissue formation [215, 216]. The data presented here shows that excessive immune reactions were induced at 1 week after transplantation of native tissues, higher than immune response of SDS and SC group implantation. This indicates that tissue fragments such as DNA and damaged ECM fragments that originated from SDS-treated tissue degradation, induced increased immune reactions compared to the SC group during tissue transplantation [217-219]. After 4 weeks of transplantation, the native group maintained a lower level of immune response compared to the 1-week time point, but still showed higher than that of the other two groups. The SDS and SC groups showed increased immune cell infiltration compared to 2 weeks. This is expected to be due to tissue disintegration and increased immune cell infiltration, with the SC group showing a relatively lower level of immune cell infiltration, as demonstrated in the earlier mechanical evaluation, due to their ability to maintain strong stiffness even after cell removal process [218, 219]

Based on the evaluation of protein preservation, mechanical strength,

and cell reactivity, as well as immunogenicity, supercritical-based decellularization was shown to be the more biocompatible method of decellularizing native nerve tissues. Next, we conducted nerve gap defect transplantation experiment to evaluate the treatment potential of decellularized tissues. The gait analysis results showed that the SC group exhibited better recovery of motor function compared to the SDS 0.5 group, and the volume and weight of the gastrocnemius were also greater compared to the no graft and SDS 0.5 groups (Figure 4.6C-D). It was confirmed through muscle images of the gastrocnemius where nerve gap defect made did not function properly, while the gastrocnemius of the normal leg (opposite limb) was particularly over developed to compensate for reduced motor function, and these differences were reflected in the relative muscle weight ratio data showing dramatic difference (Figure 4.6D).

After 2 months following nerve dECM transplantation, the nerve tissues were collected and stained with S-100 and Gap-43 antibody. The Gap-43 is known to activate the signaling system that regulates neuron sprouting and connectivity during development in nerve tissues [220, 221]. The results obtained 4 weeks after nerve transection showed no

significant differences in Gap-43 between the no graft group, SDS 0.5 group, and SC group. It seems that host nerve cells were still active even with intervention made and this expectation was also deduced from muscle in vivo data collected at 4 week time point that still sustain volumetric state of muscle (Figure 4.6). Strong Gap-43 signals in the two groups (SDS 0.5 and SC) at 4 weeks post-implantation was expected to have growing and migration of neuronal, glial cells towards the transplanted decellularized tissues (Figure 4.7A). At 8-week time point, the control group showed decreased Gap-43 signals, and the degenerated morphology in proximal and distal area both in nerve gap. It might be derived immune cell related tissue degradation and fibrotic scar formation after injury [222]. In SDS 0.5 groups, the Gap-43 signals were found in the surface area of elongated gap junctions which means neuronal cell infiltration may happen but not correct direction and depth in transplanted tissues because of neuronal cell binding protein loss after process [223, 224]. The SC group showed the evenly concentrated Gap-43 signals in transplanted areas which stand for normal neuronal tissue formation in implanted biomaterials.

The S-100 is a marker for Schwann cells in peripheral nerves that

known to be involved in nerve metabolism, bundle formation, and nerve tissue atrophy [225, 226]. Therefore, the formation of Schwann cells during nerve regeneration is an important factor in evaluating healthy neuron elongation and formal neural tissue formations in peripheral nervous systems [227]. The results for S-100 were very similar to the expression pattern of Gap-43 at both time points (4, 8 weeks). However, At 4 weeks, SDS 0.5 showed a lower S-100 signal ratio compared to the no graft group. It was expected because of low proteins and ECM contents in SDS 0.5 group that could hinder the migration of Schwann cells, expressing S-100, and the proliferation of migrated cells in adhesion site of transplanted dECM [228].

To confirm whether the neural tissue was properly formed in transplanted decellularized tissues, luxol fast blue staining was performed on cross-sections of tissues to visualize myelin sheath formed by schwann cells, rather than sagittal sections that were previously used to confirm the expression of Gap-43 and S-100 [229]. In the No graft group (Figure 4.8A), myelin was still present in the proximal area that connected to the spinal cord, but very lightly observed in the neural tissues in the intact nerve defect areas (medial, distal). In the SDS 0.5

group, myelin sheath was found in proximal area and medial area which bridged to proximal, but no certain myelin sheaths were found in the distal area (Figure 4.8B). Therefore, it was expected that myelin would be more easily maintained or repaired in the proximal area near the spinal cord and peripheral nerve entry points where the fast transmission of nerve regeneration materials occurring and stronger regeneration signal can be activated for increase of Schwann cell migration and proliferation [230]. In the SC group, condensed myelin tissues were observed in whole anatomical area in newly regenerated axon including the distal area. This result indicating that myelinated axons from the proximal origin had grown into the grafted tissue (SC) and that the microenvironment formed by the grafted tissues had helped to maintain the activity of the surrounding myelinated axons in distal area also.

4.5 Conclusion

Supercritical-based decellularization and SDS-based decellularization two different approaches used in the decellularization of the sciatic nerves with the aim of enhancing its regeneration ability. The supercritical based method showed higher preservation of ECM in

processed tissue compared to SDS-based method. By preserving the native ECM architecture, supercritical-based decellularized nerve scaffolds retain their mechanical integrity like native tissue. In contrast, SDS-based decellularized scaffolds may experience a decrease in mechanical strength due to the potential damage to the ECM structure during the decellularization process. This structural stability was crucial for surgical handling and implantation, as well as for withstanding physiological loading, cellular reactivity and facilitating the regeneration process. The higher ECM and protein preservation of supercritical-based method resulted in providing of more proper neuronal cell culture basements that supported outgrowth of axons in culture conditions. In terms of advanced regeneration ability, the supercritical-based decellularization method had shown promising results of neural tissue regeneration. Studies have demonstrated that the supercritical-based decellularized sciatic nerve scaffolds exhibited a favorable microenvironment for neuronal cell growth and Schwann cell proliferation in tissues.

4.6 Supplementary figure

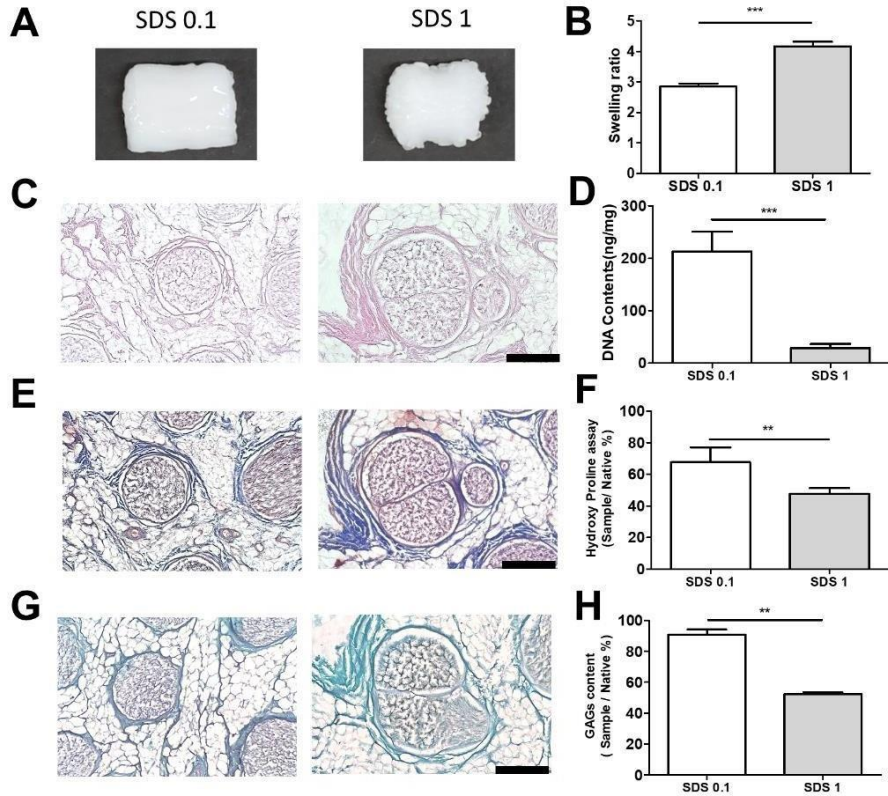


Figure S4. 6 Polymeric composition analysis and contents measurements of decellularized tissues processed with various decellularization methods. (A) Representative images decellularized nerve tissues (SDS 0.1%, 1% w/v). (B) Swelling ratios of decellularized nerve tissues (SDS 0.1%, 1% w/v). (C) Hematoxylin and eosin staining of decellularized nerve tissues (SDS 0.1%, 1% w/v). (D) DNA contents of native and decellularized tissues (E) MTC staining decellularized nerve tissues (SDS 0.1%, 1% w/v). (F) Hydroxyproline contents of decellularized nerve tissues (SDS 0.1%, 1% w/v). (G) Safranin-O staining of decellularized nerve tissues (SDS 0.1%, 1% w/v) (H) Sulfated gag contents decellularized nerve tissues (SDS 0.1%, 1% w/v). (scale bar = 50 μ m)

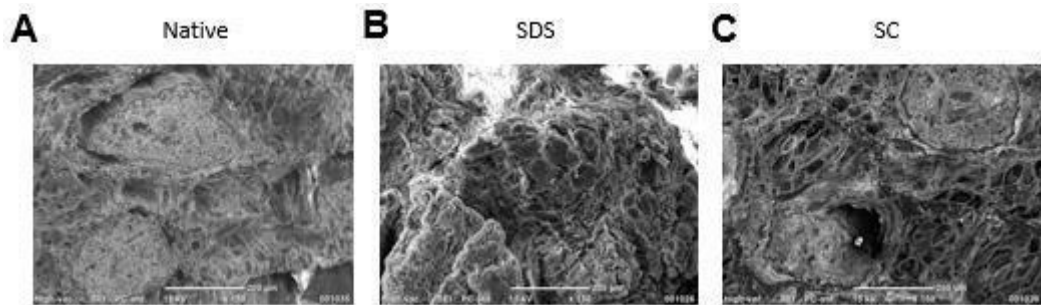


Figure S4. 7 SEM image of native tissues and decellularized tissues (A) SEM image of native tissues (B) SEM image of decellularized tissue with SDS chemical. (C) SEM image of decellularized tissue with supercritical fluids.

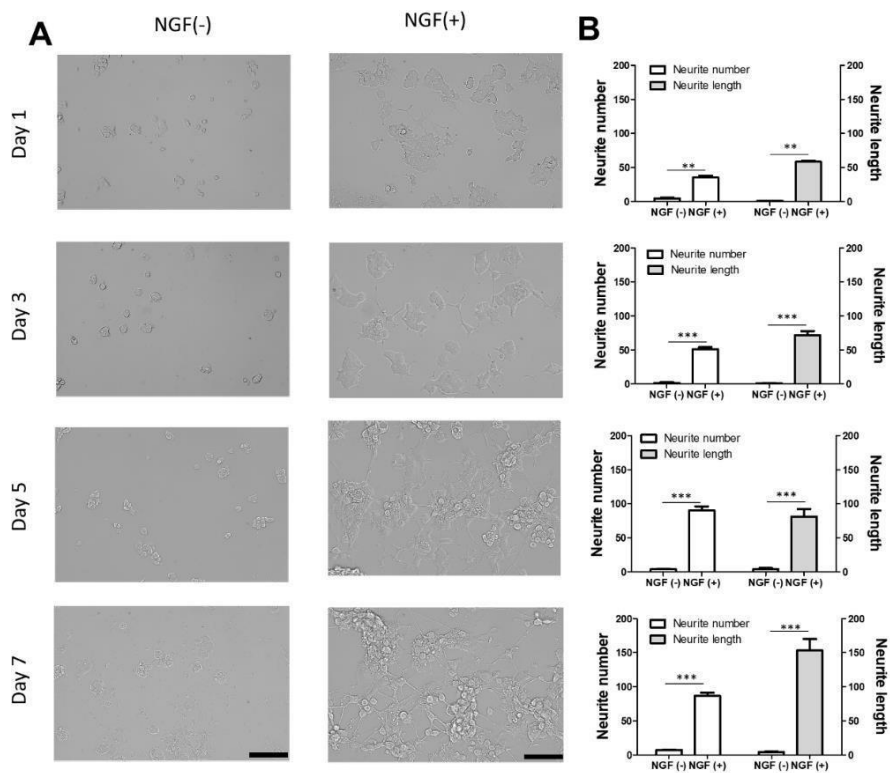


Figure S4. 8 PC12 differentiation cultured on TCP plates with/without NGF. (A) Representative images of differentiated and non-differentiated PC12 cells. (B) Neurite number and length of PC12 cells. (scale bar = 100 μ m)

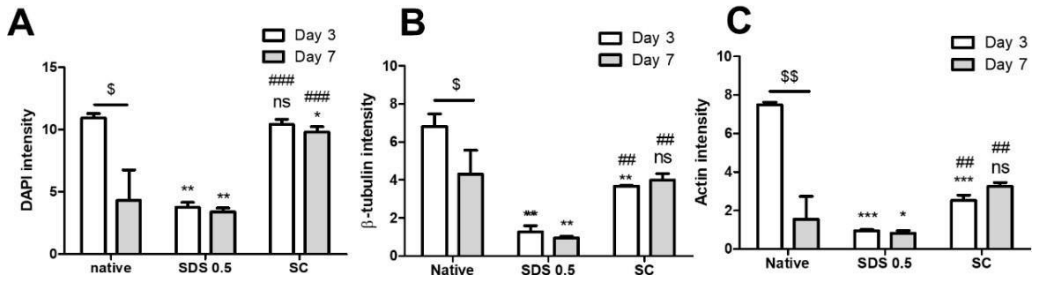


Figure S4.9 Fluorescence data of PC12 cells cultured for 3,7 days on nerve tissue slices (A) DAPI fluorescence intensity of each experimental group. (B) Class III β -tubulin fluorescence intensity of each experimental. (C) Actin fluorescence intensity of each experimental group.

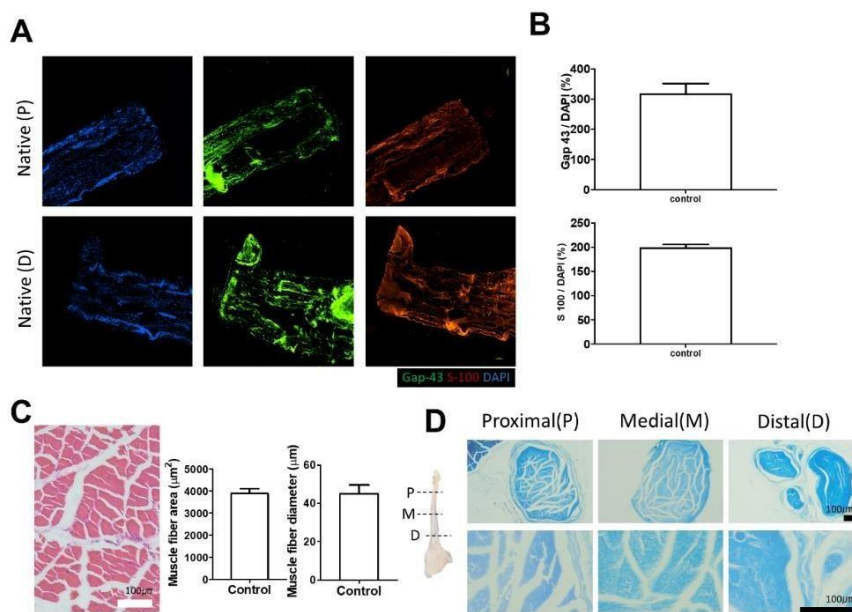


Figure S4. 10 Quantitative data of native tissues. (A) Gap-43, S-100 staining of native tissues (P: proximal, D: distal) (B) Characterization of Gap-43, S-100 signals of native tissues. (C) Muscle fiber diameter and area of native muscle tissue. (D) Luxol fast blue staining of native sciatic nerve tissues.

CHAPTER FIVE: CONCLUDING

REMARKS

In conclusion, the brain dECM cryogel fabrication and super critical decellularization method both showed overcome of current limitation of dECM fabrication and application to tissue engineering major. The use of brain-derived extracellular matrix (brain dECM) based cryogel as a scaffold for neuronal cell recruitment in brain tissue shows great potential for neuro regeneration. The brain dECM based cryogel serves as a three-dimensional scaffold that mimics the natural environment of brain tissue. It provides a supportive structure for the adhesion, growth, and migration of neuronal cells, facilitating their integration into the existing brain tissue. The unique composition of brain dECM, which includes various growth factors, cytokines, and other bioactive molecules, further enhances the recruitment and differentiation of neuronal cells. In addition, the chemical crosslinking of heparin sulfate that added to control growth factor loading ability of cryogel enhanced neuron specific regeneration in TBI model also.

Supercritical decellularization of the sciatic nerve offers several

advantages as biomaterial perspectives. Supercritical decellularization effectively removes cellular components from the nerve while preserving the native ECM architecture and biochemical cues necessary for regeneration. Furthermore, the scaffold provides a favorable microenvironment for cell adhesion and differentiation, thus promoting nerve regeneration. Moreover, the enhanced ECM retention achieved through this approach plays a crucial role in guiding cell behavior and tissue regeneration. The retained ECM components serve as signaling cues, regulating neuron cell differentiation and supportive structure, providing 3D cell binding network *in vivo*. This contributes to the successful regeneration of damaged nerve tissues.

Overall, the utilization of brain dECM based cryogel fabrication and supercritical decellularization represents a promising strategy for nerve tissue regeneration. By leveraging the inherent properties of the brain ECM and combining them with advanced tissue engineering techniques, this approach has the potential to address the challenges associated with nerve injuries and neurodegenerative diseases. Further research and optimization of this methodology are warranted to harness its full therapeutic potential and facilitate clinical translation in the future.

BIBLIOGRAPHY

1. Kim, Su-Hwan, Kyungmin Kim, **Beom Seok Kim**, Young-Hyeon An, Uk-Jae Lee, Sang-Hyuk Lee, Seunghyun L. Kim, Byung-Gee Kim, and Nathaniel S. Hwang. "Fabrication of polyphenol-incorporated anti-inflammatory hydrogel via high-affinity enzymatic crosslinking for wet tissue adhesion." *Biomaterials* 242 (2020): 119905.
2. **Beom Seok Kim**, Kim, Su-Hwan Kyungmin Kim, Young-Hyeon. An, Kyoung-Ha So, Byung-Gee Kim, and Nathaniel S. Hwang. "Enzyme-mediated one-pot synthesis of hydrogel with the polyphenol cross-linker for skin regeneration." *Materials Today Bio* 8 (2020): 100079.
3. **Beom-Seok Kim**, Jeong-Uk Kim, Kyoung-Ha So, and Nathaniel S. Hwang. "Supercritical fluid-based decellularization technologies for regenerative medicine applications." *Macromolecular Bioscience* 21, no. 8 (2021): 2100160.
4. Hyun Kim, Uk-Jae Lee, Hanbit Song, Jeongchan Lee, Won-Suk Song, Heewon Noh, Min-Ho Kang, **Beom-Seok Kim**, Jungwon Park, Nathaniel S Hwang, Byung-Gee Kim. "Synthesis of soluble melanin nanoparticles under acidic conditions using *Burkholderia cepacia* tyrosinase and their characterization." *RSC advances* 12, no. 27 (2022): 17434-17442.

국문초록

기능화와 구조특성 강화를 통한 세포외 기질 지지체

기반의 재생 치료제 개발

서울대학교

공과대학

바이오엔지니어링 협동과정

김범석

Decellularized ECM (dECM)은 뛰어난 생체적합성과 원재료 내의 조직 재생 성분 덕분에 조직공학용 재료로서 널리 이용되어 왔습니다. 이 논문에서는 탈세포화 재료의 응용방법에 대해 중점적으로 다루고 있으며, 특히 dECM 스캐폴드를 제조하기 위해 다른 기능성 고분자를 도입하거나 새로운 탈세포 방법을 사용하여 현재 사용하고 있는 dECM의 활용기술의 한계점을 극복하고자 하였습니다. 현재의 탈세포화 방법 및 dECM 응용기법들은 dECM의 재생 능력과 깊게 연관되어 있는 원조직 유래고분자, 단백질성분이 다량 손실 된다는 문제가 있기에 이를 보완하고자 조직 유래 성분을 최대한 보존하는 새로운 탈세포 방

법과 추후에 조직 특이적 단백 성분을 보충해줄 수 있는 생체 재료 제작 기법을 개발하였습니다.

먼저 음전하 특성을 갖는 헤파린 설페이트기를 뇌 조직 유래 탈세포와 가교 하여 양전하 특성의 성장인자를 담지 및 서 방출하는 cryogel 을 제작하였습니다. 이 접근법은 원 조직의 복잡한 세포외 기질 구조와 뇌 조직 재생을 위한 성장 인자를 동시에 제공할 수 있다는 장점을 가지고 있습니다. 제작된 cryogel은 다양한 스트레스 조건에서 3D 구조를 유지하였고 헤파린 설페이트 양에 따른 성장 인자 방출량을 조절할 수 있었습니다. 뇌 탈세포 조직 기반 cryogel을 이용한 외상성 뇌 손상 (traumatic brain injury) 모델 재생 실험에서 cryogel 은 뛰어난 생체 적합성을 나타내는 동시에 스캐폴드 내에서 신경세포의 부착, 증식을 촉진하는 것을 확인 하였습니다.

초임계 유체를 이용한 탈세포화 방법을 이용한 신경 조직 지지체 제작 실험에서 초임계 유체 기반 탈세포 기법은 기본 조직 구조 및 세포외 기질(ECM) 구성 요소를 보존하는데 있어 기존의 계면활성제를 이용한 기법에 비해 우수함을 증명하였습니다. 초임계 유체 기술은 탈 세포된 신경조직 내의 콜라겐 및 기타 주요 단백질이 기존의 계면활성제를 이용한 기법에 비해 더 많이 보존되었으며 또한 인장강도, 탄성도 등의 기

계적 물성변화 또한 초임계 유체 기반 탈세포 기법으로 제조된 신경 조직이 원조직과 더 가까운 특성을 보였습니다. 이러한 높은 단백질 보존율, 원조직 유사 물성을 가지는 탈세포 조직 지지체는 높은 신경 세포의 분화 효율과 동물조직에서 3차원 지지체로서 조직내의 세포 부착 지점을 제공함으로 기능성 조직의 형성을 유도함을 확인하였다.

전반적으로, 이 논문은 기본 ECM 구성 요소 보존 및 조직의 구조적 안전성 유지를 위한 초임계 유체 기술과 조직 특이적인 성장인자 전달을 위한 음전하 기반의 고분자를 화학적 가교로 탈세포 조직에 도입하는 연구를 정리하였습니다. 2개의 방법 모두 기존의 탈세포화기법의 문제점인 원조직 유래 조직 재생 인자가 탈세포 과정 중 소실되는 현상을 보완할 방법으로 개발된 실험 기법들이며 이러한 기술의 조합은 재생 의학 및 조직 공학 분야에 탈세포 조직을 도입하기 위한 새로운 솔루션을 제공하여 원조직을 이상적으로 모방하는 생체 재료를 개발하기 위한 플랫폼을 제공할 수 있을 것으로 예상됩니다.

키워드 : 탈세포, 세포외 기질, 초임계 유체, 신경조직

학번 : 2018-28861

References

1. Giannoudis PV, Pountos I: **Tissue regeneration: the past, the present and the future.** *Injury* 2005, **36**(4):S2-S5.
2. Lane SW, Williams DA, Watt FM: **Modulating the stem cell niche for tissue regeneration.** *Nature biotechnology* 2014, **32**(8):795-803.
3. Zhang Y, Yang F, Liu K, Shen H, Zhu Y, Zhang W, Liu W, Wang S, Cao Y, Zhou G: **The impact of PLGA scaffold orientation on in vitro cartilage regeneration.** *Biomaterials* 2012, **33**(10):2926-2935.
4. Shi-Wen X, Leask A, Abraham D: **Regulation and function of connective tissue growth factor/CCN2 in tissue repair, scarring and fibrosis.** *Cytokine & growth factor reviews* 2008, **19**(2):133-144.
5. Eming SA, Wynn TA, Martin P: **Inflammation and metabolism in tissue repair and regeneration.** *Science* 2017, **356**(6342):1026-1030.
6. Reddi AH: **Role of morphogenetic proteins in skeletal tissue engineering and regeneration.** *Nature biotechnology* 1998, **16**(3):247-252.
7. Laflamme MA, Murry CE: **Regenerating the heart.** *Nature biotechnology* 2005, **23**(7):845-856.
8. Van Koppen A, Joles JA, Bongartz LG, Van Den Brandt J, Reichardt HM, Goldschmeding R, Nguyen TQ, Verhaar MC: **Healthy bone marrow cells reduce progression of kidney failure better than CKD bone marrow cells in rats with established chronic kidney disease.** *Cell transplantation* 2012, **21**(10):2299-2312.
9. Kebriaei P, Isola L, Bahceci E, Holland K, Rowley S, McGuirk J, Devetten M, Jansen J, Herzig R, Schuster M: **Adult human mesenchymal stem cells added to corticosteroid therapy for the treatment of acute graft-versus-host disease.** *Biology of Blood and Marrow Transplantation* 2009, **15**(7):804-811.
10. Marler JJ, Upton J, Langer R, Vacanti JP: **Transplantation of cells in matrices for tissue regeneration.** *Advanced drug delivery reviews*

1998, **33**(1-2):165-182.

11. Dawson JI, Oreffo RO: **Bridging the regeneration gap: stem cells, biomaterials and clinical translation in bone tissue engineering.** *Archives of biochemistry and biophysics* 2008, **473**(2):124-131.
12. Wu DT, Jeffreys N, Diba M, Mooney DJ: **Viscoelastic biomaterials for tissue regeneration.** *Tissue Engineering Part C: Methods* 2022, **28**(7):289-300.
13. de Graaf CA, Kauppi M, Baldwin T, D. Hyland C, Metcalf D, Willson TA, Carpinelli MR, Smyth GK, Alexander WS, Hilton DJ: **Regulation of hematopoietic stem cells by their mature progeny.** *Proceedings of the National Academy of Sciences* 2010, **107**(50):21689-21694.
14. Trivedi P, Hematti P: **Derivation and immunological characterization of mesenchymal stromal cells from human embryonic stem cells.** *Experimental hematology* 2008, **36**(3):350-359.
15. Xie L, Zhang N, Marsano A, Vunjak-Novakovic G, Zhang Y, Lopez MJ: **In vitro mesenchymal trilineage differentiation and extracellular matrix production by adipose and bone marrow derived adult equine multipotent stromal cells on a collagen scaffold.** *Stem Cell Reviews and Reports* 2013, **9**:858-872.
16. Karp JM, Langer R: **Development and therapeutic applications of advanced biomaterials.** *Current opinion in biotechnology* 2007, **18**(5):454-459.
17. Kowalczewski CJ, Saul JM: **Biomaterials for the delivery of growth factors and other therapeutic agents in tissue engineering approaches to bone regeneration.** *Frontiers in pharmacology* 2018, **9**:513.
18. Zhuang Y, Cui W: **Biomaterial-based delivery of nucleic acids for tissue regeneration.** *Advanced Drug Delivery Reviews* 2021, **176**:113885.
19. El-Fattah A, Kenawy E-R, Kandil S: **Biodegradable polyesters as biomaterials for biomedical applications.** *International Journal of Chemical and Applied Biological Sciences* 2014, **1**(5):2-2.

20. *Jacobs IN, Redden RA, Goldberg R, Hast M, Salowe R, Mauck RL, Doolin EJ: **Pediatric laryngotracheal reconstruction with tissue-engineered cartilage in a rabbit model.** The Laryngoscope 2016, **126**:S5-S21.*
21. *Lopes MS, Jardini A, Maciel Filho R: **Poly (lactic acid) production for tissue engineering applications.** Procedia Engineering 2012, **42**:1402-1413.*
22. *Zhou H, Lawrence JG, Bhaduri SB: **Fabrication aspects of PLA-CaP/PLGA-CaP composites for orthopedic applications: a review.** Acta biomaterialia 2012, **8**(6):1999-2016.*
23. *Bogan SL, Teoh GZ, Birchall MA: **Tissue engineered airways: a prospects article.** Journal of cellular biochemistry 2016, **117**(7):1497-1505.*
24. *Elomaa L, Keshi E, Sauer IM, Weinhart M: **Development of GelMA/PCL and dECM/PCL resins for 3D printing of acellular in vitro tissue scaffolds by stereolithography.** Materials Science and Engineering: C 2020, **112**:110958.*
25. *Damme HV, Deprez M, Creemers E, Limet R: **Intrinsic structural failure of polyester (Dacron) vascular grafts. A general review.** Acta chirurgica belgica 2005, **105**(3):249-255.*
26. *Cai S, Christian DA, Tewari M, Minko T, Discher DE: **Anti-cancer polymersomes.** Polymer-based Nanostructures 2010:300.*
27. *Kim M-N, Lee B-Y, Lee I-M, Lee H-S, Yoon J-S: **Toxicity and biodegradation of products from polyester hydrolysis.** Journal of Environmental Science and Health, Part A 2001, **36**(4):447-463.*
28. *Woodruff MA, Hutmacher DW: **The return of a forgotten polymer—Polycaprolactone in the 21st century.** Progress in polymer science 2010, **35**(10):1217-1256.*
29. *Ratner BD, Zhang G: **A history of biomaterials.** In: Biomaterials Science. edn.: Elsevier; 2020: 21-34.*
30. *Moussa DG, Aparicio C: **Present and future of tissue engineering scaffolds for dentin-pulp complex regeneration.** Journal of tissue engineering and regenerative medicine 2019, **13**(1):58-75.*

31. *Islam MM, Shahruzzaman M, Biswas S, Sakib MN, Rashid TU: Chitosan based bioactive materials in tissue engineering applications-A review. Bioactive materials 2020, 5(1):164-183.*
32. *Neuendorf R, Saiz E, Tomsia A, Ritchie R: Adhesion between biodegradable polymers and hydroxyapatite: Relevance to synthetic bone-like materials and tissue engineering scaffolds. Acta biomaterialia 2008, 4(5):1288-1296.*
33. *Pradhan S, Brooks A, Yadavalli V: Nature-derived materials for the fabrication of functional biodevices. Materials Today Bio 2020, 7:100065.*
34. *Xing H, Lee H, Luo L, Kyriakides TR: Extracellular matrix-derived biomaterials in engineering cell function. Biotechnology advances 2020, 42:107421.*
35. *Fukushima M, Hirayama T, Ichikawa M, Kitazawa I, Kojima K, Sakai T, Takatsu Y, Ohtaki T: Glycosaminoglycan-conjugated insulin derivatives suitable for once-daily formulations. Acs Omega 2019, 4(3):5517-5525.*
36. *Prajapati SK, Jain A, Shrivastava C, Jain AK: Hyaluronic acid conjugated multi-walled carbon nanotubes for colon cancer targeting. International journal of biological macromolecules 2019, 123:691-703.*
37. *Garcia JMS, Panitch A, Calve S: Functionalization of hyaluronic acid hydrogels with ECM-derived peptides to control myoblast behavior. Acta biomaterialia 2019, 84:169-179.*
38. *Fan Z, Cheng P, Yin G, Wang Z, Han J: In situ forming oxidized salectan/gelatin injectable hydrogels for vancomycin delivery and 3D cell culture. Journal of Biomaterials Science, Polymer Edition 2020, 31(6):762-780.*
39. *Glowacki J, Mizuno S: Collagen scaffolds for tissue engineering. Biopolymers: Original Research on Biomolecules 2008, 89(5):338-344.*
40. *Copes F, Pien N, Van Vlierberghe S, Boccafoschi F, Mantovani D: Collagen-based tissue engineering strategies for vascular medicine. Frontiers in bioengineering and biotechnology 2019,*

7:166.

41. Nair M, Johal RK, Hamaia SW, Best SM, Cameron RE: **Tunable bioactivity and mechanics of collagen-based tissue engineering constructs: A comparison of EDC-NHS, genipin and TG2 crosslinkers.** *Biomaterials* 2020, **254**:120109.
42. Pastorino L, Dellacasa E, Scaglione S, Giulianelli M, Sbrana F, Vassalli M, Ruggiero C: **Oriented collagen nanocoatings for tissue engineering.** *Colloids and Surfaces B: Biointerfaces* 2014, **114**:372-378.
43. Frantz C, Stewart KM, Weaver VM: **The extracellular matrix at a glance.** *Journal of cell science* 2010, **123**(24):4195-4200.
44. Rosso F, Giordano A, Barbarisi M, Barbarisi A: **From cell-ECM interactions to tissue engineering.** *Journal of cellular physiology* 2004, **199**(2):174-180.
45. Murphy WL, McDevitt TC, Engler AJ: **Materials as stem cell regulators.** *Nature materials* 2014, **13**(6):547-557.
46. Lebre F, Hearnden CH, Lavelle EC: **Modulation of immune responses by particulate materials.** *Advanced Materials* 2016, **28**(27):5525-5541.
47. Huey DJ, Hu JC, Athanasiou KA: **Unlike bone, cartilage regeneration remains elusive.** *Science* 2012, **338**(6109):917-921.
48. Lu HH, Subramony SD, Boushell MK, Zhang X: **Tissue engineering strategies for the regeneration of orthopedic interfaces.** *Annals of biomedical engineering* 2010, **38**:2142-2154.
49. Dutta RC, Dutta AK: **Comprehension of ECM-Cell dynamics: A prerequisite for tissue regeneration.** *Biotechnology advances* 2010, **28**(6):764-769.
50. Gilpin A, Yang Y: **Decellularization strategies for regenerative medicine: from processing techniques to applications.** *BioMed research international* 2017, **2017**.
51. Badylak SF: **Decellularized allogeneic and xenogeneic tissue as a bioscaffold for regenerative medicine: factors that influence the host response.** *Annals of biomedical engineering* 2014, **42**:1517-

- 1527.
52. Gilbert TW, Sellaro TL, Badylak SF: **Decellularization of tissues and organs**. *Biomaterials* 2006, **27**(19):3675-3683.
 53. Swinehart IT, Badylak SF: **Extracellular matrix bioscaffolds in tissue remodeling and morphogenesis**. *Developmental Dynamics* 2016, **245**(3):351-360.
 54. Fujisaka S, Usui I, Bukhari A, Ikutani M, Oya T, Kanatani Y, Tsuneyama K, Nagai Y, Takatsu K, Urakaze M: **Regulatory mechanisms for adipose tissue M1 and M2 macrophages in diet-induced obese mice**. *Diabetes* 2009, **58**(11):2574-2582.
 55. Molina CP, Giglio R, Gandhi RM, Sicari BM, Londono R, Hussey GS, Bartolacci JG, Luque LMQ, Cramer MC, Dziki JL: **Comparison of the host macrophage response to synthetic and biologic surgical meshes used for ventral hernia repair**. *Journal of Immunology and Regenerative Medicine* 2019, **3**:13-25.
 56. Gilbert TW: **Strategies for tissue and organ decellularization**. *Journal of cellular biochemistry* 2012, **113**(7):2217-2222.
 57. Haykal S, Soleas JP, Salna M, Hofer SO, Waddell TK: **Evaluation of the structural integrity and extracellular matrix components of tracheal allografts following cyclical decellularization techniques: comparison of three protocols**. *Tissue Engineering Part C: Methods* 2012, **18**(8):614-623.
 58. Andrée B, Bela K, Horvath T, Lux M, Ramm R, Venturini L, Ciubotaru A, Zweigerdt R, Haverich A, Hilfiker A: **Successful re-endothelialization of a perfusable biological vascularized matrix (BioVaM) for the generation of 3D artificial cardiac tissue**. *Basic research in cardiology* 2014, **109**:1-13.
 59. Cui H, Chai Y, Yu Y: **Progress in developing decellularized bioscaffolds for enhancing skin construction**. *Journal of Biomedical Materials Research Part A* 2019, **107**(8):1849-1859.
 60. Syed O, Walters NJ, Day RM, Kim H-W, Knowles JC: **Evaluation of decellularization protocols for production of tubular small intestine submucosa scaffolds for use in oesophageal tissue engineering**. *Acta biomaterialia* 2014, **10**(12):5043-5054.

61. *Boccafoschi F, Botta M, Fusaro L, Copes F, Ramella M, Cannas M: Decellularized biological matrices: an interesting approach for cardiovascular tissue repair and regeneration. Journal of tissue engineering and regenerative medicine 2017, 11(5):1648-1657.*
62. *Wolf MT, Daly KA, Brennan-Pierce EP, Johnson SA, Carruthers CA, D'Amore A, Nagarkar SP, Velankar SS, Badylak SF: A hydrogel derived from decellularized dermal extracellular matrix. Biomaterials 2012, 33(29):7028-7038.*
63. *Sharma S, Tiwari S: A review on biomacromolecular hydrogel classification and its applications. International journal of biological macromolecules 2020, 162:737-747.*
64. *Ahn G, Min K-H, Kim C, Lee J-S, Kang D, Won J-Y, Cho D-W, Kim J-Y, Jin S, Yun W-S: Precise stacking of decellularized extracellular matrix based 3D cell-laden constructs by a 3D cell printing system equipped with heating modules. Scientific reports 2017, 7(1):8624.*
65. *Hwang SH, Kim J, Heo C, Yoon J, Kim H, Lee S-H, Park HW, Heo MS, Moon HE, Kim C: 3D printed multi-growth factor delivery patches fabricated using dual-crosslinked decellularized extracellular matrix-based hybrid inks to promote cerebral angiogenesis. Acta Biomaterialia 2023, 157:137-148.*
66. *Jang J, Kim TG, Kim BS, Kim S-W, Kwon S-M, Cho D-W: Tailoring mechanical properties of decellularized extracellular matrix bioink by vitamin B2-induced photo-crosslinking. Acta biomaterialia 2016, 33:88-95.*
67. *Kong MS, Koh W-G, Lee HJ: Controlled Release of Epidermal Growth Factor from Furfuryl-Gelatin Hydrogel Using in Situ Visible Light-Induced Crosslinking and Its Effects on Fibroblasts Proliferation and Migration. Gels 2022, 8(4):214.*
68. *Zhou J, Zhu Z, Ding J, Yang W, Shi J, Dong X, Xu J, Dong N: Promoting endothelialization on decellularized porcine aortic valve by immobilizing branched polyethylene glycolmodified with cyclic-RGD peptide: an in vitro study. Biomedical Materials 2015, 10(6):065014.*
69. *Wan J, Wang L, Huang Y, Fan H, Chen C, Yuan X, Guo Y, Yin L:*

Using GRGDSPC peptides to improve re-endothelialization of decellularized pancreatic scaffolds. *Artificial Organs* 2020, **44**(4):E172-E180.

70. Tong Z, Xu Z, Tong Y, Qi L, Guo L, Guo J, Gu Y: **Effectiveness of distal arterial bypass with porcine decellularized vascular graft for treating diabetic lower limb ischemia.** *The International journal of artificial organs* 2021, **44**(8):580-586.
71. Saleh T, Ahmed E, Yu L, Hussein K, Park K-M, Lee Y-S, Kang B-J, Choi K-Y, Choi S, Kang K-S: **Silver nanoparticles improve structural stability and biocompatibility of decellularized porcine liver.** *Artificial Cells, Nanomedicine, and Biotechnology* 2018, **46**(sup2):273-284.
72. Zhang Y, Fan W, Wang K, Wei H, Zhang R, Wu Y: **Novel preparation of Au nanoparticles loaded Laponite nanoparticles/ECM injectable hydrogel on cardiac differentiation of resident cardiac stem cells to cardiomyocytes.** *Journal of Photochemistry and Photobiology B: Biology* 2019, **192**:49-54.
73. Rahmati M, Mills DK, Urbanska AM, Saeb MR, Venugopal JR, Ramakrishna S, Mozafari M: **Electrospinning for tissue engineering applications.** *Progress in Materials Science* 2021, **117**:100721.
74. Kong Y, Xu J, Han Q, Zheng T, Wu L, Li G, Yang Y: **Electrospinning porcine decellularized nerve matrix scaffold for peripheral nerve regeneration.** *International Journal of Biological Macromolecules* 2022, **209**:1867-1881.
75. Hogan KJ, Smoak MM, Koons GL, Perez MR, Bedell ML, Jiang EY, Young S, Mikos AG: **Bioinspired electrospun decellularized extracellular matrix scaffolds promote muscle regeneration in a rat skeletal muscle defect model.** *Journal of Biomedical Materials Research Part A* 2022, **110**(5):1090-1100.
76. Smoak MM, Han A, Watson E, Kishan A, Grande-Allen KJ, Cosgriff-Hernandez E, Mikos AG: **Fabrication and characterization of electrospun decellularized muscle-derived scaffolds.** *Tissue Engineering Part C: Methods* 2019, **25**(5):276-287.

77. Zheng C, Yang Z, Chen S, Zhang F, Rao Z, Zhao C, Quan D, Bai Y, Shen J: **Nanofibrous nerve guidance conduits decorated with decellularized matrix hydrogel facilitate peripheral nerve injury repair.** *Theranostics* 2021, **11**(6):2917.
78. Dzobo K, Motaung KSCM, Adesida A: **Recent trends in decellularized extracellular matrix bioinks for 3D printing: an updated review.** *International journal of molecular sciences* 2019, **20**(18):4628.
79. Kim H, Kang B, Cui X, Lee SH, Lee K, Cho DW, Hwang W, Woodfield TB, Lim KS, Jang J: **Light-activated decellularized extracellular matrix-based bioinks for volumetric tissue analogs at the centimeter scale.** *Advanced Functional Materials* 2021, **31**(32):2011252.
80. Kara A, Distler T, Polley C, Schneidereit D, Seitz H, Friedrich O, Tihminlioglu F, Boccaccini AR: **3D printed gelatin/decellularized bone composite scaffolds for bone tissue engineering: Fabrication, characterization and cytocompatibility study.** *Materials Today Bio* 2022, **15**:100309.
81. Zare P, Pezeshki-Modaress M, Davachi SM, Chahsetareh H, Simorgh S, Asgari N, Haramshahi MA, Alizadeh R, Bagher Z, Farhadi M: **An additive manufacturing-based 3D printed poly ϵ -caprolactone/alginate sulfate/extracellular matrix construct for nasal cartilage regeneration.** *Journal of Biomedical Materials Research Part A* 2022, **110**(6):1199-1209.
82. Khati V, Ramachandraiah H, Pati F, Svahn HA, Gaudenzi G, Russom A: **3D bioprinting of multi-material decellularized liver matrix hydrogel at physiological temperatures.** *Biosensors* 2022, **12**(7):521.
83. Wang D, Guo Y, Zhu J, Liu F, Xue Y, Huang Y, Zhu B, Wu D, Pan H, Gong T: **Hyaluronic acid methacrylate/pancreatic extracellular matrix as a potential 3D printing bioink for constructing islet organoids.** *Acta biomaterialia* 2022.
84. Hillebrandt KH, Everwien H, Haep N, Keshi E, Pratschke J, Sauer IM: **Strategies based on organ decellularization and recellularization.** *Transplant International* 2019, **32**(6):571-585.

85. *Kajbafzadeh A-M, Khorramirouz R, Nabavizadeh B, Seyedian S-SL, Akbarzadeh A, Heidari R, Masoumi A, Azizi B, Beigi RSH: **Whole organ sheep kidney tissue engineering and in vivo transplantation: effects of perfusion-based decellularization on vascular integrity.** Materials Science and Engineering: C 2019, 98:392-400.*
86. *de Haan MJ, Witjas FM, Engelse MA, Rabelink TJ: **Have we hit a wall with whole kidney decellularization and recellularization: A review.** Current Opinion in Biomedical Engineering 2021, 20:100335.*
87. *Delgado ALJ, Carreira ACO, de Carvalho HJC, da Palma RK, de Castro Sasahara TH, de Carvalho CMF, León M, Barreto RdSN, Miglino MA: **Development of a new decellularization protocol for the whole porcine heart.** Journal of clinical and translational research 2021, 7(4):563.*
88. *Tsuchiya T, Obata T, Sengyoku H, Doi R, Hatachi G, Matsumoto K, Miyazaki T, Watanabe H, Nagayasu T: **Novel Options of Decellularization Solutions for Lung Tissue/Organ Engineering.** In: C57 EXTRACELLULAR MATRIX AND SUBCELLULAR DYNAMICS IN COMPLEX LUNG DISEASE. edn.: American Thoracic Society; 2020: A5531-A5531.*
89. *Rabbani M, Zakian N, Alimoradi N: **Contribution of physical methods in decellularization of animal tissues.** Journal of medical signals and sensors 2021, 11(1):1.*
90. *Funamoto S, Nam K, Kimura T, Murakoshi A, Hashimoto Y, Niwaya K, Kitamura S, Fujisato T, Kishida A: **The use of high-hydrostatic pressure treatment to decellularize blood vessels.** Biomaterials 2010, 31(13):3590-3595.*
91. *Wang F, Zhang J, Wang R, Gu Y, Li J, Wang C: **Triton X-100 combines with chymotrypsin: A more promising protocol to prepare decellularized porcine carotid arteries.** Bio-Medical Materials and Engineering 2017, 28(5):531-543.*
92. *Choudhury D, Yee M, Sheng ZLJ, Amirul A, Naing MW: **Decellularization systems and devices: State-of-the-art.** Acta biomaterialia 2020, 115:51-59.*

93. Collatusso C, Roderjan JG, Vieira ED, Costa FAd, Noronha Ld, Fornazari DdF: **Effect of SDS-based decellularization in the prevention of calcification in glutaraldehyde-preserved bovine pericardium: study in rats.** *Brazilian Journal of Cardiovascular Surgery* 2012, **27**:88-96.
94. Cheng J, Li J, Cai Z, Xing Y, Wang C, Guo L, Gu Y: **Decellularization of porcine carotid arteries using low-concentration sodium dodecyl sulfate.** *The International Journal of Artificial Organs* 2021, **44**(7):497-508.
95. Alshaikh AB, Padma AM, Dehlin M, Akouri R, Song MJ, Brännström M, Hellström M: **Decellularization and recellularization of the ovary for bioengineering applications; studies in the mouse.** *Reproductive Biology and Endocrinology* 2020, **18**:1-10.
96. McCrary MW, Vaughn NE, Hlavac N, Song YH, Wachs RA, Schmidt CE: **Novel sodium deoxycholate-based chemical decellularization method for peripheral nerve.** *Tissue Engineering Part C: Methods* 2020, **26**(1):23-36.
97. Liao J, Xu B, Zhang R, Fan Y, Xie H, Li X: **Applications of decellularized materials in tissue engineering: advantages, drawbacks and current improvements, and future perspectives.** *Journal of Materials Chemistry B* 2020, **8**(44):10023-10049.
98. Marin-Tapia HA, Romero-Salazar L, Arteaga-Arcos JC, Rosales-Ibáñez R, Mayorga-Rojas M: **Micro-mechanical properties of corneal scaffolds from two different bio-models obtained by an efficient chemical decellularization.** *Journal of the Mechanical Behavior of Biomedical Materials* 2021, **119**:104510.
99. El Soury M, García -García Ó D, Moretti M, Perroteau I, Raimondo S, Lovati AB, Carriel V: **Comparison of decellularization protocols to generate peripheral nerve grafts: a study on rat sciatic nerves.** *International Journal of Molecular Sciences* 2021, **22**(5):2389.
100. Zahmati AHA, Alipoor R, Shahmirzadi AR, Khori V, Abolhasani MM: **Chemical decellularization methods and its effects on extracellular matrix.** *Internal Medicine and Medical Investigation Journal* 2017, **2**(3):76-83.

101. Gregory E, Baek IH, Ala-Kokko N, Dugan R, Pinzon-Herrera L, Almodovar J, Song YH: **Peripheral Nerve Decellularization for In Vitro Extracellular Matrix Hydrogel Use: A Comparative Study.** *ACS Biomaterials Science & Engineering* 2022, **8**(6):2574-2588.
102. Fernández-Pérez J, Ahearne M: **The impact of decellularization methods on extracellular matrix derived hydrogels.** *Scientific reports* 2019, **9**(1):14933.
103. McHugh M, Krukonis V: **Supercritical fluid extraction: principles and practice:** Elsevier; 2013.
104. Zhang X, Heinonen S, Levänen E: **Applications of supercritical carbon dioxide in materials processing and synthesis.** *Rsc Advances* 2014, **4**(105):61137-61152.
105. Qamar S, Torres YJ, Parekh HS, Falconer JR: **Extraction of medicinal cannabinoids through supercritical carbon dioxide technologies: A review.** *Journal of Chromatography B* 2021, **1167**:122581.
106. Vafaei N, Rempel CB, Scanlon MG, Jones PJ, Eskin MN: **Application of supercritical fluid extraction (SFE) of tocopherols and carotenoids (hydrophobic antioxidants) compared to non-SFE methods.** *AppliedChem* 2022, **2**(2):68-92.
107. Patil PD, Patil SP, Kelkar RK, Patil NP, Pise PV, Nadar SS: **Enzyme-assisted supercritical fluid extraction: An integral approach to extract bioactive compounds.** *Trends in Food Science & Technology* 2021, **116**:357-369.
108. Yousefi M, Rahimi-Nasrabadi M, Mirsadeghi S, Pourmortazavi SM: **Supercritical fluid extraction of pesticides and insecticides from food samples and plant materials.** *Critical Reviews in Analytical Chemistry* 2021, **51**(5):482-501.
109. Lane MKM, Zimmerman JB: **Controlling metal oxide nanoparticle size and shape with supercritical fluid synthesis.** *Green Chemistry* 2019, **21**(14):3769-3781.
110. Sodeifian G, Sajadian SA, Derakhsheshpour R: **CO₂ utilization as a supercritical solvent and supercritical antisolvent in production of sertraline hydrochloride nanoparticles.** *Journal of CO₂*

Utilization 2022, **55**:101799.

111. Ahangari H, King JW, Ehsani A, Yousefi M: **Supercritical fluid extraction of seed oils—A short review of current trends**. *Trends in Food Science & Technology* 2021, **111**:249-260.
112. MY M, AP S: **Development of supercritical fluid extraction for the recovery of betacyanins from red pitaya fruit (*Hylocereus polyrhizus*) peel: a source of natural red pigment with potential antioxidant properties**. *International Food Research Journal* 2019, **26**(3).
113. Manjare SD, Dhingra K: **Supercritical fluids in separation and purification: A review**. *Materials Science for Energy Technologies* 2019, **2**(3):463-484.
114. Zhang S, Xu X, Liu C, Liu X, Dang C: **Experimental investigation on the heat transfer characteristics of supercritical CO₂ at various mass flow rates in heated vertical-flow tube**. *Applied Thermal Engineering* 2019, **157**:113687.
115. Radzali SA, Markom M, Saleh NM: **Co-solvent selection for supercritical fluid extraction (SFE) of phenolic compounds from *Labisia pumila***. *Molecules* 2020, **25**(24):5859.
116. Chaschin IS, Britikov DV, Khugaev GA, Salokhednova RR, Zubko AV, Abramchuk SS, Petlenko AA, Muratov RM, Bakuleva NP: **Decellularization of the human donor aortic conduit by a new hybrid treatment in a multicomponent system with supercritical CO₂ and Tween 80**. *The Journal of Supercritical Fluids* 2022, **180**:105452.
117. Huang C-C, Chen Y-J, Liu H-W: **Characterization of composite nano-bioscaffolds based on collagen and supercritical fluids-assisted decellularized fibrous extracellular matrix**. *Polymers* 2021, **13**(24):4326.
118. Andersson J, Bilotto P, Mears LL, Fossati S, Ramach U, Köper I, Valtiner M, Knoll W: **Solid-supported lipid bilayers—A versatile tool for the structural and functional characterization of membrane proteins**. *Methods* 2020, **180**:56-68.
119. Han Y, Zhang B, Li J, Cen L, Zhao L, Xi Z: **Preparation of**

- extracellular matrix of fish swim bladders by decellularization with supercritical carbon dioxide. Bioresources and Bioprocessing* 2023, **10**(1):14.
120. Giang NN, Trinh XT, Han J, Chien PN, Lee J, Noh SR, Shin Y, Nam SY, Heo CY: **Effective decellularization of human skin tissue for regenerative medicine by supercritical carbon dioxide technique.** *Journal of Tissue Engineering and Regenerative Medicine* 2022, **16**(12):1196-1207.
121. Gafarova ER, Grebenik EA, Lazhko AE, Frolova AA, Kuryanova AS, Kurkov AV, Bazhanov IA, Kapomba BS, Kosheleva NV, Novikov IA: **Evaluation of supercritical CO₂-assisted protocols in a model of ovine aortic root decellularization.** *Molecules* 2020, **25**(17):3923.
122. Chung S, Kwon H, Kim NP: **Supercritical extraction of decellularized extracellular matrix from porcine adipose tissue as regeneration therapeutics.** *Journal of Cosmetic Medicine* 2019, **3**(2):86-93.
123. Maas AI, Stocchetti N, Bullock R: **Moderate and severe traumatic brain injury in adults.** *The Lancet Neurology* 2008, **7**(8):728-741.
124. Burda JE, Bernstein AM, Sofroniew MV: **Astrocyte roles in traumatic brain injury.** *Experimental neurology* 2016, **275**:305-315.
125. Lozano D, Gonzales-Portillo GS, Acosta S, de la Pena I, Tajiri N, Kaneko Y, Borlongan CV: **Neuroinflammatory responses to traumatic brain injury: etiology, clinical consequences, and therapeutic opportunities.** *Neuropsychiatric disease and treatment* 2015:97-106.
126. Zhao Z, Nelson AR, Betsholtz C, Zlokovic BV: **Establishment and dysfunction of the blood-brain barrier.** *Cell* 2015, **163**(5):1064-1078.
127. Mendibil U, Ruiz-Hernandez R, Retegi-Carrion S, Garcia-Urquia N, Olalde-Graells B, Abarrategi A: **Tissue-specific decellularization methods: rationale and strategies to achieve regenerative compounds.** *International journal of molecular sciences* 2020, **21**(15):5447.
128. De Waele J, Reekmans K, Daans J, Goossens H, Berneman Z,

- Ponsaerts P: 3D culture of murine neural stem cells on decellularized mouse brain sections. Biomaterials 2015, 41:122-131.*
129. *Lin Q, Wong HL, Tian F-R, Huang Y-D, Xu J, Yang J-J, Chen P-P, Fan Z-L, Lu C-T, Zhao Y-Z: Enhanced neuroprotection with decellularized brain extracellular matrix containing bFGF after intracerebral transplantation in Parkinson's disease rat model. International journal of pharmaceutics 2017, 517(1-2):383-394.*
130. *Ravichandran A, Murekatete B, Moedder D, Meinert C, Bray LJ: Photocrosslinkable liver extracellular matrix hydrogels for the generation of 3D liver microenvironment models. Scientific Reports 2021, 11(1):1-12.*
131. *Massensini AR, Ghuman H, Saldin LT, Medberry CJ, Keane TJ, Nicholls FJ, Velankar SS, Badylak SF, Modo M: Concentration-dependent rheological properties of ECM hydrogel for intracerebral delivery to a stroke cavity. Acta biomaterialia 2015, 27:116-130.*
132. *Memic A, Colombani T, Eggermont LJ, Rezaeeyazdi M, Steingold J, Rogers ZJ, Navare KJ, Mohammed HS, Bencherif SA: Latest advances in cryogel technology for biomedical applications. Advanced Therapeutics 2019, 2(4):1800114.*
133. *Li J, Wang Y, Zhang L, Xu Z, Dai H, Wu W: Nanocellulose/gelatin composite cryogels for controlled drug release. ACS Sustainable Chemistry & Engineering 2019, 7(6):6381-6389.*
134. *He C, Ji H, Qian Y, Wang Q, Liu X, Zhao W, Zhao C: Heparin-based and heparin-inspired hydrogels: size-effect, gelation and biomedical applications. Journal of Materials Chemistry B 2019, 7(8):1186-1208.*
135. *Partington L, Mordan N, Mason C, Knowles J, Kim H, Lowdell M, Birchall M, Wall I: Biochemical changes caused by decellularization may compromise mechanical integrity of tracheal scaffolds. Acta biomaterialia 2013, 9(2):5251-5261.*
136. *Sheu M-T, Huang J-C, Yeh G-C, Ho H-O: Characterization of collagen gel solutions and collagen matrices for cell culture.*

- Biomaterials* 2001, **22**(13):1713-1719.
137. Maeda N: **Proteoglycans and neuronal migration in the cerebral cortex during development and disease**. *Frontiers in neuroscience* 2015, **9**:98.
 138. Ucar B, Humpel C: **Collagen for brain repair: therapeutic perspectives**. *Neural regeneration research* 2018, **13**(4):595.
 139. Gan D, Xu T, Xing W, Ge X, Fang L, Wang K, Ren F, Lu X: **Mussel-inspired contact-active antibacterial hydrogel with high cell affinity, toughness, and recoverability**. *Advanced Functional Materials* 2019, **29**(1):1805964.
 140. Gouda M, Gouveia W, Afonso M, Šljukić B, El Essawy N, Nassr AA, Santos D: **Poly (vinyl alcohol)-based crosslinked ternary polymer blend doped with sulfonated graphene oxide as a sustainable composite membrane for direct borohydride fuel cells**. *Journal of Power Sources* 2019, **432**:92-101.
 141. Kim I, Lee SS, Bae S, Lee H, Hwang NS: **Heparin functionalized injectable cryogel with rapid shape-recovery property for neovascularization**. *Biomacromolecules* 2018, **19**(6):2257-2269.
 142. Latifi M, Sani M, Salmannejad M, Kabir-Salmani M, Babakhanzadeh Bavanati H, Talaei-Khozani T: **Synergistic impact of platelet rich plasma-heparin sulfate with hydroxyapatite/zirconia on the osteoblast differentiation potential of adipose-derived mesenchymal stem cells**. *Cell and Tissue Banking* 2021:1-15.
 143. Lin ZP, Ngo W, Mladjenovic SM, Wu JL, Chan WC: **Nanoparticles bind to endothelial cells in injured blood vessels via a transient protein corona**. *Nano Letters* 2023, **23**(3):1003-1009.
 144. Salis A, Boström M, Medda L, Cugia F, Barse B, Parsons DF, Ninham BW, Monduzzi M: **Measurements and theoretical interpretation of points of zero charge/potential of BSA protein**. *Langmuir* 2011, **27**(18):11597-11604.
 145. Johnson D, Lanahan A, Buck CR, Sehgal A, Morgan C, Mercer E, Bothwell M, Chao M: **Expression and structure of the human NGF receptor**. *Cell* 1986, **47**(4):545-554.

146. *Metwally S, Stachewicz U: Surface potential and charges impact on cell responses on biomaterials interfaces for medical applications. Materials Science and Engineering: C 2019, 104:109883.*
147. *Zhong J, Lan C, Zhang C, Yang Y, Chen WX, Zhang KY, Zhao HL, Fang XY, Li HH, Tan L: Chondroitin sulfate proteoglycan represses neural stem/progenitor cells migration via PTPσ/α-actinin4 signaling pathway. Journal of Cellular Biochemistry 2019, 120(7):11008-11021.*
148. *Masuda T, Sankowski R, Staszewski O, Prinz M: Microglia heterogeneity in the single-cell era. Cell reports 2020, 30(5):1271-1281.*
149. *Kwon HS, Koh S-H: Neuroinflammation in neurodegenerative disorders: The roles of microglia and astrocytes. Translational neurodegeneration 2020, 9:1-12.*
150. *Dzyubenko E, Manrique-Castano D, Kleinschnitz C, Faissner A, Hermann DM: Role of immune responses for extracellular matrix remodeling in the ischemic brain. Therapeutic advances in neurological disorders 2018, 11:1756286418818092.*
151. *Huleihel L, Dziki JL, Bartolacci JG, Rausch T, Scarritt ME, Cramer MC, Vorobyov T, LoPresti ST, Swineheart IT, White LJ: Macrophage phenotype in response to ECM bioscaffolds. In: Seminars in immunology: 2017: Elsevier; 2017: 2-13.*
152. *Stolzing A, Wengner A, Grune T: Degradation of oxidized extracellular proteins by microglia. Archives of biochemistry and biophysics 2002, 400(2):171-179.*
153. *Agrawal V, Tottey S, Johnson SA, Freund JM, Siu BF, Badylak SF: Recruitment of progenitor cells by an extracellular matrix cryptic peptide in a mouse model of digit amputation. Tissue engineering Part A 2011, 17(19-20):2435-2443.*
154. *Uchida Y, Ohtsuki S, Katsukura Y, Ikeda C, Suzuki T, Kamiie J, Terasaki T: Quantitative targeted absolute proteomics of human blood-brain barrier transporters and receptors. Journal of neurochemistry 2011, 117(2):333-345.*

155. **Brightman M, Reese T: Junctions between intimately apposed cell membranes in the vertebrate brain.** *The Journal of cell biology* 1969, **40**(3):648-677.
156. **Saha B, Peron S, Murray K, Jaber M, Gaillard A: Cortical lesion stimulates adult subventricular zone neural progenitor cell proliferation and migration to the site of injury.** *Stem cell research* 2013, **11**(3):965-977.
157. **Tang M, Park SH, Petri S, Yu H, Rueda CB, Abel ED, Kim CY, Hillman EM, Li F, Lee Y: An early endothelial cell-specific requirement for Glut1 is revealed in Glut1 deficiency syndrome model mice.** *JCI insight* 2021, **6**(3).
158. **Albini M, Krawczun-Rygmaczewska A, Cesca F: Astrocytes and Brain-Derived Neurotrophic Factor (BDNF).** *Neuroscience Research* 2023.
159. **Fang J, Wang Z, Miao C-y: Angiogenesis after ischemic stroke.** *Acta Pharmacologica Sinica* 2023:1-17.
160. **Hartmann DA, Coelho-Santos V, Shih AY: Pericyte control of blood flow across microvascular zones in the central nervous system.** *Annual review of physiology* 2022, **84**:331-354.
161. **Lindahl P, Johansson BR, Leveen P, Betsholtz C: Pericyte loss and microaneurysm formation in PDGF-B-deficient mice.** *Science* 1997, **277**(5323):242-245.
162. **Hellstrom M, Kalen M, Lindahl P, Abramsson A, Betsholtz C: Role of PDGF-B and PDGFR-beta in recruitment of vascular smooth muscle cells and pericytes during embryonic.** 1999.
163. **Di Z, Wu X, Xie W, Lin X: Effect of pericytes on cerebral microvasculature at different time points of stroke.** *BioMed Research International* 2021, **2021**:1-10.
164. **Sasaki T, Larsson H, Kreuger J, Salmivirta M, Claesson-Welsh L, Lindahl U, Hohenester E, Timpl R: Structural basis and potential role of heparin/heparan sulfate binding to the angiogenesis inhibitor endostatin.** *The EMBO journal* 1999, **18**(22):6240-6248.
165. **Chiodelli P, Bugatti A, Urbinati C, Rusnati M: Heparin/Heparan**

- sulfate proteoglycans glycomic interactome in angiogenesis: biological implications and therapeutical use. Molecules* 2015, **20**(4):6342-6388.
166. Seo Y, Jeong S, Chung JJ, Kim SH, Choi N, Jung Y: **Development of an anisotropically organized brain dECM hydrogel-based 3D neuronal culture platform for recapitulating the brain microenvironment in vivo.** *ACS Biomaterials Science & Engineering* 2019, **6**(1):610-620.
167. Schabitz W-R, Berger C, Kollmar R, Seitz M, Tanay E, Kiessling M, Schwab S, Sommer C: **Effect of brain-derived neurotrophic factor treatment and forced arm use on functional motor recovery after small cortical ischemia.** *Stroke* 2004, **35**(4):992-997.
168. Kim H, Li Q, Hempstead BL, Madri JA: **Paracrine and autocrine functions of brain-derived neurotrophic factor (BDNF) and nerve growth factor (NGF) in brain-derived endothelial cells.** *Journal of Biological Chemistry* 2004, **279**(32):33538-33546.
169. Tomlinson RE, Li Z, Zhang Q, Goh BC, Li Z, Thorek DL, Rajbhandari L, Brushart TM, Minichiello L, Zhou F: **NGF-TrkA signaling by sensory nerves coordinates the vascularization and ossification of developing endochondral bone.** *Cell Reports* 2016, **16**(10):2723-2735.
170. Ma X, Cheng O, Jiang Q, Yang J, Xiao H, Qiu H: **Activation of ephrinb1/EPHB2/MAP-2/NMDAR mediates hippocampal neurogenesis promoted by transcranial direct current stimulation in cerebral-ischemic mice.** *NeuroMolecular Medicine* 2021:1-10.
171. Li S, Liao X, He Y, Chen R, Zheng WV, Tang M, Guo X, Chen J, Hu S, Sun J: **Exosomes derived from NGF-overexpressing bone marrow mesenchymal stem cell sheet promote spinal cord injury repair in a mouse model.** *Neurochemistry International* 2022, **157**:105339.
172. Zhu W, Chen L, Wu Z, Li W, Liu X, Wang Y, Guo M, Ito Y, Wang L, Zhang P: **Bioorthogonal DOPA-NGF activated tissue engineering microunits for recovery from traumatic brain injury by microenvironment regulation.** *Acta Biomaterialia* 2022, **150**:67-82.

173. Tanaka K, Tsukahara T, Kaku Y, Hashimoto N, Yonekawa Y, Ogata N, Kimura T, Taniguchi T: **Effect of nerve growth factor on delayed neuronal death and microtubule-associated protein 2 after transient cerebral ischaemia in the rat.** *Journal of Clinical Neuroscience* 1994, **1**(2):125-130.
174. Chiaretti A, Barone G, Riccardi R, Antonelli A, Pezzotti P, Genovese O, Tortorolo L, Conti G: **NGF, DCX, and NSE upregulation correlates with severity and outcome of head trauma in children.** *Neurology* 2009, **72**(7):609-616.
175. Chiaretti A, Antonelli A, Genovese O, Fernandez E, Giuda D, Mariotti P, Riccardi R: **Intraventricular nerve growth factor infusion improves cerebral blood flow and stimulates doublecortin expression in two infants with hypoxic–ischemic brain injury.** *Neurological research* 2008, **30**(3):223-228.
176. Ghuman H, Gerwig M, Nicholls FJ, Liu JR, Donnelly J, Badylak SF, Modo M: **Long-term retention of ECM hydrogel after implantation into a sub-acute stroke cavity reduces lesion volume.** *Acta biomaterialia* 2017, **63**:50-63.
177. Ghuman H, Mauney C, Donnelly J, Massensini AR, Badylak SF, Modo M: **Biodegradation of ECM hydrogel promotes endogenous brain tissue restoration in a rat model of stroke.** *Acta biomaterialia* 2018, **80**:66-84.
178. Witherel CE, Abeyayehu D, Barker TH, Spiller KL: **Macrophage and fibroblast interactions in biomaterial-mediated fibrosis.** *Advanced healthcare materials* 2019, **8**(4):1801451.
179. Pfister BJ, Gordon T, Loverde JR, Kochar AS, Mackinnon SE, Cullen DK: **Biomedical engineering strategies for peripheral nerve repair: surgical applications, state of the art, and future challenges.** *Critical Reviews™ in Biomedical Engineering* 2011, **39**(2).
180. Tapp M, Wenzinger E, Tarabishy S, Ricci J, Herrera FA: **The Epidemiology of Upper Extremity Nerve Injuries and Associated Cost in the US Emergency Departments.** *Annals of Plastic Surgery* 2019, **83**(6):676-680.

181. Zhang R-C, Du W-Q, Zhang J-Y, Yu S-X, Lu F-Z, Ding H-M, Cheng Y-B, Ren C, Geng D-Q: **Mesenchymal stem cell treatment for peripheral nerve injury: a narrative review**. *Neural Regeneration Research* 2021, **16**(11):2170.
182. Sharma AD, Wiederin J, Uz M, Ciborowski P, Mallapragada SK, Gendelman HE, Sakaguchi DS: **Proteomic analysis of mesenchymal to Schwann cell transdifferentiation**. *Journal of proteomics* 2017, **165**:93-101.
183. Fex Svenningsen Å, Dahlin LB: **Repair of the peripheral nerve—remyelination that works**. *Brain sciences* 2013, **3**(3):1182-1197.
184. Gorecka J, Kostiuk V, Fereydooni A, Gonzalez L, Luo J, Dash B, Isaji T, Ono S, Liu S, Lee SR: **The potential and limitations of induced pluripotent stem cells to achieve wound healing**. *Stem cell research & therapy* 2019, **10**(1):1-10.
185. Sulaiman W, Gordon T: **Neurobiology of peripheral nerve injury, regeneration, and functional recovery: from bench top research to bedside application**. *Ochsner Journal* 2013, **13**(1):100-108.
186. Wang S, Cai L: **Polymers for fabricating nerve conduits**. *International Journal of Polymer Science* 2010, **2010**.
187. Chrzęszcz P, Derbisz K, Suszyński K, Miodoński J, Trybulski R, Lewin-Kowalik J, Marcol W: **Application of peripheral nerve conduits in clinical practice: A literature review**. *neurologia i neurochirurgia polska* 2018, **52**(4):427-435.
188. Lee B-K, Ju YM, Cho J-G, Jackson JD, Lee SJ, Atala A, Yoo JJ: **End-to-side neuroorrhaphy using an electrospun PCL/collagen nerve conduit for complex peripheral motor nerve regeneration**. *Biomaterials* 2012, **33**(35):9027-9036.
189. Qian Y, Zhao X, Han Q, Chen W, Li H, Yuan W: **An integrated multi-layer 3D-fabrication of PDA/RGD coated graphene loaded PCL nanoscaffold for peripheral nerve restoration**. *Nature communications* 2018, **9**(1):323.
190. IJkema-Paassen J, Jansen K, Gramsbergen A, Meek M: **Transection of peripheral nerves, bridging strategies and effect evaluation**. *Biomaterials* 2004, **25**(9):1583-1592.

191. Kehoe S, Zhang X, Boyd D: **FDA approved guidance conduits and wraps for peripheral nerve injury: a review of materials and efficacy.** *Injury* 2012, **43**(5):553-572.
192. Sun B, Zhou Z, Wu T, Chen W, Li D, Zheng H, El-Hamshary H, Al-Deyab SS, Mo X, Yu Y: **Development of nanofiber sponges-containing nerve guidance conduit for peripheral nerve regeneration in vivo.** *ACS applied materials & interfaces* 2017, **9**(32):26684-26696.
193. Samadian H, Maleki H, Fathollahi A, Salehi M, Gholizadeh S, Derakhshankhah H, Allahyari Z, Jaymand M: **Naturally occurring biological macromolecules-based hydrogels: Potential biomaterials for peripheral nerve regeneration.** *International journal of biological macromolecules* 2020, **154**:795-817.
194. Sondell M, Lundborg G, Kanje M: **Regeneration of the rat sciatic nerve into allografts made acellular through chemical extraction.** *Brain research* 1998, **795**(1-2):44-54.
195. Hudson TW, Zawko S, Deister C, Lundy S, Hu CY, Lee K, Schmidt CE: **Optimized acellular nerve graft is immunologically tolerated and supports regeneration.** *Tissue engineering* 2004, **10**(11-12):1641-1651.
196. Meyer SR, Nagendran J, Desai LS, Rayat GR, Churchill TA, Anderson CC, Rajotte RV, Lakey JR, Ross DB: **Decellularization reduces the immune response to aortic valve allografts in the rat.** *The Journal of thoracic and cardiovascular surgery* 2005, **130**(2):469-476.
197. Chakraborty J, Roy S, Ghosh S: **Regulation of decellularized matrix mediated immune response.** *Biomaterials science* 2020, **8**(5):1194-1215.
198. Kim BS, Kim JU, So KH, Hwang NS: **Supercritical Fluid-Based Decellularization Technologies for Regenerative Medicine Applications.** *Macromolecular Bioscience* 2021, **21**(8):2100160.
199. Casali DM, Handleton RM, Shazly T, Matthews MA: **A novel supercritical CO₂-based decellularization method for maintaining scaffold hydration and mechanical properties.** *The Journal of*

- Supercritical Fluids* 2018, **131**:72-81.
200. Ahmad T, Masoodi F, Rather SA, Wani S, Gull A: **Supercritical fluid extraction: A review**. *J Biol Chem Chron* 2019, **5**(1):114-122.
 201. Sullivan DC, Mirmalek-Sani S-H, Deegan DB, Baptista PM, Aboushwareb T, Atala A, Yoo JJ: **Decellularization methods of porcine kidneys for whole organ engineering using a high-throughput system**. *Biomaterials* 2012, **33**(31):7756-7764.
 202. Snyder Y, Jana S: **Strategies for development of decellularized heart valve scaffolds for tissue engineering**. *Biomaterials* 2022:121675.
 203. Benzina O, Cloitre T, Martin M, Raoul C, Gergely C, Scamps F: **Morphology and intrinsic excitability of regenerating sensory and motor neurons grown on a line micropattern**. *Plos one* 2014, **9**(10):e110687.
 204. Chia JX, Efimova N, Svitkina TM: **Neurite outgrowth is driven by actin polymerization even in the presence of actin polymerization inhibitors**. *Molecular Biology of the Cell* 2016, **27**(23):3695-3704.
 205. Chua P, Lim WK: **The strategic uses of collagen in adherent cell cultures**. *Cell Biology International* 2023, **47**(2):367-373.
 206. Mehl BT, Martin RS: **Integrating 3D cell culture of PC12 cells with microchip-based electrochemical detection**. *Analytical methods* 2019, **11**(8):1064-1072.
 207. Kapalczyńska M, Kolenda T, Przybyła W, Zajączkowska M, Teresiak A, Filas V, Ibbs M, Bliźniak R, Łuczewski Ł, Lamperska K: **2D and 3D cell cultures—a comparison of different types of cancer cell cultures**. *Archives of Medical Science* 2018, **14**(4):910-919.
 208. Ravi M, Paramesh V, Kaviya S, Anuradha E, Solomon FP: **3D cell culture systems: advantages and applications**. *Journal of cellular physiology* 2015, **230**(1):16-26.
 209. Knight E, Przyborski S: **Advances in 3D cell culture technologies enabling tissue-like structures to be created in vitro**. *Journal of anatomy* 2015, **227**(6):746-756.
 210. Yang C-Y, Huang W-Y, Chen L-H, Liang N-W, Wang H-C, Lu J,

- Wang X, Wang T-W: **Neural tissue engineering: The influence of scaffold surface topography and extracellular matrix microenvironment**. *Journal of Materials Chemistry B* 2021, **9**(3):567-584.
211. Latchoumane C-FV, Chopra P, Sun L, Ahmed A, Palmieri F, Wu H-F, Guerreso R, Thorne K, Zeltner N, Boons G-J: **Synthetic Heparan Sulfate Hydrogels Regulate Neurotrophic Factor Signaling and Neuronal Network Activity**. *ACS applied materials & interfaces* 2022, **14**(25):28476-28488.
212. Dehmelt L, Smart FM, Ozer RS, Halpain S: **The role of microtubule-associated protein 2c in the reorganization of microtubules and lamellipodia during neurite initiation**. *Journal of Neuroscience* 2003, **23**(29):9479-9490.
213. **The Scaffold Immune Microenvironment: Biomaterial-Mediated Immune Polarization in Traumatic and Nontraumatic Applications**. *Tissue Engineering Part A* 2017, **23**(19-20):1044-1053.
214. Cramer MC, Badylak SF: **Extracellular matrix-based biomaterials and their influence upon cell behavior**. *Annals of biomedical engineering* 2020, **48**:2132-2153.
215. Aloysius A, Saxena S, Seifert AW: **Metabolic regulation of innate immune cell phenotypes during wound repair and regeneration**. *Current opinion in immunology* 2021, **68**:72-82.
216. Kim B, Kim S-H, Kim K, An Y-H, So K-H, Kim B-G, Hwang N: **Enzyme-mediated one-pot synthesis of hydrogel with the polyphenol cross-linker for skin regeneration**. *Materials Today Bio* 2020, **8**:100079.
217. Padma AM, Alshaikh AB, Song MJ, Akouri R, Oltean M, Brännström M, Hellström M: **Decellularization protocol-dependent damage-associated molecular patterns in rat uterus scaffolds differentially affect the immune response after transplantation**. *Journal of Tissue Engineering and Regenerative Medicine* 2021, **15**(7):674-685.
218. Tang D, Kang R, Coyne CB, Zeh HJ, Lotze MT: **PAMPs and DAMP**

- s: signal 0s that spur autophagy and immunity. Immunological reviews* 2012, **249**(1):158-175.
219. Malik AF, Hoque R, Ouyang X, Ghani A, Hong E, Khan K, Moore LB, Ng G, Munro F, Flavell RA et al: **Inflammasome components Asc and caspase-1 mediate biomaterial-induced inflammation and foreign body response.** *Proceedings of the National Academy of Sciences* 2011, **108**(50):20095-20100.
220. Burello L, De Bartolo P, Gelfo F, Foti F, Angelucci F, Petrosini L: **Functional recovery after cerebellar damage is related to GAP-43-mediated reactive responses of pre-cerebellar and deep cerebellar nuclei.** *Experimental neurology* 2012, **233**(1):273-282.
221. Chung D, Shum A, Caraveo G: **GAP-43 and BASP1 in axon regeneration: implications for the treatment of neurodegenerative diseases.** *Frontiers in cell and developmental biology* 2020, **8**:567537.
222. Lemke A, Ferguson J, Gross K, Penzenstadler C, Bradl M, Mayer RL, Gerner C, Redl H, Wolbank S: **Transplantation of human amnion prevents recurring adhesions and ameliorates fibrosis in a rat model of sciatic nerve scarring.** *Acta biomaterialia* 2018, **66**:335-349.
223. Bongolan T, Whiteley J, Castillo-Prado J, Fantin A, Larsen B, Wong CJ, Mazilescu L, Kawamura M, Urbanellis P, Jonebring A: **Decellularization of porcine kidney with submicellar concentrations of SDS results in the retention of ECM proteins required for the adhesion and maintenance of human adult renal epithelial cells.** *Biomaterials Science* 2022, **10**(11):2972-2990.
224. Zhou X, Qian Y, Chen L, Li T, Sun X, Ma X, Wang J, He C: **Flowerbed-inspired biomimetic scaffold with rapid internal tissue infiltration and vascularization capacity for bone repair.** *ACS nano* 2023, **17**(5):5140-5156.
225. Min Q, Parkinson DB, Dun XP: **Migrating Schwann cells direct axon regeneration within the peripheral nerve bridge.** *Glia* 2021, **69**(2):235-254.
226. Jessen KR, Mirsky R: **Schwann cell precursors; multipotent glial**

- cells in embryonic nerves. Frontiers in molecular neuroscience 2019, 12:69.*
227. *Nocera G, Jacob C: Mechanisms of Schwann cell plasticity involved in peripheral nerve repair after injury. Cellular and Molecular Life Sciences 2020, 77:3977-3989.*
228. *Schnell E, Klinkhammer K, Balzer S, Brook G, Klee D, Dalton P, Mey J: Guidance of glial cell migration and axonal growth on electrospun nanofibers of poly-ε-caprolactone and a collagen/poly-ε-caprolactone blend. Biomaterials 2007, 28(19):3012-3025.*
229. *Moszczyński AJ, Volkening K, Strong MJ: Neurofilament immunohistochemistry followed by Luxol fast Blue, for staining axons and myelin in the same paraffin section of spinal cord. Applied Immunohistochemistry & Molecular Morphology 2020, 28(7):562-565.*
230. *Chen B, Chen Q, Parkinson DB, Dun X-p: Analysis of Schwann cell migration and axon regeneration following nerve injury in the sciatic nerve bridge. Frontiers in molecular neuroscience 2019, 12:308.*